Novel Anionic Clay Adsorbents for Boiler-Blow-Down Waters Reclaim and Reuse

Final Report

DOE Award No.: DE-FG26-06NT42711

Principal Authors: Muhammad Sahimi and Theodore T. Tsotsis

Term: 01/2006 – 01/2010

Mork Family Department of Chemical Engineering and Materials Science

University of Southern California

925 Bloom Walk, HED 216

Los Angeles, CA 90089-1211

Phone No. 213-740-2069

Fax No. 213-740-8053

Email: tsotsis@usc.edu

Date of Report Submission: 02/10/2010

DISCLAIMER

"This report was prepared as an account of work sponsored by an agency of the United States Government. Neither the United States Government nor any agency thereof, nor any of their employees, makes any warranty, express or implied, or assumes any legal liability or responsibility for the accuracy, completeness, or usefulness of any information, apparatus, product, or process disclosed, or represents that its use would not infringe privately owned rights. Reference herein to any specific commercial product, process, or service by trade name, trademark, manufacturer, or otherwise does not necessarily constitute or imply its endorsement, recommendation, or favoring by the United States Government or any agency thereof. The views and opinions of authors expressed herein do not necessarily state or reflect those of the United States Government or any agency thereof."

Abstract

Arsenic (As) and Selenium (Se) are found in water in the form of oxyanions. Relatively high concentrations of As and Se have been reported both in power plant discharges, as well as, in fresh water supplies. The International Agency for Research on Cancer currently classifies As as a group 1 chemical, that is considered to be carcinogenic to humans.

In Phase I of this project we studied the adsorption of As and Se by uncalcined and calcined layered double hydroxide (LDH). The focus of the present work is a systematic study of the adsorption of As and Se by conditioned LDH adsorbents. Conditioning the adsorbent significantly reduced the Mg and Al dissolution observed with uncalcined and calcined LDH. The adsorption rates and isotherms have been investigated in batch experiments using particles of four different particle size ranges. As(V) adsorption is shown to follow a Sips-type adsorption isotherm. The As(V) adsorption rate on conditioned LDH increases with decreasing adsorbent particle size; the adsorption capacity, on the other hand, is independent of the particle size. A homogeneous surface diffusion model (HSDM) and a bi-disperse pore model (BPM) - - the latter viewing the LDH particles as assemblages of microparticles and taking into account bulk diffusion in the intraparticle pore space, and surface diffusion within the microparticles themselves - - were used to fit the experimental kinetic data. The HSDM estimated diffusivity values dependent on the particle size, whereas the BPM predicted an intracrystalline diffusivity, which is fairly invariant with particle size.

The removal of As(V) on conditioned LDH adsorbents was also investigated in flow columns, where the impact of important solution and operational parameters such as

influent As concentration, pH, sorbent particle size and flow rate were studied. An early breakthrough and saturation was observed at higher flow rates and at higher influent concentrations, whereas a decrease in the sorbent particle size and a decrease in influent pH resulted in an increase in the bed volumes treated at breakthrough. Both the HSDM and BPM were shown capable of predicting the column behavior.

Analysis of power plant effluents from various power plants in the greater Los Angeles area shows that, in addition to As and Se, these streams also consist of ions like fluorides, nitrates, chlorides, carbonates, sulphates and phosphates. In this study we have also tried to understand the effect of each of these individual ions on the As and Se removal capacity of LDH. For that, we carried out binary isotherm experiments with varying concentrations of As and of the individual competing ions in order to better understand the competition for the available adsorption sites. We fitted the data using the extended Sips isotherm equation. It was observed that the As adsorption capacity decreases in the presence of various individual competing ions in the order of PO_4^{2-} > SO_4^{2-} > CO_3^{2-} > Cl^- > NO_3^- ≈ F^-. For the Se removal from aqueous solutions in the presence of individual competing ions, calcined LDH proved more effective than conditioned LDH. It was also concluded that the Se adsorption capacity decreased in the presence of various individual competing ions in the order of PO_4^{2-} > SO_4^{2-} > CO_3^{2-} > Cl^- > NO_3^- > F^-, same as that observed for As.

We also studied the regeneration of LDH and it was shown that even after regenerating the LDH 15 times, the adsorption capacity only decreased by 10%, making it a very economical adsorbent. The TCLP test carried out on As- and Se-saturated LDH, showed that it can be categorized as a non hazardous waste.

Table of Contents

List of Tables 5

List of Figures 7

Executive Summary 10

Abstract 16

1. Introduction 19
   1.1. Background 19
   1.2. Scope of the Present Work 27

2. Adsorption of Arsenic on Layered Double Hydroxides: Effect of the Particle Size 32
   2.1. Introduction 32
   2.2. Model Development 33
      2.2.1. Homogeneous Surface Diffusion Model 33
      2.2.2. Bidisperse Pore Model 37
   2.3. Experimental 40
      2.3.1. Preparation of LDH 40
      2.3.2. Sorption Experiments 41
         2.3.2.1. Adsorption Isotherms 41
         2.3.2.2. Kinetics of Adsorption 42
      2.3.3. Characterization 42
   2.4. Results and Discussion 42
      2.4.1 Particle Size Distribution 42
      2.4.2. Adsorption Kinetics and Isotherms of As on LDH 48
   2.5. Conclusions 58

3. Adsorption of Arsenic on Conditioned Layered Double Hydroxides: Column Experiments and Modeling 60
   3.1. Introduction 60
   3.2. Model Development 61
      3.2.1. Homogeneous Surface Diffusion Model 64
      3.2.2. Bidisperse Pore model 65
   3.3. Experimental 70
      3.3.1. Materials 70
      3.3.2. Column Experiments 71
   3.4. Results and Discussion 72
      3.4.1. Determination of Adsorption Isotherms and Kinetics 72
      3.4.2. Column Experiments 75
         3.4.2.1. Breakthrough Studies 75
         3.4.2.2. Effect of Changing the Column Parameters 77
            3.4.2.2.1. Effect of Flow rate 77

3.4.2.2.2. Effect of the Influent As Concentration 79
3.4.2.2.3. Effect of Adsorbent Particle Size 80
3.4.2.2.4. Effect of pH 82
3.4.3. Error Analysis 83
3.5. Conclusions 84

4. Adsorption of Arsenic and Selenium on Conditioned Layered Double Hydroxides in the Presence of Various Competing Ions 86
4.1. Introduction 86
4.2. The Composition of Power Plant Effluents 88
4.3. Experimental 90
4.3.1. Materials 90
4.3.2. Batch Sorption Experiments 91
4.3.2.1. Adsorption Isotherm Experiments 92
4.3.2.1.1. Adsorption Isotherms of Competing Ions 92
4.3.2.1.2. Adsorption Isotherms of As and Individual Competing Ions 92
4.3.2.2. Kinetic Experiments 93
4.3.2.2.1. As Adsorption Kinetics in the Presence of Individual Competing Ions 93
4.3.2.3. Adsorption of Se in the Presence of Individual Competing Ions 94
4.3.3. Column Experiments for As Removal in the Presence of Individual Competing Ions 95
4.4. Results and Discussion 96
4.4.1. Adsorption Isotherms of the Competing Ions 96
4.4.2. Adsorption Isotherms of As in the Presence of Competing Ions 97
4.4.3. Adsorption Kinetics 100
4.4.4. Breakthrough Studies for As in the Presence of Individual Competing Ions 112
4.4.5. Binary Adsorption Isotherms of As and Competing Ions 118
4.4.6. Adsorption of Se in the Presence of Individual Competing Ions 124
4.5. Conclusions 128

5. Regeneration of LDH 129
5.1. Introduction 129
5.2. Regeneration Experiments 129
5.3. Conclusions 131

6. Cost Analysis for Treating Power Plant Effluents 132

7. Second Generation Adsorbents 133
7.1. Introduction 133
7.2. Experimental 133
7.2.1. Preparation of Second Generation Adsorbents 133
7.2.1.1. Mg-Al-CO_3-LDH with a Mg/Al Molar Ratio of 2 and 4 133

7.2.1.2. Mg-Al-NO_3-LDH with a Mg/Al Molar Ratio of 3 134
7.2.1.3. Mg-Fe-SO_4-LDH with a Mg/Fe Molar Ratio of 3 134
7.2.2. Sorption Isotherm Experiments 135
7.3. Results and Discussion 136
7.3.1. Adsorption Isotherms 136
7.4. Conclusions 139

8. Safe Disposal of the LDH Adsorbents 140
8.1. Introduction 140
8.2. Experimental 140
8.3. Conclusions 142

9. Nomenclature 143

10. Bibliography 148

11. Appendix 155

List of Tables

Table 2.1.	Average particle size calculated using arithmetic mean and volume mean definitions for conditioned LDH with various particle sizes	48
Table 2.2.	Measured densities and porosities for conditioned LDH with various particle sizes	48
Table 2.3.	Sorption isotherm parameters for As uptake on conditioned LDH at starting solution pH = 7	53
Table 2.4.	Surface diffusion coefficients for conditioned LDH with various particle sizes	54
Table 2.5.	D_{i0} for conditioned LDH with various particle sizes	54
Table 2.6.	Simulated D_μ / R_μ^2 for conditioned LDH with various particle sizes	56
Table 3.1.	Sorption isotherm parameters for As uptake on conditioned LDH as a function of starting solution pH for 180-300 μm particle size conditioned LDH	73
Table 3.2.	Measured densities and porosities and fitted D_μ / R_μ^2, Γ, and D_M values using the BPM, and fitted D_i values using the HSDM for conditioned LDH with various particle sizes	74
Table 3.3.	Properties of the fixed-bed column	77
Table 3.4.	RMSD values calculated for different cases for both the HSDM and BPM for data at the 8.5 cm column height	84
Table 4.1.	As and Se concentrations in various power-plant effluents	89
Table 4.2.	Concentration of various ions present in power-plant effluents	90
Table 4.3.	Initial composition of bottles for the As kinetic experiments	94
Table 4.4.	Sips isotherm parameters for various competing anions on conditioned LDH	97
Table 4.5.	Sorption isotherm parameters for As(V) uptake on conditioned	99

LDH in the presence of various competing ions

Table 4.6. Reduction in the competing ion concentrations during the isotherm experiments as a function of As concentration 99

Table 4.7. Fitted diffusion coefficients for HSDM and BPM for the As experiments in the presence of various competing ions 103

Table 4.8. Properties of the fixed-bed column 114

Table 4.9. Fitted parameters for the binary isotherm data 119

Table 4.10. Fitted parameters for the isotherm data with the power plant concentration ratios 124

Table 5.1. Adsorption efficiency of recycled conditioned LDH 130

Table 7.1 Cost analysis for treating power plant effluents 132

Table 8.1. Sorption isotherm parameters for As uptake on second generation LDHs 138

List of Figures

Figure 1.1.	Schematic view of the LDH structure and general formula.	25
Figure 2.1.	Schematic diagram of an adsorbent particle in the BPM framework.	37
Figure 2.2.	SEM pictures of LDH with mesh size of (a) 200-270 mesh (75-53μm), (b) 170-200 mesh (90-75μm), (c) 80-170 mesh (180-90μm), and (d) 50-80 mesh (300-180μm).	45
Figure 2.3.	Particle size distribution profiles for LDH.	47
Figure 2.4.	As concentration and solution pH profiles as a function of adsorption time on LDH; particle size of 75-90μm, C_0 of 205 μg/l, LDH dose of 0.04g/l.	49
Figure 2.5.	Mg and Al content in the solution as a function of time during the kinetic runs; particle size of 75-90μm, C_0 of 205 μg/l, LDH dose of 0.04g/l.	50
Figure 2.6.	Effect of particle size on the adsorption kinetics of As on LDH.	51
Figure 2.7.	Adsorption isotherm of As on LDH as a function of particle size.	51
Figure 2.8.	Sips isotherm model fit for the As adsorption on LDH for various particle sizes.	52
Figure 2.9.	Observed experimental data (symbols) and model predictions (lines) for As adsorption on LDH with various particle sizes: (a) 53-75 μm; (b) 75-90 μm; (c) 90-180 μm; (d) 180-300 μm. Solid lines denote simulated uptake curves for d_{10} and d_{30}, and the dash lines denote simulated uptake curves calculated with a loading – dependent diffusivity.	57
Figure 2.10.	Observed experimental data and model predictions (bidisperse pore model) for As adsorption on LDH with various particle sizes: (a) 53-75 μm; (b) 75-90 μm; (c) 90-180 μm; (d) 180-300 μm.	58
Figure 3.1.	Fit of the Sips isotherm for the As adsorption on LDH at three starting solution pH.	73
Figure 3.2.	Adsorption of 200 ppb As solution (pH=7.0), fed at a flow rate	77

of 8 ml/min by LDH with particle size (180-300μm) at several dimensionless bed depths $\left(\overline{V}\right)$ in a 8.5 cm column.

Figure 3.3. Effect of feed flow rate on the breakthrough curves and the corresponding simulation fittings at a bed depth of 8.5 cm $\left(\overline{V}=1.0\right)$. 79

Figure 3.4. Effect of the influent As concentration on the breakthrough curves and the corresponding simulation fittings at a bed depth of 8.5 cm $\left(\overline{V}=1.0\right)$. 80

Figure 3.5. Effect of the adsorbent particle size on the breakthrough curves and the corresponding simulation fittings at a bed depth of 8.5 cm $\left(\overline{V}=1.0\right)$. 82

Figure 3.6. Effect of the influent stream pH on the breakthrough curves and the corresponding simulation fittings at a bed depth of 8.5 cm $\left(\overline{V}=1.0\right)$. 83

Figure 4.1. Adsorption isotherms for the various anions on conditioned LDH. 97

Figure 4.2. Adsorption isotherms for As(V) on conditioned LDH in the presence of various individual competing ions at a fixed initial concentration and the Sips fit. 98

Figure 4.3. Adsorption of 20 ppb As solution as a function of time by (180-300 μm) LDH particles in the presence of various individual competing ions at concentration levels found in typical power plant effluents. 101

Figure 4.4. HSDM and BPM fits for the adsorption of 20 ppb As solution as function of time by (180-300 μm) LDH particles in the presence of various individual competing ions at concentration levels found in typical power plant effluents. 106

Figure 4.5. Reduction in the competing ion concentration as a function of time during As adsorption. 107

Figure 4.6. Reduction in As concentration as a function of time in the presence of various individual competing ions as a function of competing ion concentration. 111

Figure 4.7. Adsorption of 60 ppb As solution as a function of time by (180- 112

300 μm) LDH particles indicating the additive effect of various individual competing ions.

Figure 4.8. Adsorption of 20 ppb As solution by LDH in the presence of various individual competing ions at several column height locations in packed bed experiments and the corresponding HSDM & BPM predictions. 117

Figure 4.9. Binary adsorption isotherms for As(V) and the competing ions on conditioned LDH. 123

Figure 4.10. Adsorption isotherms for Se on calcined and conditioned LDH in the presence of individual competing ions. 127

Figure 8.1. Adsorption isotherms for As on various second generation LDHs. 138

Executive Summary

Introduction

Electric utilities are a very large user of water in the USA (132,000 Mgal/daily), putting the industry on an equal footing with farm irrigation. As the demand for electricity increases with the growing economy, so will the need for water for cooling and other plant uses. As a result, the electric power generation industry is likely to find itself in direct competition for new sources of water with the other growing sectors of the economy. The water usage issue aside for a moment, water quality issues in power generation will continue to dominate the discussion for many years to come. Renewed concerns exist today about the environmental fate of heavy metals, such as mercury, arsenic, and selenium that are found in many of these effluents, which negatively impact their disposal. Plant-wide discharges, as a result, are likely to come under increased scrutiny as future water regulations come more into focus.

These power plant effluents fall today under the category of high volume, "too clean to clean" effluents. These require highly efficient treatment techniques, particularly for the removal of trace-level metal contaminants. Very little emphasis, so far, has been placed on such discharges. The focus of the report presented is on the development of advanced concepts for reclaiming and reusing such effluents. In particular, the emphasis is on dealing with arsenic and selenium impacted boiler blow-down streams, which have, so far, only received scant attention. Arsenic and selenium contaminants in these streams are expected to be in the ppm to ppb levels, though little detail about these streams is published in the open literature.

Project Objectives

The key project objective is the study of the use of a novel class of adsorbent materials, namely layered double hydroxides (LDH), for the treatment of heavy metal (specifically As and Se) impacted power plant effluents. To meet the project objectives we carried out the following Tasks:

Task 1: Studying the removal of As and Se from model and real boiler blow-down streams in flow columns.

Task 2: Development of the 2nd generation product.

Task 3: Aspects of safe disposal of the spent adsorbents.

Project Outcomes

The overall outcome of our efforts is a reliable and efficient process utilizing novel optimal adsorbent material, namely layered double hydroxides (LDH), that is flexible to apply towards recycle and reutilization of boiler blow-down streams and, hopefully, also for the treatment of a number of other effluents of relevance to the power/electricity generation environment. The following briefly describes the work that was carried out in each of the project's tasks and the resulting outcomes:

Task 1: In this Task the removal of As and Se from model and real power plant effluents was studied in detail. In particular, this Task involved the following types of studies:

1. Adsorption of Arsenic on Layered Double Hydroxides: Effect of Particle Size

The adsorption of As(V) on conditioned LDH was investigated as a function of its particle size. It was shown that the As(V) adsorption rate on conditioned LDH increases with decreasing adsorbent particle size; the total adsorption capacity of As(V) on conditioned LDH, on the other hand, is independent of particle size. The experimental

data were then fitted to two models, the Homogeneous Surface Diffusion Model (HSDM) which considers the adsorbent to consist of uniform particles, and the Bidisperse Pore Model (BPM) which assumes that the adsorbent particle is an agglomerate of a number of equal size, single-crystal microparticles. The advantage of the HSDM is its simplicity and ease in simulation, while the BPM model provides a better representation of the true pore structure of the LDH. When the HSDM was used to describe the experimental data, the estimated diffusivity values were shown to increase with increasing particle size. On the other hand, when the BPDM was utilized to fit the experimental data it predicted that the diffusivity was particle-size independent. The latter model, therefore, appeared more appropriate for use in real flow-column experiments.

2. Adsorption of Arsenic on Conditioned Layered Double Hydroxides: Column Experiments and Modeling

The adsorption of As(V) on the conditioned LDH was then studied in flow column experiments. The experimental variables examined in this part of the study included influent As concentration, pH, sorbent particle size characteristics, and flow rate. Adsorption behavior was characterized in terms of the As concentration at the exit of the column (as well as at various lengths along the column) as a function of the number of bed volumes treated by the column. A key column characteristic is the number of the bed volumes at breakthrough, defined as the time when the effluent concentration is equal to 5% of the influent concentration. The experimental results show that the breakthrough time increased upon decreasing the sorbent particle size, the influent stream flow rate, and column feed concentration. It was also observed that, as the influent pH was

decreased, the column performance improved significantly, and the breakthrough times increased.

The two adsorption models (HSDM and BPM), developed to fit the batch experimental data, were then applied to the column experiments. Both models predicted the qualitative trends quite well. Using the root mean square deviation (RMSD) (also known as the root mean square error (RMSE)) method to compare the two models (with respect to their ability to fit the experimental data), proved inconclusive as in some cases HSDM provides a better fit (lower RMSD), while in other cases the BPM was superior.

3. Adsorption of Arsenic on Conditioned Layered Double Hydroxides in the Presence of Various Competing Ions

In this part of the study, power plant effluent data were collected and evaluated. It was found that these effluents contain various ions such as fluorides, nitrates, chlorides, carbonates, sulphates and phosphates in addition to As and Se. The effect of these competing ions on As and Se adsorption by the conditioned LDH was then investigated. Individual competing ion isotherms were measured. It was found that the carbonates adsorb the most on LDH, while nitrates adsorb the least among the various ions present in the power plant effluents. Binary isotherms of As and the individual competing ions were measured. The effect of each of these individual ions, at concentration levels that are found in typical power plant effluents, was also studied on the rates of As removal by LDH. It was observed that nitrates and fluorides have almost no effect, whereas phosphates compete the most with As for the adsorption sites on LDH. The experimental kinetic data were fitted with the HSDM and BPM. We also carried out column experiments in the presence of individual competing ions at concentration levels found in

power plant effluents and similar trends were observed as in the batch experiments. The HSDM and BPM were also able to predict the qualitative trends quite well. From the batch adsorption isotherm and kinetic experiments as well as the column experiments it can be concluded that the As adsorption capacity decreases in the presence of various individual competing ions in the order of $PO_4^{2-} > SO_4^{2-} > CO_3^{2-} > Cl^- > NO_3^- > F^-$. For Se removal from aqueous solutions in the presence of individual competing ions, calcined LDH proved more effective than the conditioned LDH.

4. Regeneration of LDH

This part of the effort focused on our ability to regenerate the spent adsorbents. A series of regeneration experiments were carried out which proved that the conditioned LDH can be regenerated and recycled for at least 15 times with minimal loss of its adsorption capacity.

5. Cost Analysis for Treating Power Plant Effluents

As part of this Task we also carried a preliminary economic analysis of the process. The cost for treating the power plant effluents using the proposed process appears to be very reasonable.

Task 2: The focus of this Task was the synthesis of second generation LDH adsorbents and comparing their As adsorption capacities to those of the base Al-Mg-LDH. Some of the approaches considered for modification of the LDH materials included:

- Varying the ratio of the M^{II}/M^{III} metal constituents.
- Substitution in the M^{III} position with selected other metal constituents.
- Substitution of the interlayer anion

We carried out batch isotherm experiments in which the various synthesized LDH were exposed to the target metal under otherwise similar experimental conditions. The data indicate that the Mg-Al-NO_3-LDH was the most effective in removing the As from aqueous solutions followed by the conditioned LDH. It was also observed that the As removal capacity decreases with the decreasing Mg/Al molar ratio in the LDH structure.

Task 3: In this Task the focus was the safe disposal of spent adsorbents. Experiments were carried out which proved that the As- and Se-saturated LDH can be characterized as non hazardous waste.

Project Report

1. Introduction

1.1. Background

One of the most important natural resources on Earth is water. The total amount of water on Earth is limited, thus making it a finite resource. Most of the world's water supply (approximately 97%) is found in oceans in the form of saltwater. Converting this saltwater into freshwater is generally too expensive to be used for industrial, agricultural or household purposes. Only 3% of the world's water supply is fresh water, and two-thirds of that is frozen, forming the polar ice caps, glaciers, and icebergs. The remaining 1% of the total world water supply is fresh water available as either surface water or ground water, the latter accounting for two-thirds of the total.

In the United States alone, everyday 450 billion gal of water are withdrawn from ground and surface waters for a variety of uses. Less than 20% of that water is consumed by humans, the rest being utilized for industrial and agricultural purposes. The increase in population and the growing economy are likely to result in an increase in the consumption of water. In the past 30 years, for example, the U.S. population has grown by 52%, while the total water use has tripled.

Electric utilities are a major user of water resources in the USA. Most electric power plants require water to operate. Nuclear and fossil fuel power plants consume over 185 billion gal of water per day. In addition, geothermal power plants use 2 billion gal of water a day. Hydropower plants use water directly to generate power. Most of the water that is utilized during power generation is for steam generation and cooling. As demand for electricity increases with the growing economy and the growing population, so is the

need for water for cooling and other purposes. As a result, in the future the electric power generation industry is likely to find itself in direct competition for new sources of water with the other growing sectors of the economy.

Recent advances in power-station design have led in reduction in water usage per megawatt (MW) of electricity generated. However, enhanced competition in the electricity market and increasing attention to sustainability issues and environmental improvements suggest that water will continue to be required for power generation in the foreseeable future. The simplest solution available to meet this increasing demand for water is to reclaim and reuse the power plant spent effluents, which is likely to reduce the pressure for finding additional sources of water for the power plant needs.

The water usage issue aside for a moment, water quality in power generation will continue to dominate the discussion for many years to come. Many of the power plant stations are located near important bodies of fresh (river, lakes, and reservoirs) or ocean water. In some instances, the reservoirs have been created by the diversion of rivers, adjacent to power plants for cooling, rinsing and the release of effluents. A variety of processes associated with fuel handling and ongoing maintenance of large thermal power plant stations create or concentrate chemical pollutants that are then discharged into nearby water bodies. Even when releases are limited to what is allowed in water-use permits, there is still the occasional but inevitable accidental release. Both these sources of pollution can be legal but, nevertheless, can cause significant harm to streams, rivers, lakes, estuaries and groundwater, and can also affect aquatic life. In addition, renewed concerns exist today about the environmental fate of heavy metals, such as mercury (Hg), arsenic (As), and selenium (Se) that are found in many of these effluents, and negatively

impact their disposal. Plant-wide discharges are, as a result, likely to come under increased scrutiny as future water regulations come more into focus.

Most of the power plant effluents fall under the category of high-volume, "too clean to clean" effluents. They require highly efficient treatment techniques, particularly for the removal of trace-level metal contaminants. Very little emphasis has, so far, been placed on such discharges. The focus of the project presented in this report is, therefore, on the development of advanced concepts for reclaiming and reusing such effluents. In particular, the emphasis is on dealing with As and Se impacted boiler blow-down streams, which have, so far, received only scant attention. The reclaim and utilization of boiler blow-down waters represent the key future challenges for utilities. As and Se contaminants in these streams are expected to be at the ppm to ppb level, though little detail about such streams is published in the open literature.

As and Se are found in waters in the form of oxyanions. Inorganic As may be present in the 3+ [As(III), arsenite] and 5+ [As(V), arsenate] oxidation states [*Ferguson et al.*, 1972]. The occurrence and distribution of the two forms of As is largely influenced by the pH and the redox conditions of the environment in which they exist. Arsenate (H_3AsO_4, $H_2AsO_4^-$, $HAsO_4^{2-}$, AsO_4^{3-}) is typically present in the mono and divalent anionic forms in oxygenated waters, while arsenite (H_2AsO_3, $H_2AsO_3^-$, and $HAsO_3^{2-}$) occurs primarily in neutral form in lower redox potential waters. As a general rule, As(III) is more likely to be found in anaerobic groundwater, while As(V) is found in aerobic surface water. Arsenate is more readily removed from water than arsenite, as it occurs as an ionic species in the pH range typically found in the aquatic environment. Protracted contact with As- containing waters is thought to cause arsenicosis, a form of

poisoning for humans [*Lepkowski*, 1998] The International Agency for Research on Cancer (IARC) currently classifies As as a group 1 chemical, which is thought to be carcinogenic to humans. Relatively high concentrations of As have been reported both in power plant discharges, as well as in fresh water supplies. Its presence has also been increasing through the use of As-containing pesticides, mining, and the burning of fossil fuels. According to the United States Environmental Protection Agency, more than 13 million people in the United States routinely obtain water from public sources that contain more than 10 parts per billion (ppb or μg/L) of As. Other nations also have a significant problem with As poisoning. Bangladesh, for example, estimates that between 35 and 77 million of its 150 million citizens are at risk of drinking contaminated water, where local populations are routinely exposed to As poisoning through the ingestion of groundwater and the eventual release into the bloodstream [*DeMarco et al.*, 2003]. Due to instances of As presence in some parts of the United States, the EPA has lowered the current maximum contaminant level (MCL) for drinking water for As to 10 μg/L from the current level of 50 μg/L [*Scharfenaker*, 2000].

Se in waters from power plants exists in the 4+ [Se(IV), or selenite] and 6+ [Se(VI), or selenate] oxidation states [*Neal et al.*, 1987]. Se also is highly toxic to humans and may be fatal if inhaled, ingested or absorbed through the skin. Acute exposure may lead to severe respiratory problems and neurological effects [*ATSDR*, 1989]. In drinking water, for example, the limit is 0.01 ppm in the USA, Europe and Japan [*Parsons et al.*, 2006; *Ohlendorf et al.*, 1986].

A recent Southern California Coastal Water Research Project report on thirteen power-generating stations [*Steinberger et al.*, 2004] for the year 2000 indicates the

presence of As and Se in power plant discharges, usually in small concentrations up to 50 ppb. Such levels may still be too high, however, to permit safe environmental discharge in the future**.**

Many techniques are currently available to remove As and Se from aqueous solutions, among them precipitation-filtration, adsorption, ion exchange, and reverse osmosis. Of these, adsorption is the simplest and the most direct approach. The development of effective adsorbents with applications in water decontamination is of current interest. So far, conventional adsorbents, such as clay minerals [*Manning et al.*, 1997], activated alumina [*Clifford et al.*, 1995; *Trotz*, 2002; *Lin et al.*, 2001], activated carbon impregnated with iron [*O'Day et al.*, 2005], mesoporous alumina [*Kim et al.*, 2004], ferric hydroxide [*Hayes et al.*, 1987; *O'Day et al.*, 2005], ferrihydrite [*Raven et al.*, 1998; *O'Day et al.*, 2005], clay membranes [*O'Day et al.*, 2005] and geological materials [*Bowell*, 1994] have been investigated. Adsorption on activated alumina, carbon, and organic strong-base anion exchangers is promising, but the approach also has a number of serious shortcomings. They include the reduction of sorbent selectivity in the presence of the chlorides and sulfates; dissolution/loss of alumina during regeneration with NaOH, and the low selectivity by the strong acid anion exchangers towards Se(IV) [*Ramana et al.*, 1992]. Though many selective cation exchangers exist for separation of metal cations [*Anthony et al.*, 1993], the same is not true for oxyanions. Therefore, removing such metal constituents remains a major hurdle.

Only in the last few years has significant attention been devoted to the development of sorbents capable of carrying out this task. Previously, goethite was reported to have high affinity towards arsenite and selenite, but its selectivity rapidly decreased in alkaline

pH [*Manceau et al.*, 1994; *Papelis et al.*, 1995]. Some researchers are using granular ferric hydroxides [*Driehaus et al.*, 1998; *Thirunavukkarasu et al.*, 2003; *Badruzzaman et al.*, 2004; *Saha et al.*, 2005; *Sperlich et al.*, 2005; *Impellitteri et al.*, 2006] to efficiently remove As from aqueous solutions, the disadvantage here being, that these materials cannot be regenerated as the As is irreversibly adsorbed on them, making them unsuitable for large-volume applications. Layered double hydroxides (LDH), also called hydrotalcite-like compounds, are also attracting current research interest as they offer a large interlayer surface to host diverse anionic species [*Cavani et al.*, 1991, *Turk et al.*, 2009] with the additional advantage that they can be easily recycled. Recently, for example, researchers at Media and Process Technologies, Inc. (M&P), the industrial collaborator in our research, reported the development and use of LDH for the separation of As for drinking water applications with significantly improved adsorption capacities.

The LDHs have the structural formula $[M^{II}_{1-x}M^{III}_{x}(OH)_2]^{z+}A_{z/n}{}^{n-} \cdot yH_2O$, where M^{II} and M^{III} represent divalent cations (e.g., Mg, Mn, Fe, Co, Cu, Ga, Ni, and Zn) and trivalent metal cations (e.g., Al, Fe, Mn, Co, Ni, La and Cr), respectively; A^{n-} represents interlayer anions, such as NO_3^-, SO_4^{2-}, OH^-, ClO_4^- and CO_3^{2-}, and x typically ranges from 0.17 to 0.33 [*Kwon et al.*, 1988] . The divalent and trivalent metal cations belong, mainly, to the third and fourth periods of the periodic classification of the elements. The ionic radii are in the range of 0.65 – 0.80 Å for divalent cations, and 0.62 – 0.69 Å for trivalent ones (with the main exception being Al for which the radius is 0.50 Å) [*Rives*, 2001].

The LDH structure is based on $M(OH)_6$ octahedral units sharing edges, in order to build $M(OH)_2$ brucite-like layers. These octahedral units contain both divalent and trivalent metal cations. The main layers are, therefore, positively charged, with the charge

density being proportional to the trivalent to the total metal ratio $x = M^{III}/(M^{II}+M^{III})$. The entire structure is constituted by stacking of such layers, held together by hydrogen bonding, intercalating charge-balancing anionic species, and water molecules, as shown in Figure. 1.1.

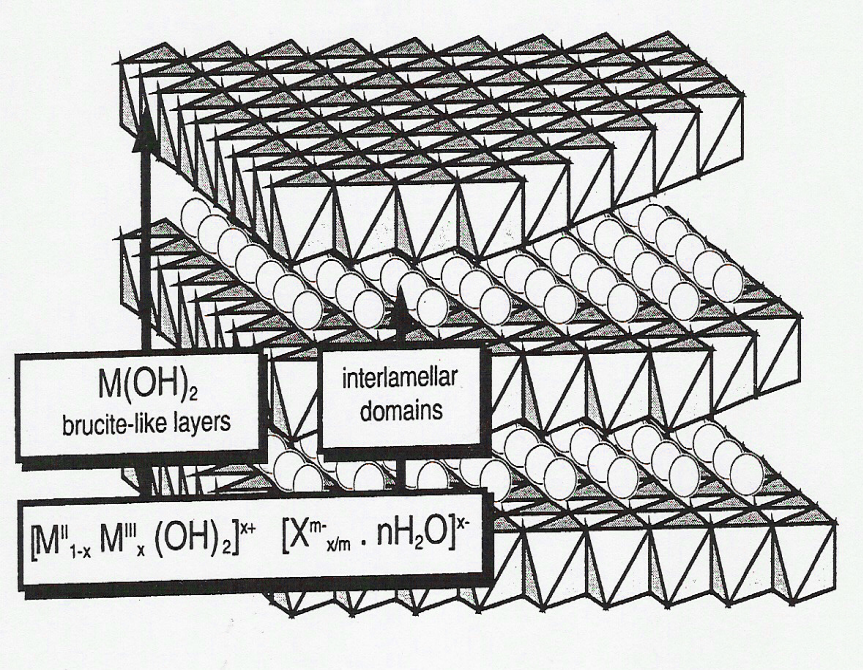

Figure 1.1. Schematic view of the LDH structure and its general formula.

The main features of the hydrotalcite structure are, therefore, determined by the nature of the brucite-like sheet, the position of the anions and water molecules in the interlayer region, and the type of stacking of the brucite-like sheets. The sheets that contain cations are built as in brucite, where they randomly occupy the octahedral holes in the close-packed configuration of the OH^- ions. The anions and the water molecules are randomly located in the interlayer region, and are free to move by breaking their bonds and forming new ones (as in liquid water). The oxygen atoms of the water molecules and of the $(CO_3)^{2-}$ groups are distributed approximately closely around the

symmetry axes that pass through the hydroxyl groups (0.56 Å apart) of the adjacent brucite-like sheet. The LDHs exhibit a high charge density in the main layers. For example, a x = 1/3 trivalent metal ratio corresponds to one charge for 50 $Å^2$ on each side of the layer, leading to one charge for 25 $Å^2$ in the interlamellar domains.

Because of the presence of large interlayer spaces and the significant number of exchangeable anions, the LDH have the potential to be good ion-exchangers and adsorbents. They (and their calcined products, heated at around 500 ^oC for 4 h) have, indeed, been reported as good adsorbents for the removal of surfactants [*Pavan et al.*, 2000], trinitrophenol [*Barriga et al.*, 2002; *Hermosin et al.*, 1996], various pesticides [*Villa et al.*, 1999], and chromate [*Lazaridis et al.*, 2004; *Rhee et al.*, 1997] from aqueous solutions. The LDH are known to uptake anions from a solution by three different mechanisms: (1) adsorption; (2) intercalation by anion exchange, and (3) intercalation by reconstruction of the structure of the calcined LDH. The latter phenomenon is known as the "memory effect," and takes place when an LDH, usually containing carbonates in its interlayer, is calcined at temperatures that are high enough to eliminate most of the interlayer anions, and then it is put in a solution containing the same or different anions. There, it rehydrates and reconstructs its original layered structure with the incorporation of anions from the solution. The ability of the LDH to "recover" their structure provides, at least in principle, the potential for reuse and recycle of the adsorbent, which is important for the large-volume applications envisioned in this report.

The LDH exist as minerals with many names, depending on the composition and the symmetry of polytypes, for example,

Hydrotalcite, Manasseite	Mg, Al
Pyroaurite, Coalignite	Mg, Fe
Stichtite, Babertonite	Mg, Cr
Takovite	Ni, Al or Ni, Ni
Reevesite	Ni, Fe
Woodwardite	Cu, Al

where the interlamellar anion is mainly carbonate, and sometimes sulphate or chloride.

Prior to the studies by our group [*Yang et al.*, 2005; *Yang et al.*, 2006; *Dadwhal et al.*, 2009], a few other groups had studied the removal of As and Se from a variety of water streams. A number of anionic clays were proposed, but for waters containing both As and Se, hydrotalcites (HTs) appear to be the adsorbent of choice [*You et al.*, 2000; *You et al.*, 2001; *Das et al.*, 2004; *Manju et al.*, 2000]. One comment concerning most of the open literature reports is that the streams studied contain significantly higher concentration of As and Se than one would typically find in power-plant streams (ppm/ppb and less trace amounts). Such streams have, so far, received only scant attention.

1.2. Scope of the Present Work

The focus of the present work is on a systematic study of adsorption of As and Se by the LDH from dilute aqueous solutions, representing "too clean to clean" model power plant effluent streams, the contaminant levels of which are expected to be in the trace ppb levels. Prior to the effort by our group, such a study was lacking in this area.

Before to the initiation of Phase II of this investigation, our group had studied the adsorption kinetics and the adsorption/desorption isotherms for As and Se on both calcined and uncalcined LDHs using batch techniques [*Yang et al.*, 2005]. Because of the

higher surface areas of the calcined materials, they were shown to exhibit greater adsorption capacity and efficiency than the uncalcined LDH. In addition, when the calcined LDH are placed in contact with anion-containing waters, they rapidly rehydrate, and adsorb the anions in the process reconstructing their original structure. In the study, the adsorption isotherms, kinetics, as well as the effects of the As oxidation state, pH, temperature and the presence of competing anions on the adsorption were investigated [*Yang et al.*, 2005].

During the adsorption runs with both the uncalcined and calcined LDH the solution pH changed significantly, which adds uncertainty in the interpretation of the data. For the calcined materials, in particular, during the batch tests significant dissolution of Al and Mg from the LDH structure was observed. Though such metals are not currently regulated, they are bound to be a source of concern for the eventual use of these materials in drinking water applications. Therefore, in this study the focus is on the calcined LDH materials, which have undergone a conditioning process (explained later in the report, in the experimental section) prior to their use in the experimental runs. Such conditioning seems to have two beneficial effects. First, it reduces significantly the Al and Mg dissolution, and, second, it tempers the solution pH change, phenomena that were both observed during our prior study [*Yang et al.*, 2005]. Using these materials we have carried out a series of experiments with the following key objectives: (i) to investigate the effect of adsorbent particle size, a key consideration for the field-testing of the materials in flow-columns, where the pressure drop and particle carry-over are concerns [*Yang et al.*, 2006]. (ii) To develop a more detailed model of the adsorption process, which better relates the batch experiments with flow-column runs and, using this model, to identify

and quantify the impact of important solution and operating parameters, such as the influent As concentration, pH, sorbent particle size, and flow rate during As removal in fixed beds [*Dadwhal et al.*, 2009]. As part of our investigation, we have also collected real power plant effluent data in the Greater Los Angeles area, in order to identify other important anionic species present in such effluents. We subsequently investigated the impact that the presence of such competing anions has on As and Se adsorption on the LDH. Finally, we have studied the regeneration and safe disposal of the spent adsorbents.

This report is organized a number of sections a brief synopsis of which follows:

- **Adsorption of Arsenic on Layered Double Hydroxides: Effect of Particle Size** [already published in *Yang et al.*, 2006]. Two models are utilized to describe the batch experimental data. The first is the classical homogeneous "surface diffusion" model (HSDM) [*Tien*, 1994] that has been previously utilized to describe adsorption of metals and other pollutants in nanoporous adsorbents such as, for example, the sorption of metal cations by hydrous amorphous aluminum, iron, and manganese oxides [*Axe et al.*, 2002], the adsorption of arsenate into granular ferric hydroxide (GFH) [*Badruzzaman et al.*, 2004] and in natural manganese oxide, and the adsorption of basic dyes in natural clays [*El-Geundi,* 1991]. The adsorption experimental data, generated with the LDH adsorbents of varying particle size are investigated using, first, this model, and the effect of particle size on the adsorption characteristics and the intraparticle diffusivity are reported. In addition, we utilize a bidisperse pore model (BPM), which assumes that the individual adsorbent particles are agglomerates of individual single crystal microparticles. Two transport processes are included in this model, the first taking place in the porous region in between the microcrystallites, and the second describing transport within the

crystallites themselves. The BPM is consistent with the TEM experimental observations of the particles themselves, and the presence of a mesoporous region, as indicated by the BET measurements.

- **Adsorption of Arsenic on Conditioned Layered Double Hydroxides: Column Experiments and Modeling** [already published in *Dadwhal et al.*, 2009]. The principal objective of these experiments is to identify and quantify mass transport processes that limit the rate of As(V) adsorption in packed beds containing conditioned LDH. The impact of important solution and operation parameters, such as influent As concentration, pH, sorbent particle size and flow rate, are investigated for As(V) removal in fixed beds. The two adsorption models used to describe the batch experiments, namely, the HSDM and the BPM, are incorporated into the flow column models, in order to account for the effect of both external mass transfer and intraparticle diffusion resistance, and are applied to analyze the fixed-bed data.

- **Adsorption of Arsenic on Conditioned Layered Double Hydroxides in the Presence of Various Competing Ions**. Analysis of power plant effluents from various plants in the Greater Los Angeles area shows that, in addition to As and Se, such streams also contain a variety of other ions, such as fluorides, nitrates, chlorides, carbonates, sulphates and phosphates. We try to understand here the effect of such ions on the As removal capacity of the LDH in both batch and column experiments.

- **Regeneration of the LDH.** We study the recycling and reuse of spent LDH adsorbents. The LDH have the unique property, known as the "memory effect," that allows them to reconstruct into their original structure when they are exposed to a regenerating ionic solution, thus making them an ideal and economical adsorbent.

- **Cost Analysis for Treating Power Plant Effluents**. Here we carry out the cost calculations for packed-bed columns used for treating the effluents in a typical power plant.
- **Second generation adsorbents.** We synthesize a class of second generation adsorbent, and study their adsorption capacities.
- **Safe Disposal of spent adsorbent**. We study the safe disposal of the spent adsorbents, as it is also an important criterion in selecting an adsorbent for any given application. TCLP tests are carried out, and it is shown that As- and Se-saturated LDH can be classified as a non-hazardous waste.

2. Adsorption of Arsenic on Layered Double Hydroxides: Effect of the Particle Size

2.1. Introduction

In our Phase I study, our group investigated the use of LDH in the removal of trace levels of As and Se from aqueous solutions [*Yang et al.*, 2005]. They were shown to be efficient adsorbents for As and Se from waters containing dilute concentrations (ppb-level) of these metals. Both uncalcined (as prepared) and calcined (materials that have been heated at 500 ^{o}C for four hours) LDH adsorbents were investigated. However, with these materials there were two issues: first, during the adsorption run the solution pH changed significantly, and second there was significant dissolution of Al and Mg from the LDH structure during the batch experiments. Therefore in this report, our focus is on calcined LDH materials, which have undergone a conditioning process (details provided in the experimental section below) prior to their use in the experimental runs. Such conditioning seems to have resolved both of the above issues, i.e., by reducing significantly the Al and Mg dissolution, and also by tempering the solution pH change. Additionally, in the previous study [*Yang et al.*, 2005] the adsorption data were modeled using a simple empirical exponential rate model, which does not provide significant physical insight into the adsorption of these metals onto the LDH. Here we have carried out a series of studies with these materials, the goal of which was (i) to investigate the effect of the adsorbent particle size, a key consideration for the field-testing of these materials in flow-columns, where pressure drops and particle carry-over are concerns; and (ii) to develop a more detailed model of the adsorption process, which better relates batch experiments with flow-column runs.

Two models are utilized to describe the batch experimental data. The first is the classical homogeneous surface diffusion model (HSDM) [*Tien*, 1994] that assumes that the adsorbent is made of spherical homogeneous particles. The second model is a bidisperse model (BPM), which assumes that the individual adsorbent particles are agglomerates of individual single crystal microparticles. Two transport processes are described by this model, the first taking place in the porous region in between the microcrystallites, and the second describing transport within the crystallites themselves. This latter model is consistent with TEM experimental observations of the particles themselves, and the presence of a mesoporous region as indicated by BET measurements. The adsorption experimental data, generated with adsorbents of various particle sizes are investigated using both these models, and the effect of particle size on the adsorption characteristics and the intraparticle diffusivities are analyzed and reported here.

2.2. Model Development

2.2.1. Homogeneous Surface Diffusion Model

The homogeneous surface diffusion model [*Tien,* 1994] is first used here to describe the experimental adsorption data. The HSDM is based on the assumption that the transport of species is determined by external mass transfer in the liquid phase, and by intraparticle diffusion resistance in the form of surface diffusion within the adsorbent particle. According to this model, the following mass balance equation describes adsorption in a spherical homogeneous sorbent particle,

$$\frac{\partial q}{\partial t} = \frac{1}{r_M{}^2} \frac{\partial}{\partial r} (r_M{}^2 D_i \frac{\partial q}{\partial r}) \qquad (2.1)$$

where q (μg adsorbate/g sorbent) is the adsorbate concentration, r_M (cm) is the radial distance, t (s) is time, and D_i (cm^2/s) is the intraparticle diffusion coefficient. In general, the diffusivity D_i of adsorbed molecules is concentration-dependent [*Crepaldi et al.*, 2002]. We have fitted this coefficient first by assuming that it is concentration-independent, and then also by assuming that it is concentration-dependent and described by the classical Darken correlation given by

$$D_i = D_{i0} \frac{\partial \ln C}{\partial \ln q} \tag{2.2}$$

where D_{i0} is the diffusivity at zero loading. For a Sips-type isotherm (see discussion below) Equation (2.2) is reduced to

$$D_i = \frac{D_{i0}}{n} \left(\frac{1}{1 - \frac{q}{q_s}} \right) \tag{2.3}$$

where q_s is the saturation loading, and n is the exponential factor in the Sips-type isotherm. A concentration-dependent surface diffusivity and the Sips isotherm have been previously utilized to describe adsorption of cadmium and copper metals onto bone char [*Ko et al.*, 2003].

At the external particle surface ($r_M = R_M$), instantaneous equilibrium is assumed between the metal species concentrations in the liquid and solid phases, which are coupled using the Sips isotherm equation, as obtained from the adsorption experiments (see further discussion below).

$$q = \frac{K q_s C_{MS}^{\ n}}{1 + K C_{MS}^{\ n}}, \qquad r_M = R_M \tag{2.4}$$

where C_{MS} is the liquid phase concentration (μg/l) at the solid-liquid interface. Equations (2.5) and (2.6) below are the initial condition (IC), and the boundary condition (BC) at the particle center:

$$q = 0, \qquad 0 \le r_M \le R_M, \; t = 0 \tag{2.5}$$

$$\frac{\partial q}{\partial r_M} = 0, \qquad r_M = 0 \tag{2.6}$$

In flow-column experiments, external mass transfer limitations are often of concern, and the following equation is utilized to describe mass transport from the bulk liquid phase bulk to the particle-liquid interface.

$$\rho D_i \left. \frac{\partial q}{\partial r_M} \right|_{r_M = R_M} = k_f (C - C_{MS}), \quad r_M = R_M \tag{2.7}$$

where ρ (g/cm^3) is the particle density, k_f (cm/s) is the external mass transfer coefficient, and C (μg/l) is the bulk liquid-phase concentration.

In the batch experiments described here, the vials containing the adsorbent and solutions were vigorously agitated in order to eliminate external mass transport limitations; we have determined the conditions for which external mass transfer limitations are no longer important, by varying the rate of agitation and measuring the corresponding rates of adsorption. An agitation speed of 170 rpm was deemed sufficient to eliminate external mass transport limitations, and afterwards all batch experiments were carried out under such conditions, so that $C = C_{MS}$.

For loading-independent diffusivity, Equations (2.1) and Equations (2.4) – (2.6) above must be coupled with the overall mass balance equation for the batch adsorption vials given by

$$V(C_0 - C) = M\bar{\bar{q}} \tag{2.8}$$

where C_0 (μg/l) is the initial liquid phase concentration, V (ml) is the initial volume of solution, M (mg) is the initial adsorbent mass, and $\bar{\bar{q}}$ (μg/g) is the volume-averaged adsorbate concentration in the adsorbent particle defined as:

$$\bar{\bar{q}} = \frac{3}{R_M{}^3}\int_0^{R_M} q\ r_M{}^2 dr_M \tag{2.9}$$

For loading-dependent diffusivity, Equations (2.1) – (2.6) together with Equations (2.8) and (2.9) are solved instead.

To consider adsorption by an adsorbent sample consisting of particles with a size distribution (PSD), Equation (2.1) and Equations (2.4) – (2.6) are modified as follows:

$$\frac{\partial q_i}{\partial t} = \frac{1}{r_{Mi}{}^2}\frac{\partial}{\partial r_{Mi}}(r_{Mi}{}^2 D_i \frac{\partial q_i}{\partial r_{Mi}}) \tag{2.10}$$

where i denotes the ith fraction of the particle size distribution corresponding to particles of average radius R_{Mi}.

BC and IC are:

$$q_i = 0, \qquad t = 0 \tag{2.11}$$

$$\frac{\partial q_i}{\partial r_i} = 0, \qquad r_{Mi} = 0 \tag{2.12}$$

$$q_i = \frac{Kq_s C_{MS}{}^{1/n}}{1 + KC_{MS}{}^{1/n}}, \qquad r_{Mi} = R_{Mi} \tag{2.13}$$

$$\bar{\bar{q}}_i = \frac{3}{R_{Mi}{}^3}\int_0^{R_{Mi}} q_i r_{Mi}{}^2 dr_{Mi} \tag{2.14}$$

$$\bar{\bar{q}} = \frac{1}{M}\sum_i M_i \bar{\bar{q}}_i = \sum_i \phi_i \bar{\bar{q}}_i \tag{2.15}$$

ϕ_i being the mass fraction of particles with average radius equal to R_{Mi}. Equations (2.10)-(2.15) together with Equation (2.8) are solved to obtain the diffusivity D_i.

2.2.2. Bidisperse Pore Model

The bidisperse pore model assumes that the adsorbent particle is an agglomerate of a number of equal size, single crystal microparticles. The schematic diagram of the adsorbent particle in the bidisperse framework is shown in Figure 2.1. A porous intercrystalline region forms in between the microparticles.

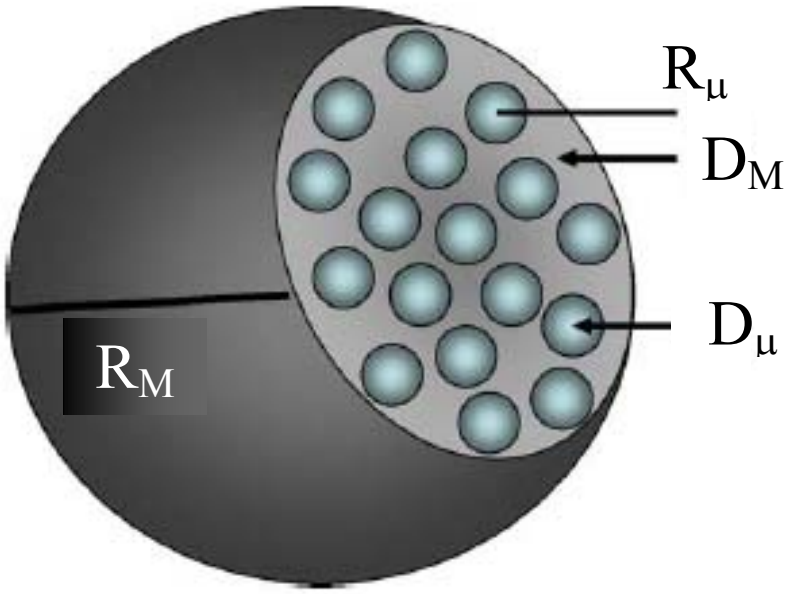

Figure 2.1. Schematic diagram of an adsorbent particle in the BPM framework.

Before the metal anion adsorbs inside the microparticle structure, it must be transported from the particle surface, through the intercrystalline region to the surface of the microparticles. The diffusivity of the intercrystalline porous region is taken to be the bulk diffusivity of As ion, whereas the diffusivity of the microparticles is calculated by fitting the experimental kinetic data (however, later on in the report we have fitted the

adsorption kinetic data again with the BPM, where we fit both diffusivity values). The following assumptions are made in this analysis:

(1) Constant diffusion coefficients.

(2) Spherical particle composed of spherical equal-sized microparticles.

(3) Adsorption following the Sips isotherm.

(4) Isothermal conditions.

In the intercrystalline porous region transport is described by the following equations [*Runkenstein et al.*, 1971; *Lee at al.*, 1976; *Lee*, 1978].

$$\frac{\partial C_M}{\partial t} + \frac{(1-\varepsilon_M)}{(\varepsilon_M)} \rho_s \frac{\partial \bar{q}_\mu}{\partial t} = \frac{D_M}{r_M{}^2} \frac{\partial}{\partial r_M} \left[r_M{}^2 \frac{\partial C_M}{\partial r_M} \right] \tag{2.16}$$

BC and IC are:

$$C_M = 0, \qquad t = 0 \tag{2.17}$$

$$\frac{\partial C_M}{\partial r_M} = 0, \qquad r_M = 0 \tag{2.18}$$

$$C_M = C(t), \qquad r_M = R_M \tag{2.19}$$

where C_M is the solute concentration in the intercrystalline porous region (μg/l), $\bar{q}_\mu$ is the volume-averaged solute concentration in the solid phase (microparticles) (μg/g) – see Equation (2.26) below, D_M (cm^2/s) is the mesopore diffusivity, R_M is the particle external radius, and ε_M is the void fraction in the porous region.

Transport and adsorption in the microparticles are described by

$$\frac{\partial q_\mu}{\partial t} = \frac{D_\mu}{r_\mu{}^2} \frac{\partial}{\partial r_\mu} \left(r_\mu{}^2 \frac{\partial q_\mu}{\partial r_\mu} \right) \tag{2.20}$$

BC and IC are:

$$q_\mu = 0, \qquad t = 0 \tag{2.21}$$

$$\frac{\partial q_\mu}{\partial r_\mu} = 0, \qquad r_\mu = 0 \tag{2.22}$$

$$q_\mu = \frac{K q_s C_M{}^n(r_M, t)}{1 + K C_M{}^n(r_M, t)}, \qquad r_\mu = R_\mu \tag{2.23}$$

where q_μ is the solute concentration (μg/g) in the microparticle, D_μ (cm^2/s) is the microparticle diffusivity, and R_μ is the microparticle radius. The bulk concentration, C, can be found by applying the following equation, which is Equation (2.8) modified to account for the presence of a bidisperse structure:

$$V(C_0 - C) = M\bar{\bar{q}} \tag{2.24}$$

where,

$$\bar{\bar{q}} = \frac{3}{\rho R_M{}^3} \int_0^{R_M} \left[(1 - \varepsilon_M)\rho_s \bar{q}_\mu + \varepsilon_M C_M \right] r_M{}^2 dr_M \tag{2.25}$$

Equations (2.16) –(2.25) above must be solved with $\bar{q}_\mu$ being given by

$$\bar{q}_\mu = \frac{3}{R_\mu{}^3} \int_0^{R_\mu} q_\mu r_\mu{}^2 dr_\mu \tag{2.26}$$

Equations (2.16)-(2.26) are made dimensionless, and are solved and fitted to the experimental data to calculate the value of $\frac{D_\mu}{R_\mu{}^2}$; D_M is taken to be the bulk diffusivity of $H_2AsO_4^-$ in water [*Lide*, 1996-1997] (this assumption may not be entirely correct, as diffusion in the porous region may be hindered, and effective diffusivity may be lower than that in the bulk [*Lin et al.*, 2001]; however, relaxing this assumption will not change the qualitative conclusions using the bidisperse model. We have, however, relaxed this

assumption later on in the report, where we fit the adsorption kinetic data again, by fitting both diffusivity values).

2.3. Experimental

2.3.1. Preparation of LDH

The Mg-Al-CO_3-LDH utilized in these experiments (with a Mg/Al molar ratio of 2.87) was prepared by the co-precipitation method [*Roelofs et.al.*,2002]. 140 ml of a solution containing 0.7 mol NaOH and 0.18 mol Na_2CO_3 were added all at once to a second solution containing 0.115 mol of $Mg(NO_3)_2 \cdot 6H_2O$ (90ml) and 0.04 mol of $Al(NO_3)_3 \cdot 9H_2O$ (90 ml) (corresponding to a Mg/Al ratio equal to 2.87) under vigorous stirring. The thick gel obtained was aged for 24 h at 333 K, followed by filtration and washing with distilled water, and was then dried at 333 K. ICP-MS analysis of the resulting LDH material indicated that its Mg/Al mole ratio is ~2.9, very close to the Mg/Al ratio of the starting salts.

The calcined Mg-Al-LDH was obtained by heating the original LDH in a muffle furnace at 773 K for 4 h in an air atmosphere with heating and cooling rates of 2 $K \cdot min^{-1}$. The calcined LDH was conditioned by shaking it in deionized water for 24 h (changing the deionized water every 6 h), and then drying in air atmosphere at 353 K for 12 h. The conditioned LDH was crushed and sieved using standard testing sieves (VWR) into four different fractions with mesh sizes of 200-270 mesh (75-53μm), 170-200 mesh (90-75μm), 80-170 mesh (180-90μm), and 50-80 mesh (300-180 μm). For the particles in the various sizes we have measured the density using an Electronic Densimeter SD-200L, and the porosity (BJH -- Barret-Joyner-Halenda-- pore volume) and surface area with N_2 adsorption at 77K using a Micrometrics ASAP 2010 instrument. The samples were

prepared for the surface area BET analysis by heating them at 150 °C in vacuum overnight.

2.3.2. Sorption Experiments

The arsenate solutions used for the adsorption experiments were prepared by dilution from 1000 ppm ICP standard solutions (As(V) in 2% HNO_3 purchased from Exaxol) using deionized water. No effort was made to minimize contact with the atmospheric air during the preparation of the various solutions. All experiments were carried out in 1000 ml polyethylene bottles at 298 K and at 170 rpm. The details of the isotherm and kinetic experiments are described below.

2.3.2.1. Adsorption Isotherms

The adsorption isotherm experiments were carried out in 1000 ml polyethylene bottles at a temperature of 298 K using conditioned LDH. 20 mg of the adsorbent were added to 500 ml of an aqueous solution of As(V) of varying concentrations, ranging from 60 ppb to 300 ppb. The initial pH of these solutions was adjusted to ~7.0 using a 0.1M NaOH solution. The bottles containing the LDH suspension and the As(V) solutions were placed in a reciprocal shaking water-bath (Precision Model 25) and were shaken at 170 rpm (rotations per min) for at least 5 days in order for the adsorption on the conditioned LDH to reach equilibrium. 5 ml samples from each bottle were taken and centrifuged, and the As concentrations in the supernatant solutions were determined by ICP-MS (Perkin-Elmer ELAN-9000). The instrument detection limit was found to be 0.043 μg/l for As using the EPA 200.8 method.

2.3.2.2. Kinetics of Adsorption

As(V) solutions with initial concentration of 205 ppb were prepared. The initial pH was adjusted to around 7 using a 0.1 M NaOH solution. The pH was not adjusted during the adsorption period. pH changes were measured and recorded using an Accumet Basic AB 15 pH meter. 20 mg of adsorbent mass was added to the 500 ml aqueous solutions in 1000 ml flasks, which were then shaken at 170 rpm. At selected time intervals, 5 ml samples were extracted, centrifuged, and the As concentrations as well as the dissolved Mg and Al in solution were determined by ICP-MS. The adsorption runs were repeated for the various particle size ranges.

2.3.3. Characterization

Scanning electron microscopy (SEM) using a Cambridge 360 SEM instrument (Cambridge Instruments, UK) was used to measure the adsorbent particle sizes. The SEM images were analyzed using the software Image J, in order to obtain the average particle size, and particle size distribution (PSD).

2.4. Results and Discussion

2.4.1. Particle Size Distribution

For each particle size range, several SEM pictures are taken and are analyzed using the software Image J, to determine the average particle size and the particle size distribution (PSD) of the adsorbent. Figure 2.2 shows the SEM pictures of the conditioned LDH for the four different particle size ranges. Representative particle size distribution profiles of the conditioned LDH are shown in Figure 2.3. There are a number of ways to define the average particle-size, characterizing every range, namely the arithmetic mean, volume mean, volume-surface mean, volume-moment mean, etc. The

two most popular definitions [*Kaczmarski et al.*, 2003], the arithmetic mean and the volume mean are utilized to calculate the average particle size.

1. The arithmetic mean:

$$d_{10} = \frac{\sum_i n_i d_i}{N} \tag{2.27}$$

where $N = \sum_i n_i$, i is an index of the population, and d_i is the particle diameter of population i.

2. The volume mean:

$$d_{30} = \left(\frac{\sum_i n_i {d_i}^3}{N} \right)^{1/3} \tag{2.28}$$

Fairly similar average particle sizes are obtained (generally d_{30} is somewhat larger than d_{10}) based on these two definitions, and the results are shown in Table 2.1. Table 2.2 includes the measured densities, porosities and surface areas for the four different samples (these porosities reflect the pore volume, as measured by BET, occupied by pores with diameters in the range 1.7 nm-300 nm). The densities are very similar, however, the porosities vary somewhat with particle size (~20%). Similar variations in porosity with particle size were previously also reported by other investigators [*Badruzzaman et al.*, 2004; *Kaczmarski et al.*, 2003].

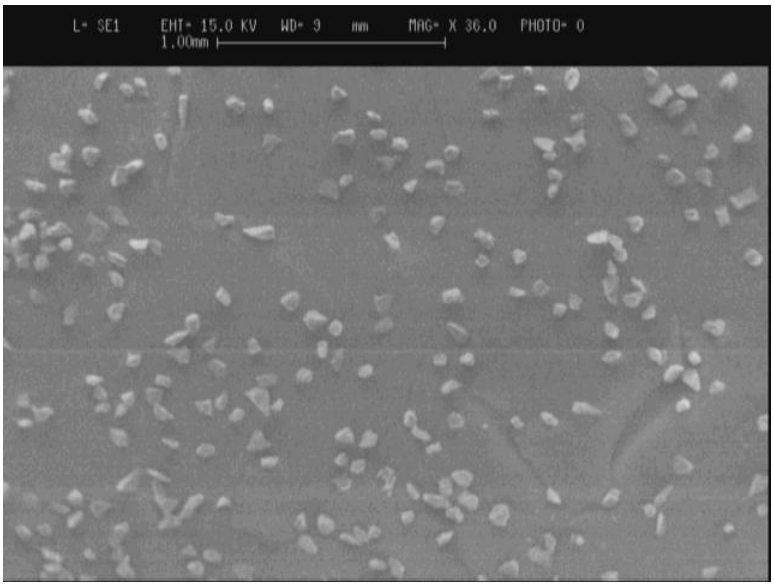
L= SE1 EHT= 15.0 KV WD= 9 mm MAG= X 36.0 PHOTO= 0
1.00mm

(a)

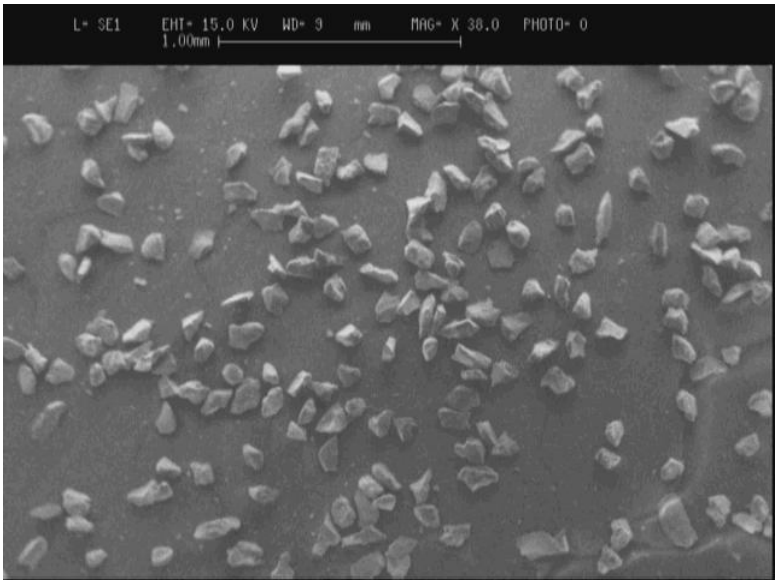
L= SE1 EHT= 15.0 KV WD= 9 mm MAG= X 38.0 PHOTO= 0
1.00mm

(b)

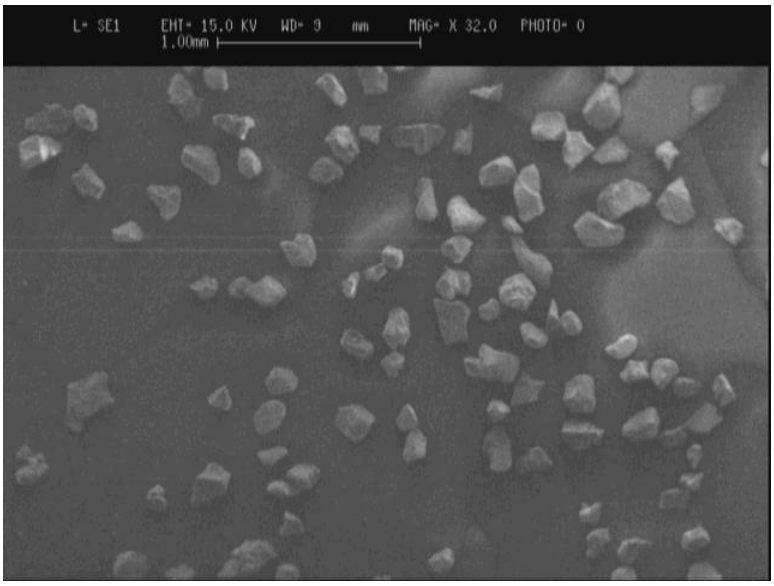

(c)

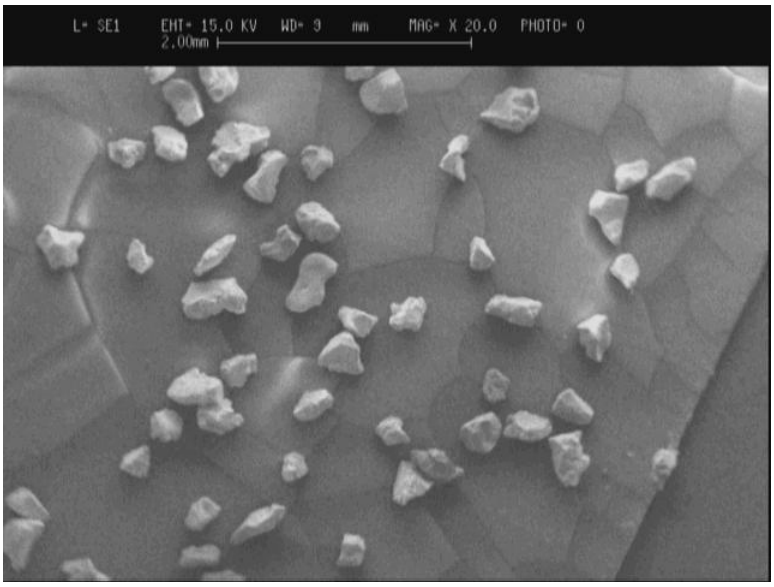

(d)

Figure 2.2. SEM pictures of LDH with mesh size of (a) 200-270 mesh (75-53μm), (b) 170-200 mesh (90-75μm), (c) 80-170 mesh (180-90μm), and (d) 50-80 mesh (300-180μm).

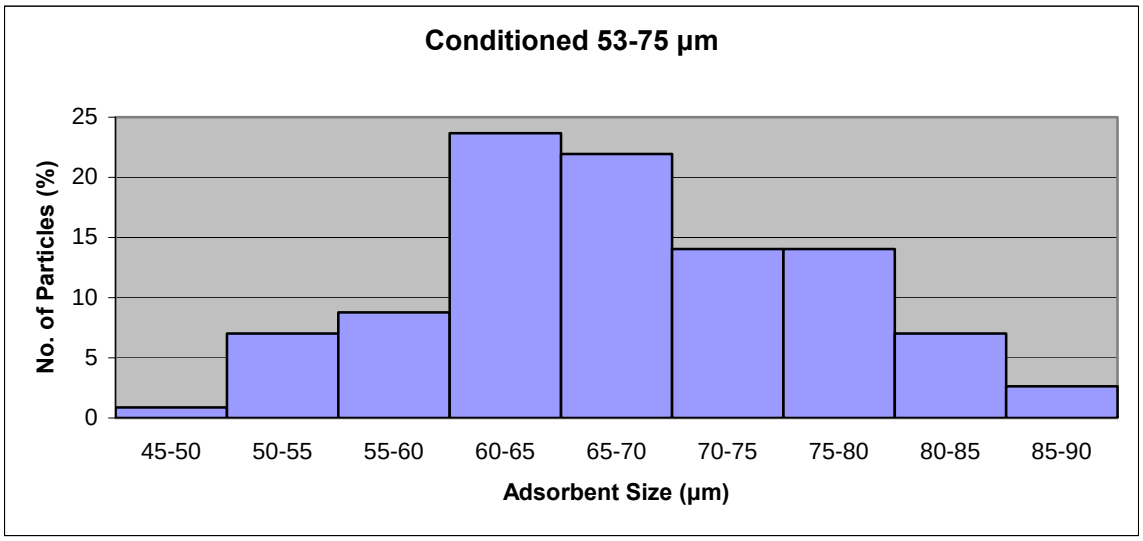
Conditioned 53-75 µm
No. of Particles (%)
25
20
15
10
5
0
45-50
50-55
55-60
60-65
65-70
70-75
75-80
80-85
85-90
Adsorbent Size (µm)

(a)

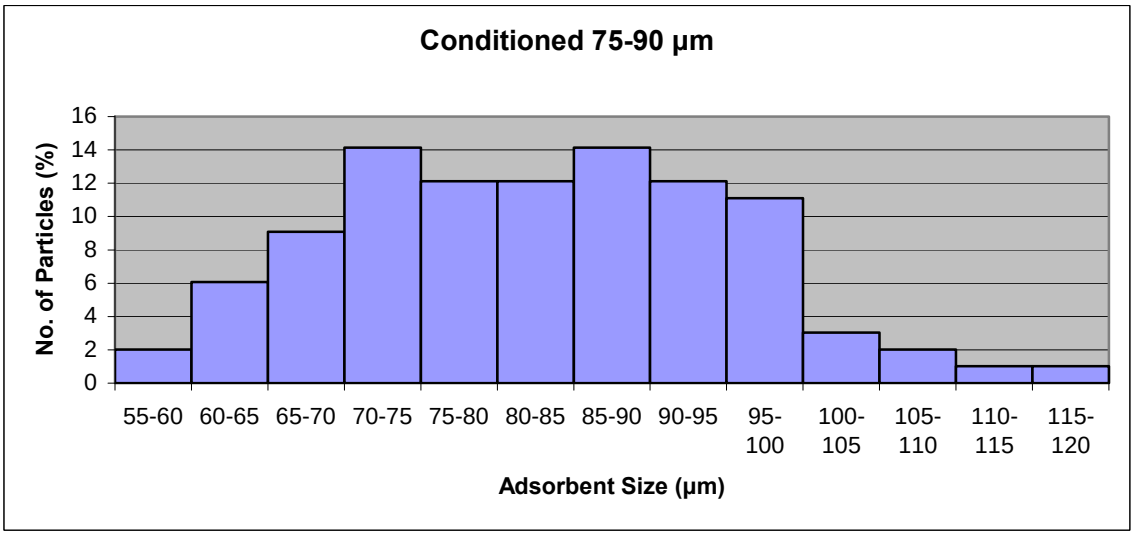
Conditioned 75-90 µm
No. of Particles (%)
16
14
12
10
8
6
4
2
0
55-60
60-65
65-70
70-75
75-80
80-85
85-90
90-95
95-100
100-105
105-110
110-115
115-120
Adsorbent Size (µm)

(b)

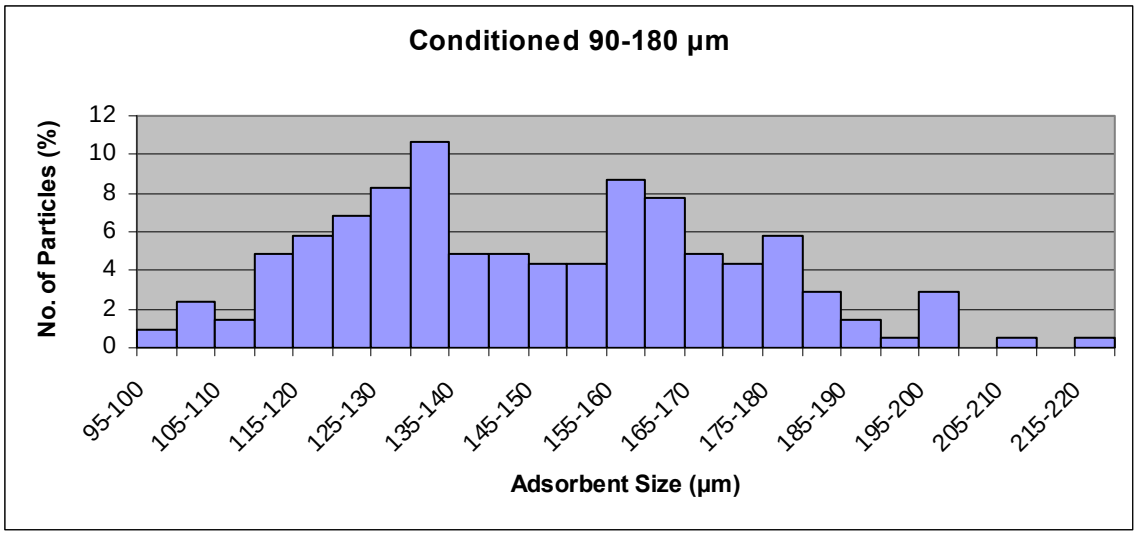

(c)

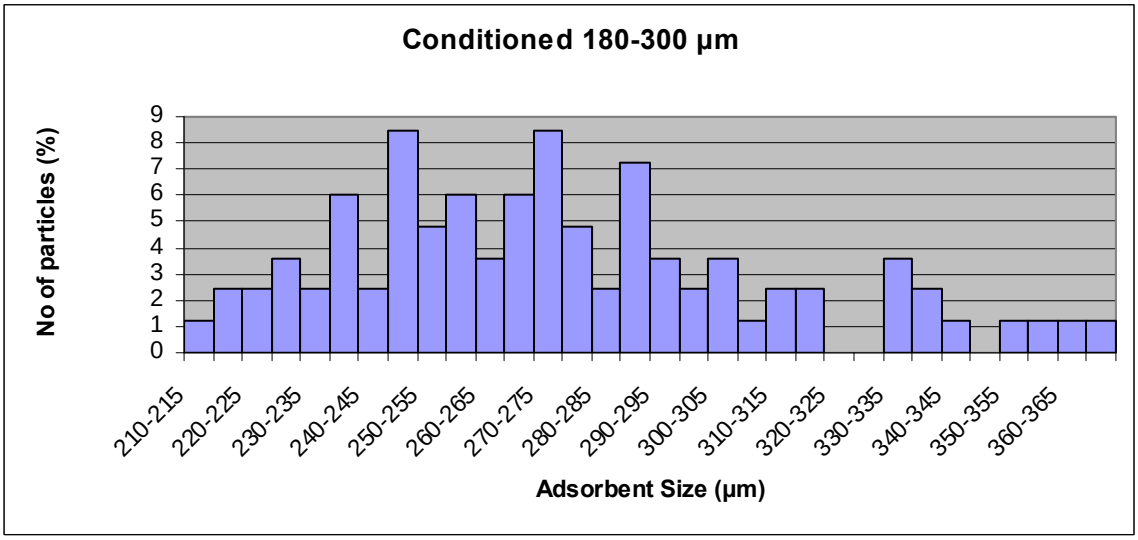

(d)

Figure 2.3. Particle size distribution profiles for LDH.

Table 2.1. Average particle size calculated using the arithmetic mean and volume mean definitions for conditioned LDH with various particle sizes

Mesh size	d_{10} (μm)	d_{30} (μm)
200-270	68.1	69.2
170-200	82.7	84.6
80-170	146.3	150.5
50-80	274.5	279.4

Table 2.2. Measured densities and porosities for conditioned LDH with various particle sizes

Mesh Size	Density ρ_s (g/cm^3)	Porosity ε_M	Surface Area (m^2/g)
200-270	1.964	0.58	32.64
170-200	1.983	0.53	29.82
80-170	1.975	0.46	26.05
50-80	1.986	0.48	27.06

2.4.2. Adsorption Kinetics and Isotherms of As on LDH

A typical example of the time dependence of As (V) concentration in solution during adsorption on the conditioned LDH (particle size of 75-90μm) with an initial As concentration of 205 μg/l and a starting solution pH of 6.7 is shown in Figure 2.4. During the adsorption experiment, as also shown on the same figure, the pH in the solution changes gradually from an initial value of 6.7 to a final value of 7.1. pH increases were also reported by Kang *et al.* when they investigated the adsorption of I^- on Mg/Al LDH [*Kang et al.*, 1999], and by Seida *et al*. for the adsorption of dilute lead on pyroaurite-like compounds [*Seida et al.*, 2001]. This pH change for the conditioned LDH is significantly smaller than what is observed with an uncalcined and calcined LDH in our previous paper [*Yang et al.*, 2005] (for the starting solution pH of 7.0, the final pH increased to as

high as pH 9.0) after it had also be en repeatedly washed and used to adsorb As from its solution.

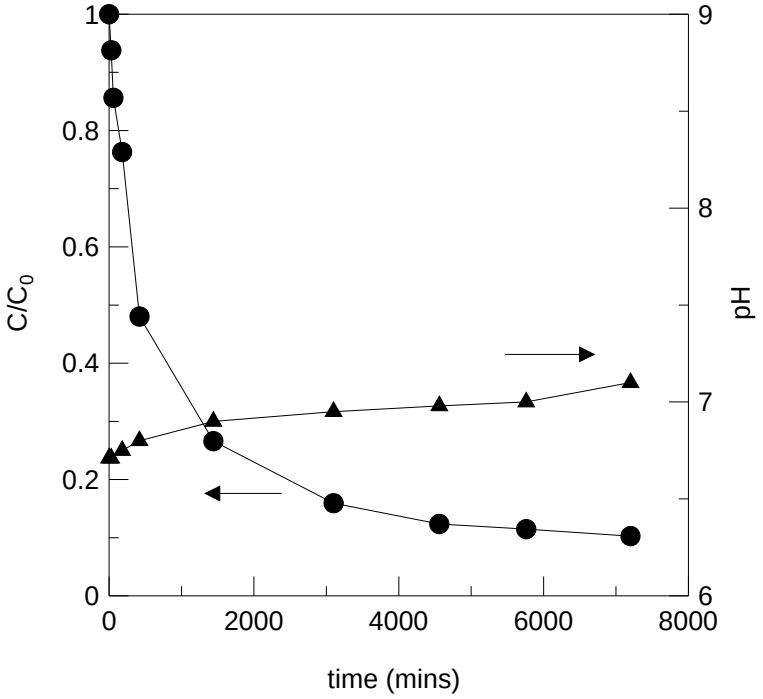

Figure 2.4. As concentration and solution pH profiles as a function of adsorption time on LDH; particle size of 75-90μm, C_0 of 205 μg/l, LDH dose of 0.04g/l.

Figure 2.5 shows that during the adsorption process there is some dissolution of the conditioned LDH, as it is manifested by the presence of Al and Mg in solution. As shown in the figure, the concentration of Al, as detected by ICP-MS analysis, first increases with time and finally levels off at 40 ppb; the Mg concentration, on the other hand, gradually increases throughout the whole experiment. (Independent experiments using Al and Mg soluble salts have shown that the Al and Mg present have no influence on the As adsorption, and they do not interfere with the ICP/MS analysis for As). Recently, aluminum is attracting attention, because exposure to it is thought of as a potential risk factor for the development or the acceleration of the onset of Alzheimer disease in

humans [*Guidelines for Drinking Water Quality*, 1998] which is a form of brain disorder that destroys the person's memory and ability to learn, communicate, etc. Though not currently regulated, the National Secondary Drinking Water Regulation (NSDWR) for Al stipulates a range of 0.05-0.2 mg/l. The Al levels in Figure 2.5 are below the lower limit of the NSDWR range.

Figure 2.6 shows the adsorption kinetics of As(V) for an initial solution pH of 6.7 measured with the four different particle size ranges, described in section 2.3.2.2 above. It reveals that the adsorption rate increases with decreasing particle size of the conditioned LDH. Lazaridis *et al*. investigated the adsorption of Cr(VI) on Mg-Al-CO_3 hydrotalcite, and also reported that decreasing the size of the sorbent had a significant effect on the sorption rate, but not on the equilibrium sorption loading [*Lazaridis et al.*, 2004]. The same appears to be true here for the adsorption of As(V) on the conditioned LDH.

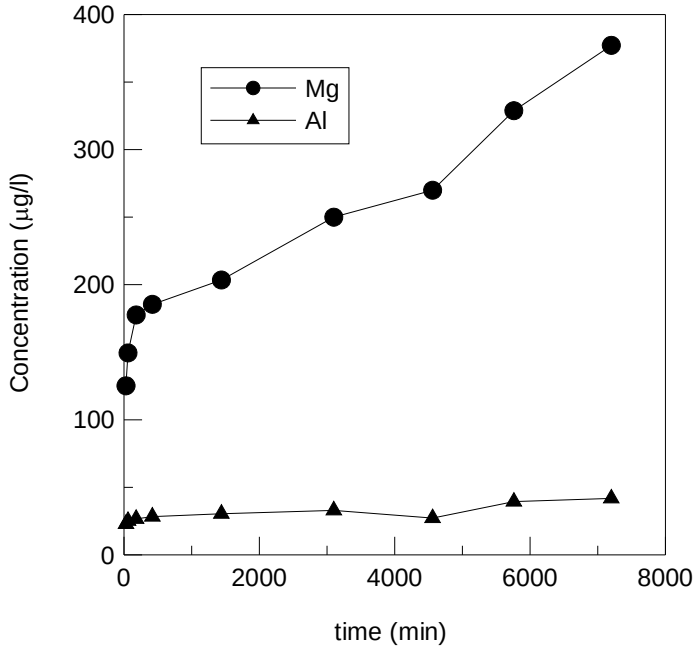

Figure 2.5. Mg and Al content in the solution as a function of time during the kinetic runs; particle size of 75-90µm, C_0 of 205 µg/l, LDH dose of 0.04g/l.

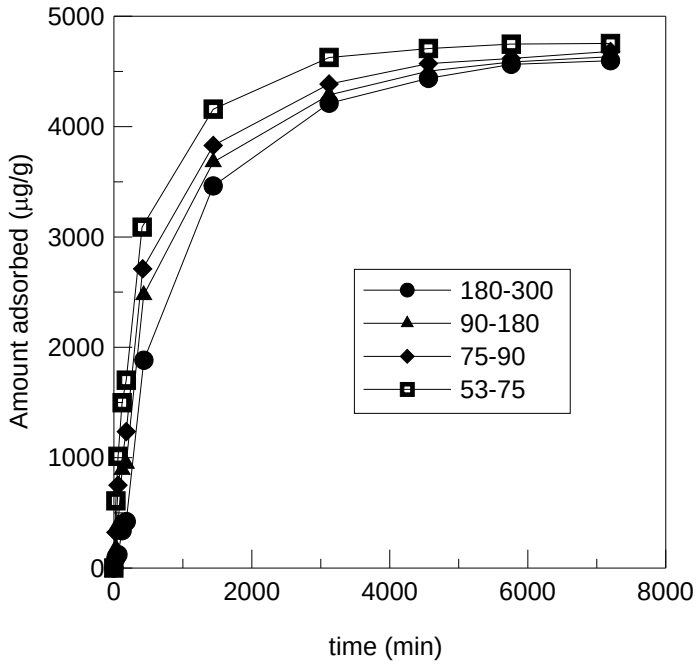

Figure 2.6. Effect of particle size on the adsorption kinetics of As on LDH.

The adsorption isotherms of As(V) (at an initial pH of ~6.7) on the conditioned LDH for various particle sizes are shown in Figure 2.7. There are no significant differences in the isotherms generated with the different particle sizes.

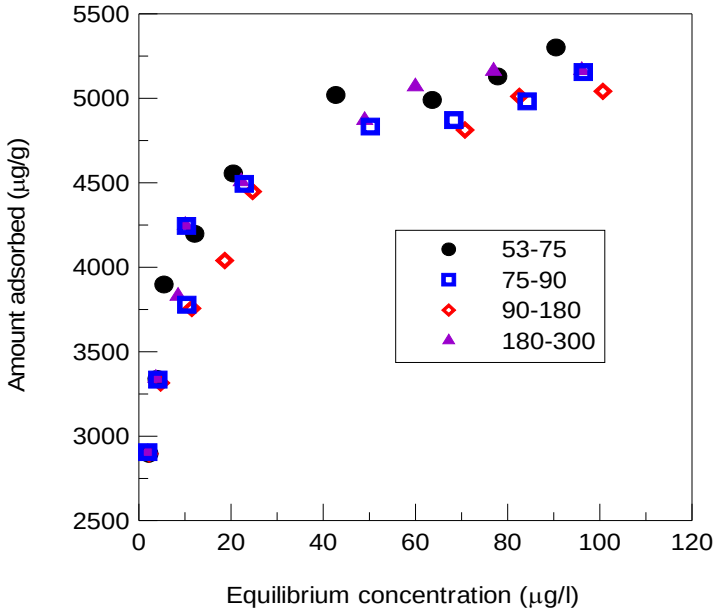

Figure 2.7. Adsorption isotherm of As on LDH as a function of particle size.

It is found that the As adsorption on conditioned LDH can be expressed well by the Sips equation shown below

$$q = \frac{Kq_s C^n}{1 + KC^n} \tag{2.29}$$

where q_s and K are the maximum sorption capacity and the Sips constant respectively, and n is the parameter characterizing the system heterogeneity.

In Figure 2.8 the data for different particle sizes are fitted to the Sips isotherm. The various isotherm parameters and the "goodness of fit," as manifested by the R^2, are shown in Table 2.3. The Sips isotherm has been previously utilized by a number of other investigators. Ko *et al.*, for example, have used the Sips isotherm to describe the adsorption of metal ions on bone char [*Ko et al.*, 2000, 2003].

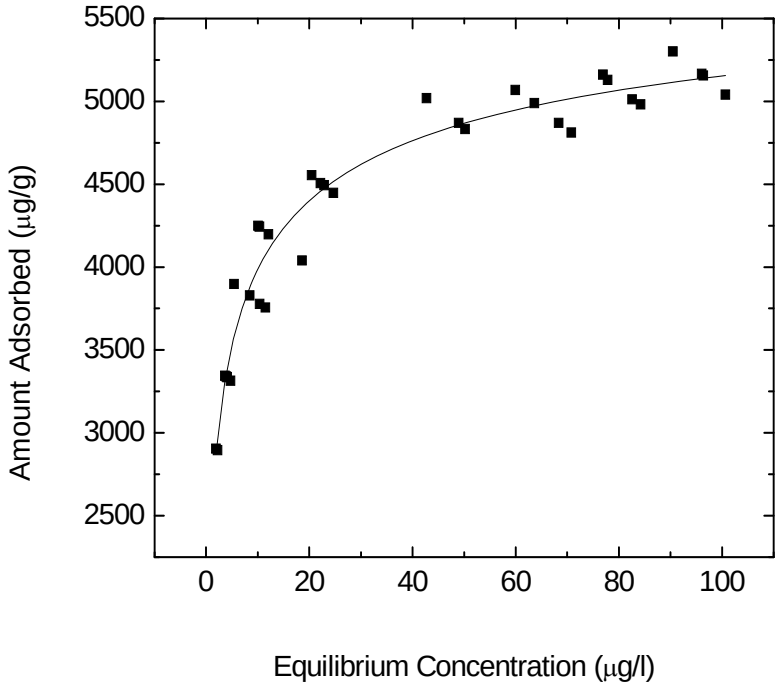

Figure 2.8. Sips isotherm model fit for the As adsorption on LDH for various particle sizes.

Table 2.3. Sorption isotherm parameters for As uptake on conditioned LDH at starting solution pH = 7

Sips Isotherm			
q_s **(μg/g)**	K **(l/μg)**	n	R^2
6130.28	0.65	0.45	0.96

The data in Figure 2.6 are fitted first to the homogeneous surface diffusion model, and the fitted lines together with the experimental data are shown in Figure 2.9 for the different particle sizes. The solid lines correspond to the homogeneous model with a constant diffusivity, and the particles assumed to be of uniform size with an average diameter equal either to d_{10} or d_{30}. The dashed lines are calculated assuming that the particles are again of uniform size (with an average diameter equal either to d_{10} or d_{30}), but the diffusivity is concentration-dependent, following the Darken correlation. The estimated diffusivity values for the different cases are shown in Tables 2.4 and 2.5. For all cases, the diffusivity values are shown to depend on the particle size. For the first case (where the d_{10} is utilized) the D_i values range from 1.64×10^{-11} cm^2/s to 10.03×10^{-11} cm^2/s and increase with increasing adsorbent particle size. For the second case using the d_{30} the D_i values range from $1.69\text{x}10^{-11}$ cm^2/s to 10.39×10^{-11} cm^2/s. For the case when diffusivity is loading -dependent the values for D_{i0} (when the d_{10} is utilized) range from 2.57×10^{-12} cm^2/s to 16.06×10^{-12} cm^2/s (for cadmium and copper ion adsorption onto bone char, in contrast, using a concentration-dependent diffusivity resulted in D_{i0} values which do not vary with particle size [*Ko et al.*, 2003]). The estimated D_i values are similar in magnitude to diffusivity values that have been reported for the adsorption of

arsenate in granular ferric hydroxide [*Badruzzaman et al.*, 2004], as well as cadmium on iron-bearing materials [*Smith*, 1996]. Axe and Trivedi, for example, investigated intraparticle surface diffusion of metal contaminants in microporous amorphous Al, Fe, and Mn oxides. The surface diffusivities were observed to range from 10^{-16} to 10^{-10} cm^2/s for strontium, cadmium, zinc, and nickel on hydrous amorphous aluminum, iron, and manganese oxides correspondingly [*Axe et al.*, 2002]. On the other hand, these diffusivities are significantly lower than the values measured during arsenite and arsenate adsorption onto activated alumina [*Lin et al.*, 2001] and arsenate onto natural manganese oxide [*Ouvrand et al.*, 2002] (of the order of ~10^{-7}-10^{-8} cm^2/s). They are also lower than the diffusivities we measure for carbon dioxide in the same materials.

Table 2.4. Surface diffusion coefficients for conditioned LDH with various particle sizes

Mesh size	d_{10} **(μm)**	D_i **($\times 10^{11}$ cm^2/s)**	d_{30} **(μm)**	D_i **($\times 10^{11}$ cm^2/s)**	D^* **($\times 10^{11}$ cm^2/s)**
200-270	68.1	1.64	69.2	1.70	1.12
170-200	82.7	1.65	84.6	1.72	1.02
80-170	146.3	3.91	150.5	4.13	2.59
50-80	274.5	10.03	279.4	10.39	6.47

D^* obtained considering the particle size distribution

Table 2.5. D_{i0} for conditioned LDH with various particle sizes

Mesh size	d_{10} **(μm)**	D_{i0} **($\times 10^{11}$ cm^2/s)**	d_{30} **(μm)**	D_{i0} **($\times 10^{11}$ cm^2/s)**
200-270	68.1	0.26	69.2	0.27
170-200	82.7	0.26	84.6	0.27
80-170	146.3	0.61	150.5	0.65
50-80	274.5	1.61	279.4	1.66

The strong variation of diffusivity with particle size has also been reported by a number of other investigators. Badruzzaman *et al*. during adsorption of arsenate in

granular ferric hydroxide (GFH) reported, for example, a non-linear relationship (D_i = $3.0x10^{-9}$ $R_P^{1.4}$) between D_i and GFH particle radius (R_p) [*Badruzzaman et al.*, 2004]. Lin and Wu reported that during arsenate and arsenite adsorption onto activated alumina that the diffusivity also increased with particle size [*Lin at al.*, 2001]. The same behavior was reported by Ouvrard *et al.* [2002] for arsenate adsorption in natural manganese oxide. On the other hand, the opposite trend was observed during adsorption of cadmium on iron-bearing materials derived from surface finishing operations in the manufacturing of cast iron components [*Smith*, 1996]. To verify whether this particle size dependence on diffusivity is the result of using an average particle size rather than the experimental particle size (approximation of the PSD by use of an average diameter has been shown in the past to lead to misinterpretation of the experimental data [*Kaczmarski et al.*, 2003]), the data were also fitted using Equations (2.10)-(2.15) and the experimentally measured particle size distribution. Despite taking into account the particle size distribution, the estimated D^* values are still particle size dependent, and range from 1.12×10^{-11} cm^2/s to 6.47×10^{-11} cm^2/s.

Finally, the experimental data were also fitted to the bidisperse pore model, described by Equations (2.16) – (2.26). Since we do not have accurate experimental data on the radius of the single crystal microparticles constituting the larger particle, we opted instead to estimate the values of D_μ / R_μ^2 (in s^{-1}). The diffusivity of the metal anions in the porous region was taken to be equal to its bulk diffusivity value, which has already been reported in the technical literature [*Lide*, 1996-1997]. The D_μ / R_μ^2 values are reported in Table 2.6, and the data and parameter fit are shown in Figure 2.10. Note, that

though there is still some variation with respect to particle size, it is significantly less than the estimated diffusivity values from the homogeneous model. This observation is consistent with the understanding that the surface diffusivity within the microparticles should remain unaffected by the overall size of the aggregate particle. Similar observation was also made by us with CO_2 adsorption on calcined LDH [*Dadwhal et al.*, 2008]. The HSDM exhibited strong particle dependence with D_i varying from 3.3×10^{-9} cm^2/s to 58.61×10^{-9} cm^2/s, whereas BPM predicted D_μ / R_μ^2 values that were not dependent on particle size [*Dadwhal et al.*, 2008]. Given the uncertainty in the assumption that the microparticles are all of uniform size, it is probably safe to say that the bidisperse model offers a more accurate representation of the particle size effect, in lieu of the commonly utilized homogeneous surface diffusion model.

Table 2.6. Simulated D_μ / R_μ^2 for conditioned LDH with various particle sizes

Mesh Size	$\frac{D_\mu}{R_\mu^2}$ **($\times 10^7$ s^{-1})**
200-270	5.01
170-200	5.50
80-170	5.68
50-80	5.82

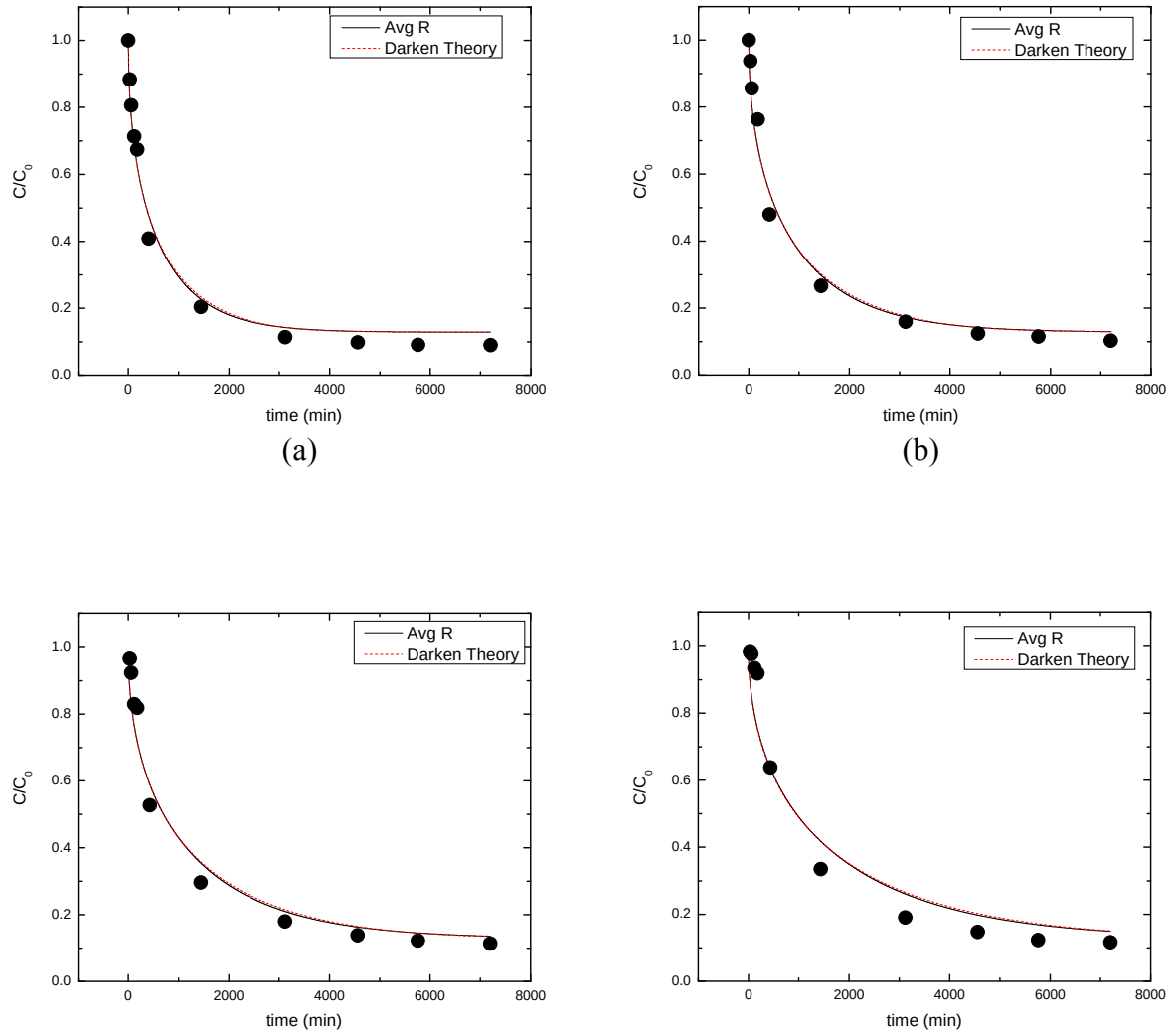

Figure 2.9. Observed experimental data (symbols) and model predictions (lines) for As adsorption on LDH with various particle sizes: (a) 53-75 μm; (b) 75-90 μm; (c) 90-180 μm; (d) 180-300 μm. Solid lines denote simulated uptake curves for d_{10} and d_{30}, and the dash lines denote simulated uptake curves calculated with a loading - dependent diffusivity.

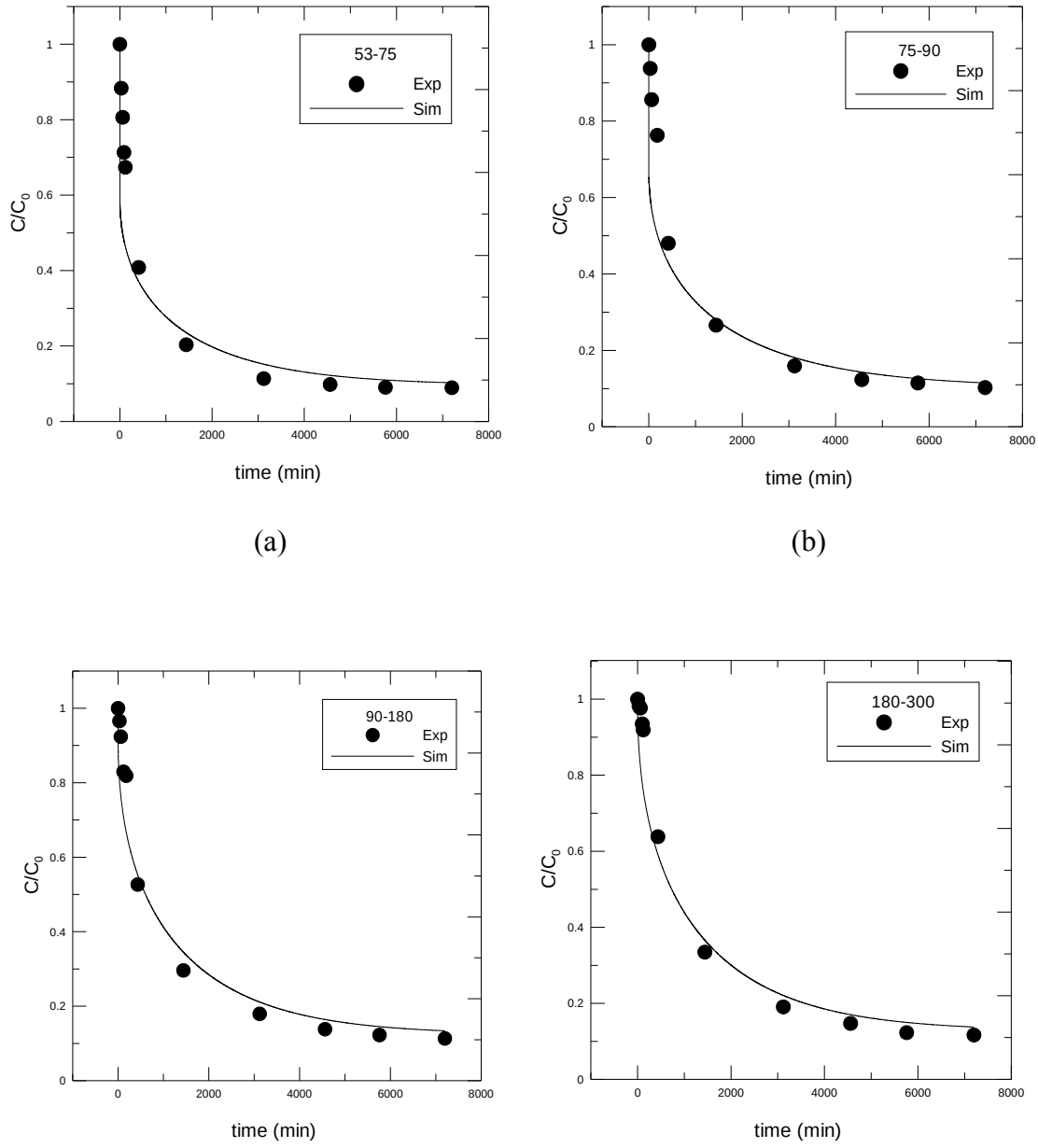

Figure 2.10. Observed experimental data and model predictions (bidisperse pore model) for As adsorption on LDH with various particle sizes: (a) 53-75 μm; (b) 75-90 μm; (c) 90-180 μm; (d) 180-300 μm.

2.5. Conclusions

The adsorption of As(V) on the conditioned LDH has been investigated. The As(V) adsorption has been shown to follow a Sips-type adsorption isotherm. The As(V)

adsorption rate on conditioned LDH increases with decreasing adsorbent particle size; the adsorption capacity of As(V) on conditioned LDH, on the other hand, is independent of particle size. The experimental data have been fitted to two models, the Homogeneous Surface Diffusion Model (HSDM) which considers the adsorbent particle to be a single particle, and the Bidisperse Pore Model (BPM) which assumes that the particle is an agglomerate of a number of equal size, single-crystal microparticles. The advantage of the HSDM is its simplicity and ease in simulation, while the BPM model provides a better representation of the true pore structure of the LDH. When a homogenous surface diffusion model is used to describe the experimental data, the estimated diffusivity values are shown to increase with increasing particle size. On the other hand, when a bidisperse pore model is utilized to fit the experimental data it predicts that the diffusivity is particle-size independent. The latter model, therefore, appears more appropriate for use in real flow-column experiments.

3. Adsorption of Arsenic on Conditioned Layered Double Hydroxides: Column Experiments and Modeling

3.1. Introduction

In the previous section we reported the adsorption kinetics and isotherms on a number of conditioned LDH, each with a different average particle size, in batch experimental runs [*Yang et al.*, 2006]. The data were fitted using both a conventional homogeneous surface diffusion model, as well as a bidisperse pore model which views the LDH particles as assemblages of microparticles and takes into account both the bulk diffusion in the interparticle pore space, and the surface diffusion within the microparticles themselves. When the homogenous surface diffusion model was used to describe the experimental data, the estimated effective particle diffusivities were shown to increase with increasing particle size. On the other hand, the bidisperse pore model predicted that the diffusivities for the microparticles are fairly insensitive to their size.

The ability of LDH to remove As (and Se) has been confirmed by the batch experiments [*Yang et al.*, 2005; *Yang et al.*, 2006] , but the performance of practical packed-bed sorption column using such LDH materials needs further investigation, as there are currently no data and design methodologies available for the efficient optimal design of such systems. This is also generally true for the design of all large-scale adsorption systems used for environmental remediation which, typically, requires copious quantities of preliminary design information, usually gathered in an extensive series of pilot-plant experiments that are time-consuming and expensive. The methodology proposed here aims to alleviate some of the design burden. It involves conducting small-scale batch experimental runs aimed at studying the kinetics as well as the equilibrium

sorption characteristics of various proposed adsorbents, including the effect of such parameters as the feed concentration, pH, and temperature. The batch experiments are combined with a mathematical model that properly describes the mass transfer and adsorption processes within the adsorbent in packed-bed sorption columns, in order to predict full-scale column performance and dynamics, and to study the effect of various design and operating parameters. With the aid of such a design model the optimal conditions for the column operation can be predicted without the need for extensive pilot-plant experiments that are time-consuming and expensive.

The principal objectives of this section [already published as *Dadwhal et al.*, 2009] are, therefore, (i) to validate the proposed design methodology, and (ii) to use the models developed to identify and quantify the impact of important solution and operating parameters, such as the influent As concentration, pH, sorbent particle size, and flow rate during As removal in fixed-beds. In what follows, we first describe the design models developed; we then describe the experimental data that have been generated, and use them to validate the design models. The models are then utilized to describe the column dynamics as a function of the various parameters that characterize column behavior.

3.2. Model Development

Any model describing As uptake in flow columns must take into account the phenomena that occur at the column level, as well as the transport and sorption phenomena within the adsorbent particles themselves. We assume that axial dispersion and channeling effects in the column are negligible, and since the As influent concentration is typically low, solution flow velocity is taken to be constant. Therefore,

the mass balance for As in the flowing liquid phase in a packed column configuration is given by:

$$u\frac{\partial C}{\partial z}+\frac{\partial C}{\partial t}+\frac{1-\varepsilon}{\varepsilon}\frac{\partial \bar{q}}{\partial t}\cdot\rho=0 \tag{3.1}$$

where u is the average axial velocity of the flowing fluid (cm/min), described by the following equation

$$u=\frac{Q_0}{\pi D^2\varepsilon/4} \tag{3.2}$$

where Q_0 is the volumetric flow rate fed to the column, D is the inside column diameter, and ε is the column void fraction (assumed to be the same with the void fraction in the cross-sectional area). In Equation (3.1), C is the solute (As(V)) concentration in the fluid phase (μg/l), t is the time (min), z is the axial coordinate (cm), $\bar{q}$ is the average concentration of solute in the solid phase (μg/g), and ρ is the adsorbent particle density (g/cm^3).

The initial (IC) and boundary (BC) conditions, consistent with the laboratory experiments, are:

$$C=0,\quad \bar{q}=0, \qquad t=0 \tag{3.3}$$

$$C=C_0, \qquad z=0 \tag{3.4}$$

Equations (3.1)-(3.4) must be coupled with the equation that describes solute transport at the liquid-solid interface. Equating the solute uptake term ($\rho\frac{\partial \bar{q}}{\partial t}$ in Equation (3.1)) to the flux from the bulk phase to the particle surface through the liquid boundary layer surrounding the spherical adsorbent particle yields the desired equation:

$$\rho \frac{\partial \bar{q}}{\partial t} = \frac{3k_f}{R_M}(C - C_{MS}) \ , \qquad (3.5)$$

where k_f is the external mass transfer coefficient, C_{MS} is the liquid-phase solute concentration at the solid-liquid interface (μg/l), and R_M is the particle radius (cm).

The value of the external mass transfer coefficient (k_f) depends on the flow conditions in the column. In this study, k_f is determined by an empirical correlation obtained by Williamson *et al.* [1963], namely,

$$\text{Sh} = 2.4\varepsilon^{0.66}\,\text{Re}^{0.34}\,\text{Sc}^{0.33} \qquad \text{for } 0.04 < \text{Re} < 52 \qquad (3.6)$$

In the above Equation (3.6), Sh is the dimensionless Sherwood number,

$$\text{Sh} = \frac{2k_f R_M}{D_b} \qquad (3.7)$$

where D_b is the bulk diffusivity of the As species (see below), while the Reynolds (Re) and Schmidt (Sc) numbers are defined by

$$\text{Re} = \frac{2R_M G_0}{\mu}; \qquad G_0 = \varepsilon \times u \times \rho_f \qquad (3.8)$$

$$\text{Sc} = \frac{\nu}{D_b} \qquad (3.9)$$

For the range of pH studied here (5.5 - 8.5), As(V) exists in two anionic forms [*Yang et al.*, 2005], namely, $H_2AsO_4^-$ and $HAsO_4^{2-}$. For pH in the range (4.5-5.5), As(V) mostly exists as the monovalent $H_2AsO_4^-$ ion; for pH in the range (8-10) it exists as the divalent $HAsO_4^{2-}$ ion, while in the range of neutral pH (6.5-7) it consists approximately of equal amounts of both ions. The bulk diffusivity of $H_2AsO_4^-$ in water has been reported to be $D_b(H_2AsO_4^-) = 9.05\text{x}10^{-6}$ cm^2/s [*Lide*, 1996-1997], while that of $HAsO_4^{2-}$ $D_b(HAsO_4^{2-}) =$

3.23×10^{-6} cm^2/s [*Vrijenhoek et al.*, 2000]. Most of the experiments reported here (other than those in Figures 3.1 and 3.6) are at pH=7. For the simulations at pH=7, we use an average value of $D_b = 6.14 \times 10^{-6}$. For the simulations at pH=5.5 (Figures 3.1 and 3.6) $D_b = 9.05 \times 10^{-6}$, while at pH=8.5, $D_b = 3.23 \times 10^{-6}$. It should be noted, however, that for the flow rates used here, the exact choice of D_b in the range of values $[3.23 - 9.05] \times 10^{-6}$ cm^2/s has little impact on the simulated As(V) adsorption profiles. In Equations (3.7)-(3.9), ρ_f, μ, and ν are the density, and the dynamic and kinematic viscosity of the fluid, taken to be equal to those of water at the corresponding temperature, since the As solutions studied here are very dilute. The porosity of the column was determined experimentally based on the mass of adsorbent used, its bulk density, and the volume of the column occupied by the adsorbent.

To describe the solute uptake in packed-bed column experiments, we again utilize the two models developed in the previous section, namely, a homogeneous surface diffusion model and a bidisperse pore model. The equations used are the same as described before (the previous section), the only difference being that at the particle surface we no longer assume infinite mass transfer resistance as assumed in batch experiments. Instead we equate the flux from the bulk phase to the liquid particle boundary layer to the intraparticle flux at the particle surface. We briefly describe below the two models again.

3.2.1. Homogenous Surface Diffusion Model

The HSDM is based on the assumption that the transport of species is determined by external mass transfer in the liquid phase, and by intraparticle diffusion resistance in the form of surface diffusion within the adsorbent particle. Assuming homogeneous spherical adsorbent particles, a concentration-independent diffusivity (this assumption was relaxed

in the previous section, without offering any particular advantage in model fit), the intraparticle transport and solute uptake is described by the following equation,

$$\frac{\partial q}{\partial t} = \frac{D_i}{r_M{}^2} \frac{\partial}{\partial r_M} (r_M{}^2 \frac{\partial q}{\partial r_M}) \tag{3.10}$$

where q is the solute loading in the sorbent phase (μg/g), D_i is the intraparticle diffusion coefficient (cm^2/s), r_M is the radial distance (cm) measured from the center. The BC and IC are:

$$q = 0, \qquad t = 0 \tag{3.11}$$

$$\frac{\partial q}{\partial r_M} = 0, \qquad r_M = 0 \tag{3.12}$$

$$\rho D_i \left. \frac{\partial q}{\partial r_M} \right|_{r_M = R_M} = k_f (C - C_{MS}), \quad r_M = R_M \tag{3.13}$$

At the external surface of the particle ($r_M = R_M$), instantaneous equilibrium is assumed between the metal concentrations in the liquid and solid phases, which are coupled using the Sips isotherm, as obtained from the adsorption experiments (see further discussion below).

$$q = \frac{K q_s C_{MS}{}^n}{1 + K C_{MS}{}^n}, \qquad r_M = R_M \tag{3.14}$$

The average solute concentration in the adsorbent particle is defined as:

$$\bar{q} = \frac{3}{R_M{}^3} \int_0^{R_M} q \; r_M{}^2 dr_M \tag{3.15}$$

3.2.2. Bidisperse Pore Model

The BPM assumes that the adsorbent particle is an agglomerate of a number of equal size microparticles. A porous intercrystalline region forms in between the microparticles.

Before the metal anion adsorbs inside the microparticle, it must be transported from the particle surface through the intercrystalline region to the surface of the microparticles. In the intercrystalline porous region transport is described by the following equations [*Yang et al.*, 2006; *Cen et al.*, 1986],

$$\varepsilon_M \frac{\partial C_M}{\partial t} + (1-\varepsilon_M)\rho_s \frac{\partial \bar{q}_\mu}{\partial t} = \varepsilon_M \frac{D_M}{r_M{}^2} \frac{\partial}{\partial r_M}\left[r_M{}^2 \frac{\partial C_M}{\partial r_M} \right] \tag{3.16}$$

The BC and IC are:

$$C_M = 0, \qquad t = 0 \tag{3.17}$$

$$\frac{\partial C_M}{\partial r_M} = 0, \qquad r_M = 0 \tag{3.18}$$

$$\varepsilon_M D_M \left. \frac{\partial C_M}{\partial r_M} \right|_{r_M = R_M} = k_f (C - C_{MS}), \; r_M = R_M \tag{3.19}$$

where C_M is the solute concentration in the intercrystalline porous region (μg/l), $\bar{q}_\mu$ is the volume-averaged solute concentration in the solid phase (microparticles) (μg/g) -- see Equation (3.25) below-- R_M is the particle external radius, D_M is the intercrystalline porous region diffusivity (cm^2/s), given by $\frac{\varepsilon_M}{\Gamma} D_b$ with ε_M being the void fraction in the porous region, and Γ, the tortuosity.

Transport and adsorption in the microparticles are described by

$$\frac{\partial q_\mu}{\partial t} = \frac{D_\mu}{r_\mu{}^2} \frac{\partial}{\partial r_\mu}\left(r_\mu{}^2 \frac{\partial q_\mu}{\partial r_\mu} \right) \tag{3.20}$$

with the BC and IC being

$$q_\mu = 0, \qquad t = 0 \tag{3.21}$$

$$\frac{\partial q_\mu}{\partial r_\mu} = 0, \qquad r_\mu = 0 \tag{3.22}$$

$$q_\mu = \frac{K q_s C_M{}^n(r_M, t)}{1 + K C_M{}^n(r_M, t)}, \qquad r_\mu = R_\mu \tag{3.23}$$

where q_μ is the solute concentration (μg/g) in the microparticle, D_μ is the microparticle diffusivity (cm^2/s), and R_μ is the microparticle radius. Equation (3.23) is the Sips isotherm, which has been shown experimentally to describe As sorption in the LDH adsorbent (see below). The average concentration throughout the adsorbent particle is defined as:

$$\bar{\bar{q}} = \frac{3}{\rho R_M{}^3} \int_0^{R_M} r_M{}^2 \left[(1-\varepsilon_M)\rho_s \bar{q}_\mu + \varepsilon_M C_M \right] dr_M \tag{3.24}$$

where q_μ is given by

$$\bar{q}_\mu = \frac{3}{R_\mu{}^3} \int_0^{R_\mu} q_\mu r_\mu{}^2 dr_\mu \tag{3.25}$$

Equations (3.1)-(3.25) above are made dimensionless by defining the following dimensionless variables and groups:

$$\eta = \frac{r_M}{R_M} \qquad \beta = \frac{r_\mu}{R_\mu} \qquad \overline{V'} = \frac{V'}{V_0'}$$

$$\overline{C}_M = \frac{C_M}{C_0} \qquad \overline{C}_{MS} = \frac{C_{MS}}{C_0} \qquad \overline{C} = \frac{C}{C_0}$$

$$Q = \frac{q}{q_s} \qquad \bar{\bar{Q}} = \frac{\bar{\bar{q}}}{q_s} \qquad Q_\mu = \frac{q_\mu}{q_s}$$

$$\bar{Q}_\mu = \frac{\bar{q}_\mu}{q_s} \qquad t_R = \frac{V_0}{Q_0} \qquad \tau = \frac{t}{t_R}$$

and setting

$$\overline{D}_i = \frac{D_i t_R}{R_M{}^2} \qquad \overline{D}_M = \frac{D_M t_R}{R_M{}^2} \qquad \overline{D}_\mu = \frac{D_\mu t_R}{R_\mu{}^2}$$

$$\Lambda = KC_0{}^n \qquad \chi = \frac{R_M t_R}{k_f} \qquad \omega = \frac{\rho q_s}{C_0}$$

$$\overline{\omega} = \frac{\rho_s q_s}{C_0} \qquad \psi = \frac{D_i}{R_M k_f} = \frac{2}{\mathrm{Sh}^{'}} \qquad \overline{\psi} = \frac{D_M}{R_M k_f} = \frac{2}{\mathrm{Sh}^{''}}$$

$$\mathrm{Sh}^{'} = \frac{2R_M k_f}{D_i} \qquad \mathrm{Sh}^{''} = \frac{2R_M k_f}{D_M}$$

The column equations above are converted to the following dimensionless form,

$$\frac{\partial \overline{C}}{\partial \overline{V}} + \varepsilon \frac{\partial \overline{C}}{\partial \tau} + (1-\varepsilon)\omega \frac{\partial \overline{\overline{Q}}}{\partial \tau} = 0 \tag{3.26}$$

with the BC and IC being

$$\overline{C} = 0, \quad \overline{\overline{Q}} = 0, \qquad \tau = 0 \tag{3.27}$$

$$\overline{C} = 1, \qquad \overline{V} = 0 \tag{3.28}$$

$$\chi\omega \frac{\partial \overline{\overline{Q}}}{\partial \tau} = 3\ (\overline{C} - \overline{C}_{MS}) \tag{3.29}$$

The HSDM equations reduce to,

$$\frac{\partial Q}{\partial \tau} = \frac{\overline{D}_i}{\eta^2} \frac{\partial}{\partial \eta}(\eta^2 \frac{\partial Q}{\partial \eta}) \tag{3.30}$$

with the IC and BC being

$$Q = 0, \qquad \tau = 0 \tag{3.31}$$

$$\frac{\partial Q}{\partial \eta} = 0, \qquad \eta = 0 \tag{3.32}$$

$$\omega\,\psi\left.\frac{\partial Q}{\partial \xi}\right|_{\eta=1} = (\overline{C} - \overline{C}_{MS}), \qquad \eta = 1 \tag{3.33}$$

$$Q = \frac{\Lambda \overline{C}_{MS}{}^{n}}{1 + \Lambda \overline{C}_{MS}{}^{n}}, \qquad \eta = 1 \tag{3.34}$$

$$\overline{\overline{Q}} = 3\int_0^1 Q\eta^2 d\eta \tag{3.35}$$

In the intercrystalline region, the BPM equations are reduced to

$$\frac{\partial \overline{C}_M}{\partial \tau} + \frac{(1-\varepsilon_M)}{\varepsilon_M}\frac{}{\omega}\frac{\partial \overline{Q}_\mu}{\partial \tau} = \frac{\overline{D}_M}{\eta^2}\frac{\partial}{\partial \eta}\left[\eta^2 \frac{\partial \overline{C}_M}{\partial \eta}\right] \tag{3.36}$$

with the BC and IC given by

$$\overline{C}_M = 0, \quad \overline{Q}_\mu = 0, \quad , \qquad \tau = 0 \tag{3.37}$$

$$\frac{\partial \overline{C}_M}{\partial \eta} = 0, \qquad \eta = 0 \tag{3.38}$$

$$\overline{\psi}\ \varepsilon_M \left.\frac{\partial \overline{C}_M}{\partial \eta}\right|_{\eta=1} = (\overline{C} - \overline{C}_{MS}), \qquad \eta = 1 \tag{3.39}$$

whereas in the micro-particles we have

$$\frac{\partial Q_\mu}{\partial \tau} = \frac{\overline{D}_\mu}{\beta^2}\frac{\partial}{\partial \beta}\left(\beta^2 \frac{\partial Q_\mu}{\partial \beta}\right) \tag{3.40}$$

with BC and IC being

$$Q_\mu = 0, \qquad \tau = 0 \tag{3.41}$$

$$\frac{\partial Q_\mu}{\partial \eta} = 0, \qquad \beta = 0 \tag{3.42}$$

$$Q_\mu = \frac{\Lambda \overline{C}_M{}^{n}(\eta,\tau)}{1 + \Lambda \overline{C}_M{}^{n}(\eta,\tau)}, \qquad \beta = 1 \tag{3.43}$$

$$\overline{Q}_{\mu} = 3\int_0^1 Q_{\mu}\beta^2 d\beta \tag{3.44}$$

$$\overline{\overline{Q}} = \frac{3}{\rho}\int_0^1 \left[(1-\varepsilon_M)\rho_s \overline{Q}_{\mu} + \varepsilon_M \frac{C_0}{q_s}\overline{C}_M \right] \eta^2 d\eta \tag{3.45}$$

To solve the above dimensionless equations, a FORTRAN program was developed, by which the governing equations for the fluid and solid phases were solved by using a finite-difference technique, which gives rise to tridiagonal matrices. For the HSDM model Equations (3.26)-(3.35) were solved simultaneously, with $\overline{\overline{Q}}$, the average dimensionless solute concentration in the adsorbent particle, calculated using Equation (3.35). For the BPM model, Equations (3.26)-(3.29) were simultaneously solved with Equations (3.36)-(3.45), with $\overline{\overline{Q}}$ calculated using both $\overline{Q}_{\mu}$, the average dimensionless solute concentration in the microparticles, and $\overline{C}_M$, the dimensionless solute concentration in the macropores.

3.3. Experimental

3.3.1. Materials

The sorbent material used in the experiments is conditioned Mg-Al-CO_3-LDH with a Mg/Al mole ratio of 2.87. It was prepared by the co-precipitation method described before in the report. To obtain different particle size fractions, the conditioned LDH was crushed and sieved using standard testing sieves (VWR). The size fraction collected at 50-80 mesh (180-300 μm) was used for most of the packed-bed adsorption experiments reported in this section (other than the experiment for the particle size effect).

As(V) was the metal investigated in the study. The As(V) solutions used for the adsorption experiments were prepared by dilution from a 1000 ppm ICP standard solution

(As(V) in 2% HNO_3 purchased from Exaxol) using deionized water. For the adsorption experiments, the pH of the working solution was adjusted to the desired initial value using 1M NaOH solution. The pH was not adjusted during the adsorption period, but any pH drift was measured and recorded. The As(V) concentration was determined by ICP-MS.

3.3.2. Column Experiments

Fixed-bed experiments were conducted in laboratory glass columns with internal diameter, $D = 0.7$ cm, and height, $H = 8.5$ cm. Two columns with the same diameter and height were employed in the study in order to speed-up the experiments (the flow rate and particle size effect experiments were carried out in one column, while the concentration and pH effect experiments were done in the second column – see discussion to follow). They were packed with conditioned LDH (cotton-wool was placed at the bottom of the column to prevent the LDH particles from eluding from the column during the flow experiments). They were then rinsed with deionized water for 24 h to ensure that the LDH particles were densely packed prior to the initiation of the experiments. The feed solution containing As, with a prescribed initial concentration and pH, was then continuously pumped in a down-flow mode from the reservoir through the columns at various flow rates using a peristaltic pump (Alitea model-XV). During the study, the performance of the pump was checked periodically by collecting solution samples at the outlet of the column for predetermined periods of time. Four sample ports (located at heights of 2.2, 4.4, 6.6, and 8.5 cm for the first column, and at heights of 1.9, 4.0, 6.0, and 8.5 cm for the second column) enabled withdrawing samples from the column for the analysis using 3 cm^3 sample syringes. Samples were taken at regular time

intervals, until the metal ion concentration in the effluent stream at the bottom of the bed became equal to the feed concentration. The metal ion concentrations were determined using ICP-MS. The pH of the influent solution was adjusted (in the reservoir) using 0.1 M NaOH solutions. No pH adjustment was done in the column, but the pH of the effluent from the column was measured and recorded with an Accumet Basic AB 15 pH meter. There was not much change in the pH of the solution in the column, with the effluent pH being typically 0.1 to 0.2 pH units higher than the pH of the feed. All column experiments were carried out at 25 °C. Temperature control was carried out by controlling the temperature of the feed solution, and by wrapping the column with a flexible coil through which water at 25 °C was circulated.

3.4. Results and Discussion

3.4.1. Determination of Adsorption Isotherms and Kinetics

We reported in our paper [*Yang et al.*, 2006] that the adsorption isotherm on conditioned LDH is well expressed by the Sips equation

$$q = \frac{Kq_s C^n}{1 + KC^n} \tag{3.46}$$

where q_s and K are the maximum sorption capacity and the Sips constant respectively, and n is the parameter characterizing the system heterogeneity. Furthermore, the adsorption parameters are not dependent on the adsorbent particle size. The adsorption isotherms for As(V) on the conditioned LDH for three different initial pH, namely, 5.5, 7.0, and 8.5, are shown in Figure 3.1. The various isotherm parameters (and the "goodness of fit", as manifested by the R^2 test) that are used in the simulations below are shown in Table 3.1. Comparing the adsorption capacity at these three different pH values

shows that lower pH significantly enhances As removal, which may be explained as follows. Since the point of zero charge (pH_{pzc}) for the LDH was reported to be in the range (6.8-8.9) [*Das et al.*, 2003; *Manju et al.*, 1999], the surface of LDH is negatively charged when $pH > pH_{pzc}$. Therefore, in the higher pH range the arsenate anionic species will be repelled by the LDH surface. For $pH < pH_{pzc}$, the LDH surface is positively charged, which is normally beneficial for the adsorption of the negatively charged anionic species.

Table 3.1. Sorption isotherm parameters for As uptake on conditioned LDH as a function of starting solution pH for 180-300 μm particle size conditioned LDH

Sips Isotherm				
pH	q_s **(μg/g)**	K **(l/μg)**	n	R^2
5.5	8045.37	0.66	0.51	0.94
7.0	6130.28	0.65	0.453	0.96
8.5	3619.90	0.65	0.58	0.91

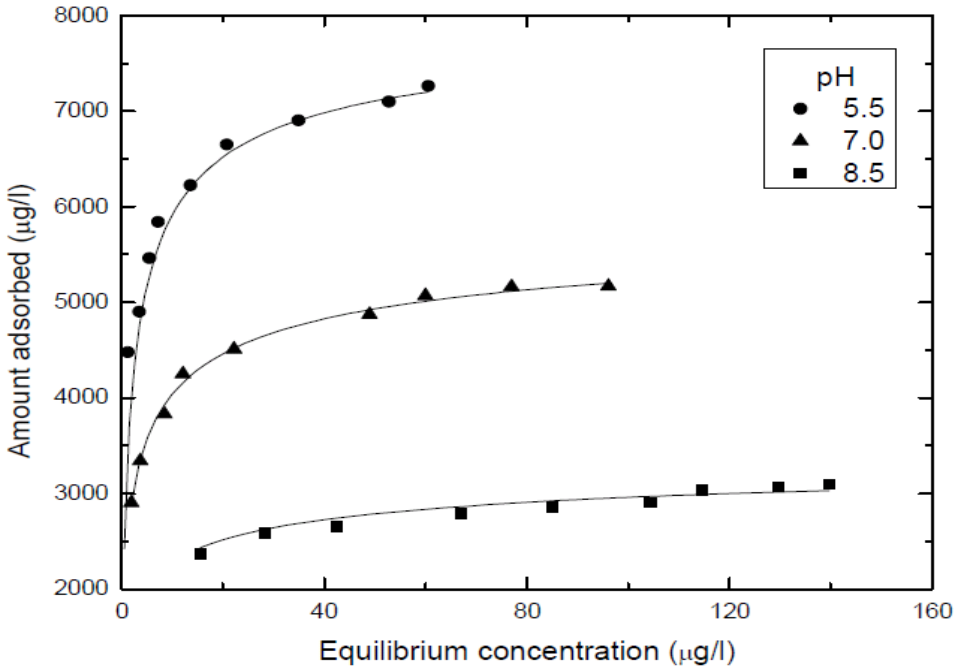

Figure 3.1. Fit of the Sips isotherm for the As adsorption on LDH at three starting solution pH.

Adsorption kinetics for As(V) were studied in well-stirred batch reactors and presented in the previous section. The data are reanalyzed here using both the HSDM and BPM. For the BPM we assumed previously that D_M is equal to D_b (visualizing the intercrystalline pore region as consisting of straight nonintersecting pores). Here, we relax this assumption and fit the data to estimate D_M. Assuming that $D_M = \frac{\varepsilon_M}{\Gamma} D_b$, allows one to calculate a pore structure tortuosity. Table 3.2 shows the parameters for both models calculated by fitting the experimental data. Note that the BPM provides estimates of $\frac{D_\mu}{R_\mu^2}$ and D_M that depend only weakly on the particle size. As also noted in the previous section [*Yang et al.*, 2006], that is not the case with the HSDM. Accounting for a concentration-dependent surface diffusivity, or for the particle size distribution of the adsorbent, does not change this conclusion much, with the surface diffusivity still remaining a strong function of the particle size.

Table 3.2. Measured densities and porosities and fitted D_μ / R_μ^2, Γ, and D_M values using the BPM, and fitted D_i values using the HSDM for conditioned LDH with various particle sizes

Particle Size (μm)	**Solid Density** ρ_s **(g/cm^3)**	**Particle Porosity** ε_M	**BPM**			**HSDM**
			Tortuosity Factor Γ	D_M **(×10^6 cm^2 s^{-1})**	$\frac{D_\mu}{R_\mu^2}$ **(×10^6 s^{-1})**	D_i **(×10^{11} cm^2 s^{-1})**
53 – 75	1.964	0.38	3.27	1.05	1.35	1.64
75 – 90	1.983	0.35	4.19	0.75	1.14	1.65
90 – 180	1.975	0.30	5.00	0.54	1.00	3.91
180 - 300	1.986	0.31	5.52	0.51	0.86	10.03

3.4.2. Column Experiments

In practice, the performance of a packed-bed column is evaluated in terms of monitoring the effluent concentration (and comparing it with the feed concentration) as a function of the number of the bed volumes (BV) treated. The number of bed volumes (BV) is defined as the volume of metal-laden waste stream treated divided by the volume of the adsorbent bed [*Chen et al.*, 2000].

$$\text{BV}=\frac{\text{Volume of solution treated}}{\text{Volume of packed bed}}=\frac{Q_0 t}{V_0}=\tau \qquad (3.47)$$

From the above definition, BV turns out to be equivalent to the dimensionless time τ, as defined previously. Column "breakthrough" occurs when the effluent concentration from the column is about 5% of the influent concentration. To utilize the models for fitting the experimental data, we use the parameters in Tables 3.1 and 3.2 and the external mass transfer coefficient (k_f), calculated by Equations (3.6)-(3.9), as described in the previous section.

3.4.2.1. Breakthrough Studies

Figure 3.2 shows the dimensionless effluent concentration $\overline{C}=\frac{C}{C_0}$ vs. dimensionless time τ (BV) at four different dimensionless bed heights ($\overline{V}=\frac{V}{V_0}$), of 0.22, 0.47, 0.7, and 1.0, and the HSDM and BPM predictions. The time at which the concentration reaches its breakthrough value, $\overline{C}=0.05$, depends on the bed height, of course, in addition to all other column parameters, see discussion to follow. In Figure 3.2, for example, the breakthrough time τ_{br} at a dimensionless bed height of 0.22 is 1,996, while it is 23,378 at the exit of the column. The adsorption curves in Figure 3.2 show the constant pattern

behavior, typical of favorable isotherms obtained in our earlier studies [*Yang et al.*, 2005; *Yang et al.*, 2006], with a sharp initial breakthrough followed by a slow approach to equilibrium. An overshoot is observed in the column experiments reported in Figure 3.2, with the effluent concentration at intermediate bed heights being slightly higher than one (as high as 1.15), while the exit concentration has yet to reach saturation ($\overline{C} \leq 1.0$). The same behavior is observed with the experiments carried out with the pH of 5.5. The experiments at the higher pH of 8.5 did not exhibit any overshoots, on the other hand. The same overshooting behavior was also reported by Chen and Wang, while removing Cu, Pb using activated carbon. Chen and Wang theorize that the overshoot indicates that as the adsorption (mass transfer) zone moves down along the column length, some desorption must be occurring in the upper saturated parts of the column [*Chen et al.*, 2000]. Neither the HSDM nor the BPM, as presented here, account for such desorption phenomena, and are not, therefore, capable of predicting the overshoots in concentration. This deficiency aside, however, both models do perform well in describing the experimental data at the exit as well as all the internal positions in the column, see also discussion to follow.

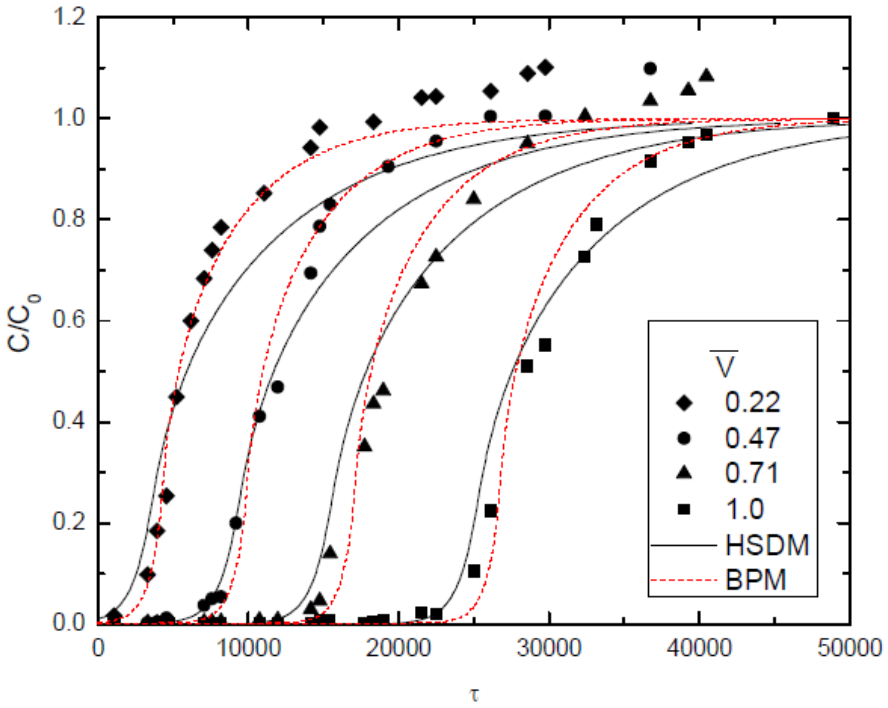

Figure 3.2. Adsorption of 200 ppb As solution (pH=7.0), fed at a flow rate of 8 ml/min by LDH with particle size (180-300μm) at several dimensionless bed depths $\left(\overline{V}\right)$ in a 8.5 cm column.

Table 3.3. Properties of the fixed-bed column

Parameters		**Value**
Height, H **(cm)**		8.5
Diameter, D **(cm)**		0.7
Bed porosity, ε	**90-180 (μm)**	0.28
	180-300 (μm)	0.27

3.4.2.2. Effect of Changing the Column Parameters

3.4.2.2.1. Effect of Flow Rate

The effect of flow rate on the column behavior was studied using a 200 ppb As(V) solution (pH 7.0), pumped at various flow rates, (6 - 20 ml/min) through the column. This range of flow rates correspond to a range of column residence times, t_R, of 0.54 to 0.16 min. Figure 3.3 shows the concentration at the exit of the column as a function of t

(min), for four flow rates (6, 8, 10, and 20 ml/min). Shown on the same figure are the HDSM and BPM predictions. Again, the models perform generally well in predicting the overall column behavior, without any need for adjustable parameters other than the measured values in Tables 3.1 and 3.2, and the mass transfer coefficient calculated by Equations (3.6)-(3.9). From the figure we can calculate the corresponding breakthrough times, t_{br}, for different flow rates. As expected, the breakthrough times are a strong function of the column residence times, t_R. For a flow rate of 6 ml/min ($t_R = 0.54$ min), for example, t_{br} = 13,205 (the HSDM model predicts t_{br} = 14,505, while the BPM yields t_{br} = 15,624), while for a flow rate of 20 ml/min ($t_R = 0.16$ min), t_{br} = 2,678 (for the HSDM, t_{br} = 2,206, and the BPM yields t_{br} = 3,010). On the other hand, the breakthrough time τ_{br} varies from 24,233 (for the HSDM, τ_{br} = 26,619, while for the BPM, τ_{br} = 28,672) for 6 ml/min to 16,381 (for the HSDM, τ_{br} = 13,494, and for the BPM τ_{br} = 18,412) for 20 ml/min. This decrease in the breakthrough time with increasing flow rate is expected, of course, and was also reported by previous investigators. Ko *et al.* [2001], for example, reported a decrease in the uptake with increasing flow rate for the sorption of cadmium and copper ions on bone-char in fixed-beds, and Kundu *et al.* [2005] also reported similar results while treating As(V) with iron oxide-coated cement.

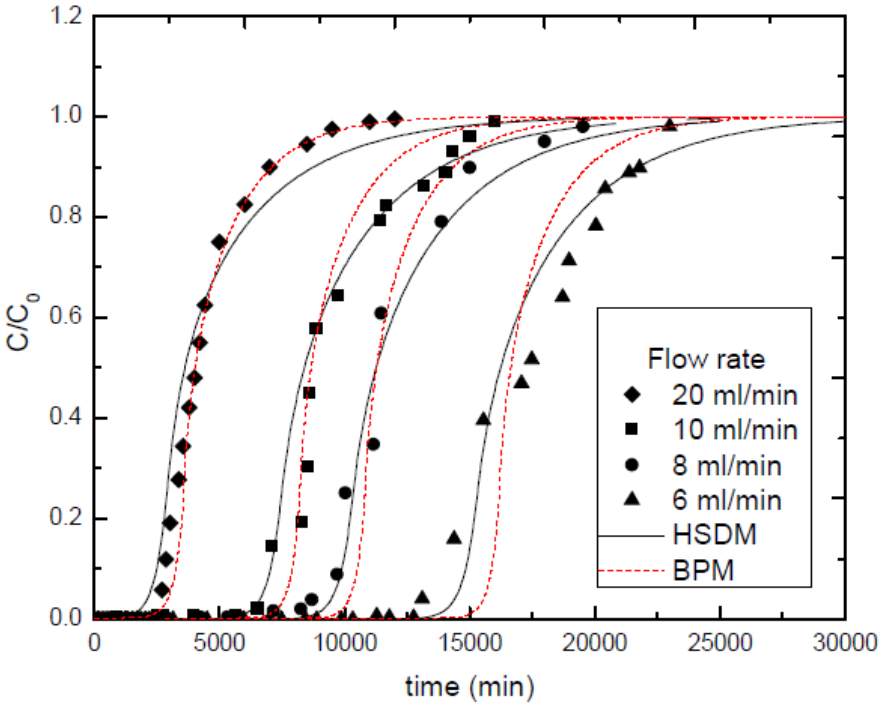

Figure 3.3. Effect of feed flow rate on the breakthrough curves and the corresponding simulation fittings at a bed depth of 8.5 cm $\left(\overline{V}=1.0\right)$.

3.4.2.2.2. Effect of the Influent As Concentration

The influent As ion concentration has a significant effect on the column behavior. To investigate this effect, sorption experiments were conducted in a fixed-bed column with a varying influent As concentration (100, 200, and 300 ppb) at a fixed pH=7, and a feed flow rate of 8 ml/min ($t_R = 0.41$ min). Figure 3.4 shows the concentration at the exit of the column as a function of τ for three influent concentrations. Again, the models perform well in predicting the column behavior without the need for any adjustable parameters. For feed concentrations of 300, 200, and 100 ppb the corresponding experimental τ_{br} values are 15,546, 23,378 and 49,056. As expected, the breakthrough times are a strong function of the influent concentrations. Similar findings were also reported by other researchers [*Chen et al.*, 2003; *Han et al.*, 2006]. In terms of the models' ability to predict

the breakthrough times, τ_{br}, the predicted values by the HSDM are (13,641, 23,418, and 47,373), while those by the BPM model are (17,005, 25,143, and 47,439).

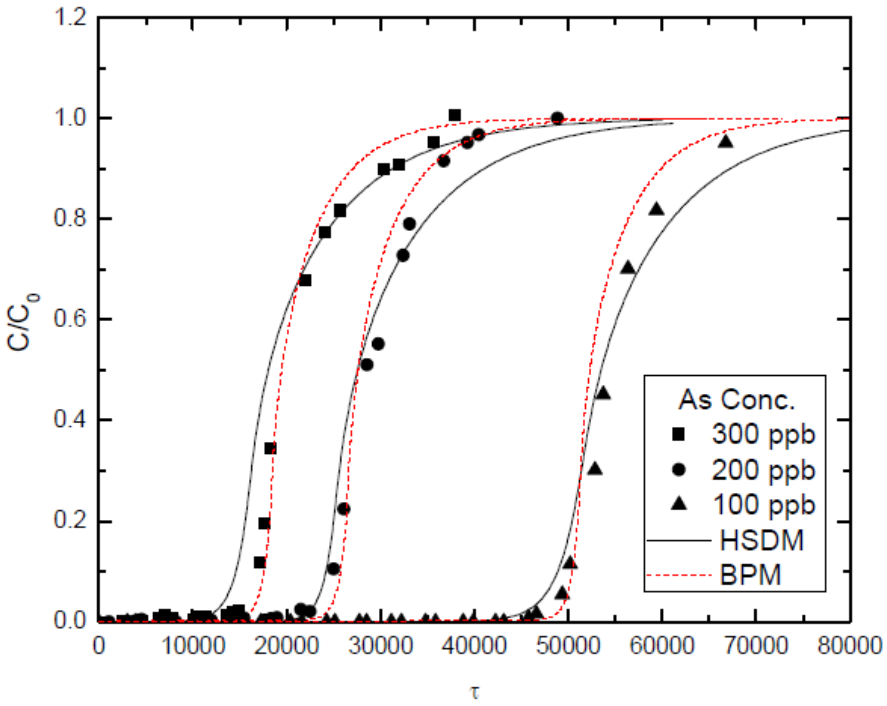

Figure 3.4. Effect of the influent As concentration on the breakthrough curves and the corresponding simulation fittings at a bed depth of 8.5 cm $\left(\overline{V}=1.0\right)$.

3.4.2.2.3. Effect of Adsorbent Particle Size

Though most experiments reported here were carried with an adsorbent sample with a particle size distribution in the range [180 – 300 μm], in order to investigate the effect of particle size on the column behavior, we also carried out column experiments with a sample with a particle size distribution in the range [90 – 180 μm]. Previously, we showed that particle size has a significant effect on the adsorption kinetics, and that the BPM seems to provide a more realistic explanation of this effect (see Table 3.2). Figure 3.5 compares column behavior (in terms of the concentration at the exit of the column as a function of τ) for the two samples with a different particle size distribution (other conditions for the experiments are influent concentration C_0(As) = 200 ppb, pH = 7.0,

and a flow rate of 8 ml/min). The results in Figure 3.5 indicate the strong influence that the particle size has on the column behavior. The experimental breakthrough time for the adsorbent with the smaller particle size (τ_{br} = 36,305) is greater than the breakthrough time of that with the larger particle size (τ_{br} = 21,812). The increased breakthrough times have also been reported by other investigators, and were explained by the faster adsorption kinetics exhibited by the smaller particles [*Vaishya et al.*, 2006; *Malkoc et al.*, 2006].

When plotting (using either the HSDM or the BPM), for example, the As(V) concentration profiles inside the particles (at a large enough τ for the column to have reached saturation) at different column positions, one notes that though for both types of adsorbents the concentration at the particle surface is very close to the equilibrium concentration value (corresponding to the bulk concentration at the position in the column) the same is not true for the interior of the particle. There, for the smaller particles the As(V) concentration is significantly higher than that for the larger particles. The differences in the concentration profiles are smaller at the inlet of the column, and larger at the end of the column, as expected. When plotting the adsorbed As(V) concentration (per unit volume of column) profiles along the length of the column, again at saturation, one again notes that the column containing the smaller particles has adsorbed more As(V). However, for large size practical columns smaller particles may result in higher flow resistances through the column [*Inglezakis et al.*, 2004]. Both the HSDM and the BPM provide a reasonable fit of the data. They also predict the differences in τ_{br}. The HSDM predicts τ_{br} values of 37,786 and 23,416, while the BPM predicts τ_{br} values of 39,072 and 25,648.

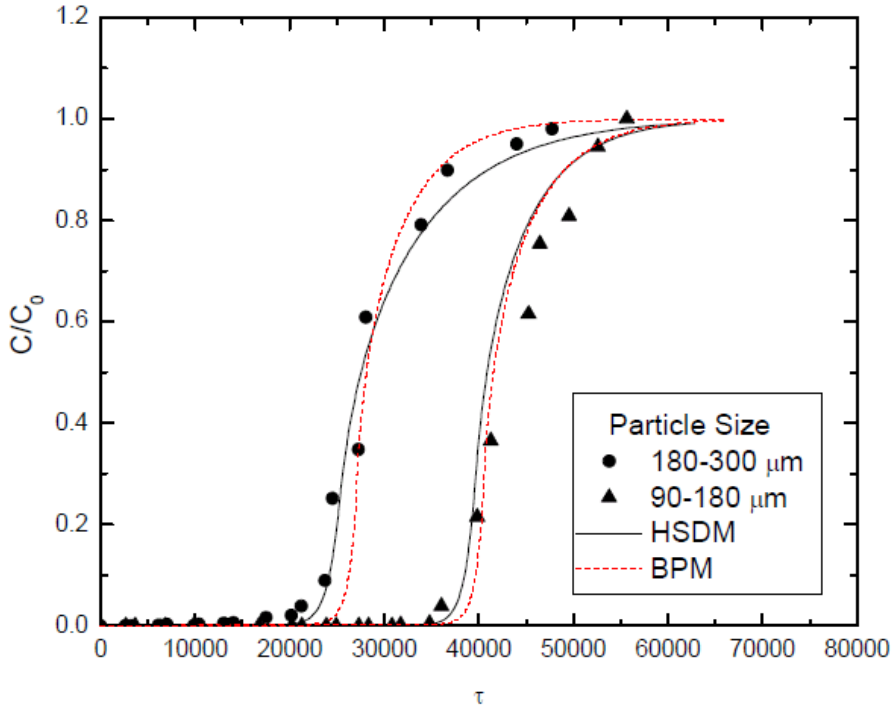

Figure 3.5. Effect of the adsorbent particle size on the breakthrough curves and the corresponding simulation fittings at a bed depth of 8.5 cm $\left(\overline{V}=1.0\right)$.

3.4.2.2.4. Effect of pH

Finally, to examine the effect that the pH has on the column behavior, experiments were carried out in which the feed pH was varied in the range [5.5 -8.5]. Figure 3.6 compares column behavior for three different pH (5.5, 7.0, and 8.5), for the adsorbent with particle size in the range [180 – 300 μm], and with an initial As concentration of 200 ppb. Lower pH generally result in better column behavior, as was expected based on the isotherm studies reported in Figure 3.1. The experimental τ_{br} are 36,521 (pH=5.5), 23,378 (pH=7), and 12,308 (pH=8.0). The corresponding τ_{br} values predicted by the HSDM are (39,308, 23,418, 14,174), while the values predicted by the BPM are (42,717, 26,052, 17,004).

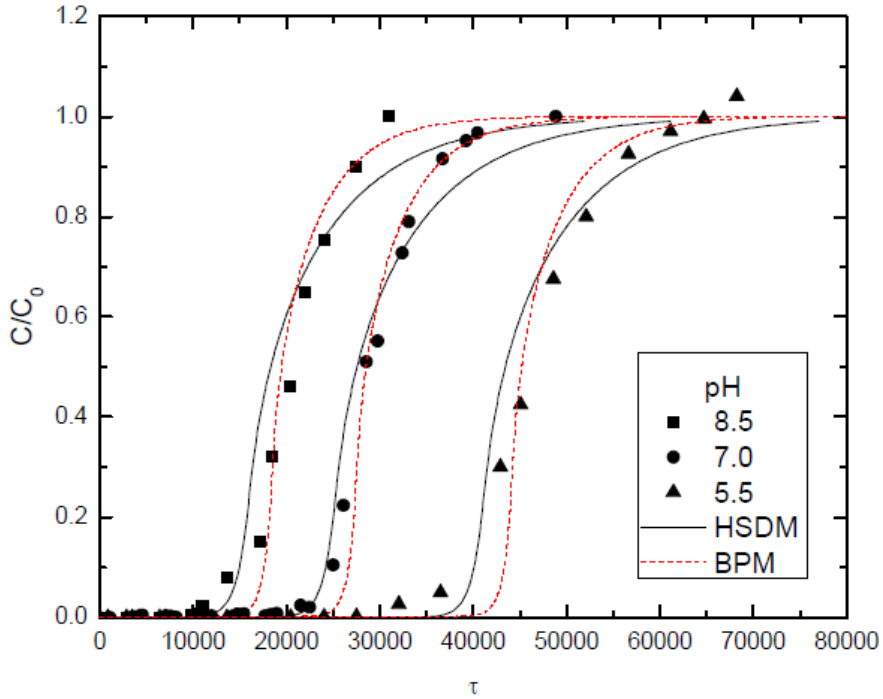

Figure 3.6. Effect of the influent stream pH on the breakthrough curves and the corresponding simulation fittings at a bed depth of 8.5 cm $\left(\overline{V}=1.0\right)$.

3.4.3. Error Analysis

It is observed from the figures above that both the HSDM and the BPM predicted the experimental data quiet well. However to have an idea that which model provides a better fit, we have compared the two models using the root mean square deviation (RMSD) (also known as the root mean square error (RMSE)) method. This method is commonly used to give a measure of the differences between the values predicted by a model (or an estimator) and the actual experimental data. The RMSD is calculated using the following formula,

$$RMSD=\sqrt{\frac{\Sigma_{i=1}^{N}(x_{1,i}-x_{2,i})^2}{N}} \tag{3.48}$$

where $x_{1,i}$ is the i_{th} experimental point value, $x_{2,i}$ is the corresponding model prediction, and N is the total number of experimental points. The Table 3.4 below indicates the

calculated RMSD for the various figures reported in this section. Based on the information provided in the Table, one cannot really conclude which model is better, as in some cases the HSDM provides a better fit (lower RMSD), while in other cases the BPM does the same.

Table 3.4. RMSD values calculated for different cases for both the HSDM and BPM for data at the 8.5 cm column height

		RMSD	
		HSDM	**BPM**
Flowrate	**6 ml/min**	0.056	0.101
	8 ml/min	0.044	0.059
	10 ml/min	0.08	0.064
	20 ml/min	0.067	0.044
Concentration	**100 ppb**	0.037	0.062
	200 ppb	0.046	0.044
	300 ppb	0.095	0.036
Particle Size	**90-180 μm**	0.064	0.051
	180-300 μm	0.045	0.062
pH	**5.5**	0.055	0.059
	7.0	0.046	0.042
	8.5	0.09	0.051

3.5. Conclusions

The focus in the section was to study As adsorption in flow column experiments. The variables examined in this study included influent As concentration, pH, sorbent particle size characteristics, and flow rate. Adsorption behavior was characterized in terms of As concentration at the exit of the column (as well as at various lengths along the column) as a function of the number of bed volumes treated by the column. A key column characteristic is the number of bed volumes at breakthrough, defined as the time when the effluent concentration is equal to 5% of the influent concentration. The experimental results show that the breakthrough time increases upon decreasing the sorbent particle size, the influent stream flow rate, and column feed concentration. It was also observed

that, as the influent pH was decreased, the column performance improved significantly, and the breakthrough times increased.

Two adsorption models (HSDM and BPM), previously developed to fit the batch experimental were applied to the column experiments. Both models predicted the qualitative trends quite well. Using the root mean square deviation (RMSD) (also known as the root mean square error (RMSE)) method to compare the two models (with respect to their ability to fit the experimental data) proved inconclusive, as in some cases HSDM provides a better fit (lower RMSD), while in other cases the BPM was superior.

4. Adsorption of Arsenic and Selenium on Conditioned Layered Double Hydroxides in the Presence of Various Competing Ions

4.1. Introduction

The ability of LDH to remove As (and Se) has been confirmed previously with both batch [*Yang et al.*, 2005; *Yang et al.*, 2006] and column experiments [*Dadwhal et al.*, 2009], but the performance of these materials in real practical conditions still needs further investigation. In other words, the ability of LDH to remove As and Se from real power plant effluents, which contain various others ions in addition to As and Se, still needs to be tested, because such ions can compete with As and Se for the available adsorption sites on LDH. Our group did carry out a preliminary study on the effect of some competing ions on As and Se adsorption capacity of uncalcined and calcined LDH in the past [*Yang et al.*, 2005]. In these studies, 10 ml of 20 ppb As and Se solutions containing additional competing ions, such as NO_3^-, CO_3^{2-}, SO_4^{2-} and HPO_4^{2-}, with concentrations ranging from 40 ppb to 1000 ppm were treated. It was found that the effect of competing anions on the adsorption of As(V) decreases in the order $HPO_4^{2-} > CO_3^{2-} > SO_4^{2-} > NO_3^-$, and for Se(IV) in the order $HPO_4^{2-} > SO_4^{2-} > CO_3^{2-} > NO_3^-$.

A few other researchers also studied the effect of competing ions on the adsorption process of As and Se on LDH; however, their efforts were limited to adsorption experiments where they study the effect of a single ion at a fixed concentration on the As and Se adsorption, with As and Se concentration also being fixed. Based on such experiments You and Zhao [2001] concluded that competing ions like phosphates, sulphates, carbonates, fluorides, chlorides, bromides, iodides and nitrates strongly affected the As adsorption on LDH in the order $HPO_4^{2-} > SO_4^{2-} > CO_3^{2-} > F^- > Cl^- > Br^- \approx$

$I^- > NO_3^-$. They also studied the affect of competing ions on selenite adsorption, and concluded that the competing anions strongly affected the adsorption behavior of SeO_3^{2-}, its adsorption increasing in the order $HPO_4^{2-} < SO_4^{2-} < CO_3^{2-} < NO_3^-$ [*You et al.*, 2001]. Similarly Wang and coworkers [*Wang et al.*, 2009] studied the affect of these competing ions on As adsorption and reported almost the same order in terms of the affect on As adsorption capacity of LDH, namely, $HPO_4^{2-} > HCO_3^{2-} > SO_4^{2-} > F^- > Cl^-$. Delorme and coworkers [*Delorme et al.*, 2007] studied the potential of removing a mixture of anionic pollutants (e.g., F^-, $HAsO_4^{2-}$, and NO_3^-) from water by mixed oxides resulting from the thermal treatment of quintinite (a Mg_4Al_2-LDH) at moderate temperatures.

To summarize the above discussion, to date no detailed investigation of how competing ions effect the As adsorption kinetics and isotherms on LDH has been published. Furthermore, prior to our investigation there was no study as to what ions are typically present in power plant effluents and at what concentration levels. How each of the ions present in these effluents affect the As adsorption, and how they compete for the available sites on LDH is, of course, very important in terms of understanding the use of these materials in real situations. The principal objective of the research presented in this section was, therefore, to understand the effect of each of these individual ions on As adsorption on LDH in both batch and column experiments at concentration levels typical of those encountered in power plant effluents. As part of our study, and prior to initiating our experimental effort, we first collected power plant effluent data in the Greater Los Angeles area in order to tabulate what their typical compositions are in terms of the concentration of As, Se and of other commons ions. We then carried out batch isotherm and kinetic experiments of As on LDH in the presence of each of the individual ions at

fixed concentrations typical to those found in power plant effluents. Packed-bed column experiments were also carried out to see whether and how the column results relate to the batch adsorption results. The HSDM and BPM are used to fit the batch data and in predicting the column behavior. We also carried further binary (As and the individual competing ion) adsorption isotherm experiments in a broader range of conditions with initial concentration ratios of As to the individual competing ion being 1:1, 1:2 and 1:4 respectively, in order to better understand how these ions compete for the available adsorption sites and how they affect each other's adsorption. In addition we also carried out kinetic experiments in the presence of all the ions to study their additive effect on the As adsorption capacity of LDH. The experimental results obtained, and presented in this section, are instructive we believe towards gaining a better understanding of the potential and limitations of the use of conditioned LDHs for the treatment of power plant effluents and the remediation of trace levels of As found in these effluents.

4.2. The Composition of Power Plant Effluents

As part of our study we collected data on various power plant effluents in the Greater Los Angeles area, the goal here being to identify the concentrations of the various species present in these effluents. The data were collected with collaboration from the Department of Water Quality in Los Angeles and are reported in Tables 4.1 and 4.2. Table 4.1 tabulates the concentrations of the heavy metals, and Table 4.2 shows the concentrations of common anions found in these effluents. Based on these data, the following average metal and anion concentrations were selected to represent a typical power plant effluent for our batch and column experiments.

As and Se concentration: 20 ppb

Anion concentration:

F^-: 1 ppm; **NO_3^-:** 5 ppm; **Cl^-:** 100 ppm; **CO_3^{2-}:** 5 ppm; **SO_4^{2-}:** 100 ppm; **PO_4^{2-}:** 1 ppm

pH: 8.0

Table 4.1. As and Se concentrations in various power-plant effluents

Station	Month (2006-2007)	As (ppb)	Se (ppb)
Haynes	May	172.00	ND
		179.00	
		174.00	
		1.10	
Harbor	Jan	1.18	0.60
		6.35	5.90
Aes Alamitos	Oct	1.44	0.04
		1.56	0.02
		0.78	0.01
		0.92	0.02
		4.56	1.20
Long Beach	Dec	1.40	0.02
		5.00	ND
		4.00	
		3.50	
		4.20	1.30
Long Beach Range	Jan	2.6 – 4.6	0.2 – 0.3
		5.2-9.8	1.0 – 1.4
Mandalay	March	10.00	5.00
		6.01	10.00
Scattergood	May	185.00	2.90
		179.00	2.00
		195.00	4.10
		159.00	2.50
	June	7.23	0.33
El Segundo	June	0.21	0.06
		1.58	0.04
		1.06	0.03
		1.56	0.01
		2.15	0.07

Table 4.2. Concentration of various ions present in power-plant effluents

Parameters	Units	Long Beach	Aes Alamitos	Redondo	Mandalay	El Segundo Refinery
pH		7.78	7.6	7-8.3	7.6-7.9	8-8.1
Temp	°F			60 - 85	60-80	
Chlorine	ppm			0.01 - 0.10	0.08-0.17	
$CaCO_3$	ppm	3.9	5.98			
Ammonia (as N)	ppm	0.9 - 2.2			0.1	12.5
Organic N	ppm	ND - 1.8				
Nitrite (as N)	ppm	ND - 0.17		0.1	0.1	
Nitrate (as N)	ppm	3.58 - 7.89		2.5	0.1	
Nitrate + Nitrite	ppm	3.62 - 7.93		2.5-4.0	0.6	
TOTAL Nitrogen	ppm	2.7 - 10.4		4.5-5.5	3.5	
Chloride (Cl-)	ppm	107 - 124 (215)	80-90	75-105	60-80	
Sulphate (SO4--)	ppm	61-118 (448)	50-85	70-85	45	
Ortho Phosphate-P	ppm	ND - 2.9	ND	ND	ND	
Total Phosphate	ppm	ND - 3.2	ND	ND	ND	
Total Phosphorus	ppm	ND - 1.04	ND	ND	ND	
Sulfide	ppm					0.75

4.3. Experimental

4.3.1. Materials

The sorbent material used in all the experiments is conditioned Mg-Al-CO_3-LDH with a Mg/Al mole ratio of 2.87, except for the Se adsorption experiments where we also

used calcined LDH. The LDH was prepared by the co-precipitation method described before. To obtain different particle size fractions, the LDH was crushed and sieved using standard testing sieves (VWR). The size fraction collected at 50-80 mesh (180-300 μm) was used for all the experiments reported in this section.

As and Se were the metals investigated in the study in the presence of various competing ions such as fluorides (F^-), nitrates (NO_3^-), chlorides (Cl^-), carbonates (CO_3^{2-}), sulphates (SO_4^{2-}) and phosphates (PO_4^{2-}). The As and Se solutions used for the adsorption experiments were prepared from As_2O_5 and Na_2SeO_3 powder purchased from Sigma Aldrich using deionized water. The solutions with various ion concentrations were prepared using NaF, $NaNO_3$, NaCl, Na_2CO_3, Na_2SO_4 and K_2HPO_4 salts.

4.3.2. Batch Sorption Experiments

No effort was made to minimize contact with the atmospheric air during the preparation of the various solutions. For the adsorption experiments, the pH of the working solution was adjusted to the desired initial value (around 8.0) using 0.1M NaOH solution. The pH was not adjusted during the adsorption period, but any pH drift was measured and recorded using an Acumet Basic AB 15 pH meter. All the experiments were performed at 298 K and 170 rpm in 1000 mL polyethylene bottles, and with an adsorbent particle size of 180-300 μm, and an adsorbent loading (dose) of 0.016 g/L.

The As and Se concentration was determined by the ICP-MS (Perkin-Elmer ELAN-9000). In order to measure the nitrates, fluorides and chlorides concentration, we have used the corresponding ion-selective electrodes purchased from Daigger. The reproducibility of the measurement with these electrodes was ±2%. To measure phosphates and sulphates, we carried out lead-perchlorate titrations, and used a

corresponding lead ion-selective electrode. The error involved in the measurement of phosphates and sulphates was around ±4%. The carbonates concentration, on the other hand, was measured by titrating with HCl, using a phenolphthalein indicator with a corresponding error of ±2%.

4.3.2.1. Adsorption Isotherm Experiments

4.3.2.1.1. Adsorption Isotherms of Competing Ions

Before carrying out experiments on the effect of competing anions on As concentration we carried out isotherm experiments in order to investigate the adsorption capacity of the various single ions on LDH in the absence of the metals. The experiments were performed with 500 ml aqueous solutions of various individual salts with predetermined initial concentration ranging from 20 ppb to 5000 ppb at 298 K with 8 mg of the 180-300 μm conditioned LDH. The bottles containing the salt and the LDH suspension were then shaken at 170 rpm for at least 5 days or as long as it is needed in order for the adsorption to reach equilibrium. The mixture in each bottle was then centrifuged and the ion concentrations in the supernatant solution were determined.

4.3.2.1.2. Adsorption Isotherms of As and Individual Competing Ions

The adsorption isotherms of As in the presence of individual anions at initial concentrations equal to the level found in the "typical" power plant effluent were investigated. To carry out these experiments, we varied the initial As(V) concentration from 20 to 240 ppb while the initial competing ion concentration remained constant. For the experiments a constant mass of 8 mg of LDH was added to 500 mL aqueous solutions. The bottles containing the LDH suspension, the As and the competing ion were kept in a reciprocal shaking water-bath (Precision model 25) and were shaken at 170 rpm

for 5 days, a time that was confirmed to be long enough for the adsorption on the LDH to reach equilibrium. The mixture in each bottle was then centrifuged and the As and the final competing ion concentration in the supernatant solutions were determined.

Binary adsorption isotherms of As and the individual competing ions for a broader range of competing ion concentrations were also investigated. For these experiments we utilized ratios of the initial concentration of As to competing ion equal to 1:1, 1:2 and 1:4 and the aqueous solutions of As(V) of predetermined concentration ranging from 20 to 5000 ppb were mixed with the corresponding concentrations of the competing individual salts, namely fluorides, nitrates, chlorides, carbonates, sulphates and phosphates. The other experimental conditions are similar with those for the fixed competing ion concentration experiments.

4.3.2.2. Kinetic Experiments

4.3.2.2.1. As Adsorption Kinetics in the Presence of Individual Competing Ions

In order to further understand the effect of the individual competing ions, we measured the kinetics for As(V) adsorption in the presence of the individual salts at initial concentration levels equal to those in the typical power plant effluents. For these experiments As(V) solutions with an initial concentration of 20 ppb were prepared with addition of the individual salts. 8 mg of the adsorbent was added to 500 ml of aqueous solution containing As and the individual salt in 1000 ml flasks, which were then shaken at 170 rpm. At selected time intervals, samples were extracted and centrifuged, and the As concentrations as well as the dissolved individual ion concentration were measured.

In order to further quantify the effect of these competing ions, we varied the initial concentrations of these ions, while keeping the As concentration constant at 20 ppb. For

these kinetic experiments, 8 mg of LDH were accurately weighed and added to 500 ml of 20 ppb As(V) solutions containing various individual competing ions, with their initial concentrations ranging from 10 ppb to 100 ppm. Samples were withdrawn at regular time intervals, centrifuged and the As concentration determined using ICP-MS.

Then we carried out another set of kinetic experiments to study the additive effect of these ions on As adsorption capacity of LDH. For these experiments 7 different bottles were used with As initial concentration of 60 ppb for which the amount of LDH used was 30 mg. The initial composition of the bottles is shown in Table 4.3. Samples were withdrawn at regular time intervals, centrifuged and the As concentration determined using ICP-MS.

Table 4.3. Initial composition of bottles for the As kinetic experiments

Bottle No.	As (60 ppb) + Ions (1 ppm each)
1	As
2	As + Fl^-
3	As + Fl^- + NO_3^-
4	As + Fl^-+ NO_3^-+ Cl^-
5	As + Fl^- + NO_3^- + Cl^- + CO_3^{2-}
6	As + Fl^- + NO_3^- + Cl^- + CO_3^{2-} + SO_4^{2-}
7	As + Fl^- + NO_3^- + Cl^- + CO_3^{2-} + SO_4^{2-} + PO_4^{2-}

4.3.2.3. Adsorption of Se in the Presence of Individual Competing Ions

We have also studied the effect of competing ions on Se adsorption on LDH. For these experiments, the LDH was accurately weighed (1.2 mg) and added to 10 ml of 20 ppb Se solutions containing additional competing ions, such as fluorides, nitrates, chlorides, carbonates, sulphates and phosphates, with concentrations ranging from 40 ppb to 100 ppm. For Se the adsorption experiments were carried out on both calcined as well as conditioned LDH. The bottles containing the LDH suspension, the Se and the

competing ion were placed in the reciprocal shaking water-bath (Precision model 25) and were shaken at 170 rpm for 5 days. The mixture in each bottle was then centrifuged and the Se concentrations in the supernatant solutions were determined by ICP-MS.

4.3.3. Column Experiments for As Removal in the Presence of Individual Competing Ions

Fixed-bed experiments were conducted in laboratory glass columns with internal diameter, $D = 0.7$ cm, and a height, $H = 8.5$ cm. The column was packed with conditioned LDH (cotton-wool was placed at the bottom of the column to prevent the LDH particles from eluding from the column during the flow experiments). It was then rinsed with deionized water for 24 h to ensure that the LDH particles were densely packed prior to the initiation of the experiments. The feed solution containing As and the individual competing ion, with a prescribed initial concentration and pH, was then continuously pumped in a down-flow mode from the reservoir through the columns at a flow rate of 2 ml/min using a peristaltic pump (Alitea model-XV). During the study, the performance of the pump was checked periodically by collecting solution samples at the outlet of the column for predetermined periods of time. Four sample ports (located at heights of 2.2, 4.4, 6.6, and 8.5 cm) enabled withdrawing samples from the column for the analysis using 3 cm^3 sample syringes. Samples were taken at regular time intervals, until the metal ion concentration in the effluent stream at the bottom of the bed became equal to the feed concentration. The metal ion concentrations were determined using ICP-MS. The pH of the influent solution was adjusted (in the reservoir) to 8.0 using 0.1 M NaOH solutions. No pH adjustment was done in the column, but the pH of the effluent from the column was measured and recorded with an Accumet Basic AB 15 pH meter.

There was not much change in the pH of the solution in the column, with the effluent pH being typically 0.1 to 0.2 pH units higher than the pH of the feed. All column experiments were carried out at 25 °C. Temperature control was carried out by controlling the temperature of the feed solution, and by wrapping the column up with a flexible coil through which water at 25 °C was circulated.

4.4. Results and Discussion

4.4.1. Adsorption Isotherms of the Competing Ions

Adsorption isotherm data for the various competing ions are shown in Figure 4.1. We used the Sips isotherm to fit the data, which is given by

$$q = \frac{Kq_s C^n}{1 + KC^n} \tag{4.1}$$

where q_s and K are the maximum sorption capacity and the Sips constant respectively, and n is the parameter characterizing the system heterogeneity. The fitted Sips parameters and the goodness of fit (R^2) are shown in Table 4.4 and the corresponding plots are shown in Figure 4.1, where points represent the experimental data and the solid lines represents the Sips isotherm fits. Of all ions the carbonates get adsorbed the most on conditioned LDH with q_s being 46010.4 µg/g, followed by sulphates, phosphates, fluorides, chlorides and nitrates which get adsorbed the least with q_s being 30017.3 µg/g. The adsorption data in Figure 4.1 are in agreement with the fact that the LDHs are known to have greater affinities for multivalent (CO_3^{2-}, SO_4^{2-} and PO_4^{2-}) rather than monovalent anions (Fl^-, Cl^- and NO_3^-) [*Miyata*, 1983; *Rives*, 2001]. The K values also decrease in the same order as the q_s values for the various ions, being the highest for carbonates (0.029

l/g) and the lowest for nitrates (0.006 l/g). All ions have fairly high n values, the highest being ~0.95 for nitrates, indicative of single site adsorption.

Table 4.4. Sips isotherm parameters for various competing anions on conditioned LDH

Sips Isotherm				
	q_s **(µg/g)**	K **(l/g)**	n	R^2
Carbonates	46010.4	0.029	0.88	0.99
Sulphates	41868.4	0.019	0.89	0.99
Phosphates	38251.1	0.018	0.90	0.99
Fluorides	34927.2	0.013	0.90	0.99
Chlorides	32394.7	0.011	0.92	0.99
Nitrates	30017.3	0.006	0.95	0.99

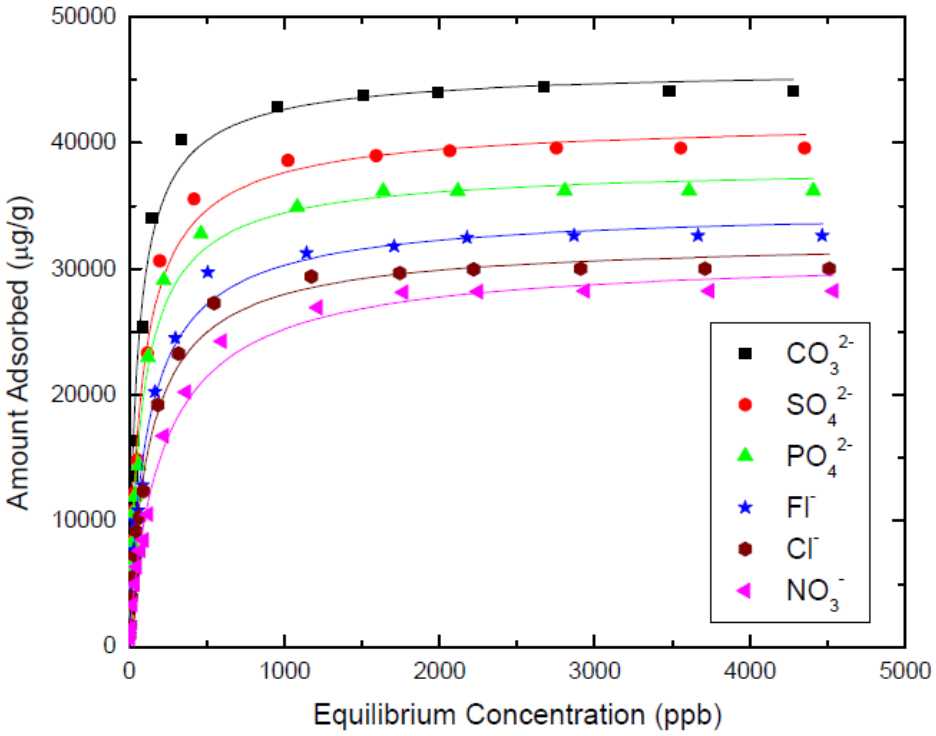

Figure 4.1. Adsorption isotherms for the various anions on conditioned LDH.

4.4.2. Adsorption Isotherms of As in the Presence of Competing Ions

As adsorption isotherms in the presence of the competing ions at a fixed initial concentration of that of the "typical" power plant effluents are shown in Figure 4.2,

where the points represent the experimental data and the solid lines represent the Sips fits. The various fitted isotherm parameters (and the "goodness of fit", as manifested by the R^2 test) are reported in Table 4.5, and Table 4.6 reports the initial and final competing ion concentrations as a function of initial As concentration (Note that the concentration changes for the chlorides and sulfates are less that the experimental measurement error). Note that the presence of various anions significantly affects the parameters of the Sips isotherm. Though fluorides and nitrates have a relatively minor impact on the maximum adsorption q_s, they do impact the adsorption equilibrium constant K. On the other hand, chlorides, carbonates, sulphates, and phosphates impact severely both the q_s as well as the K.

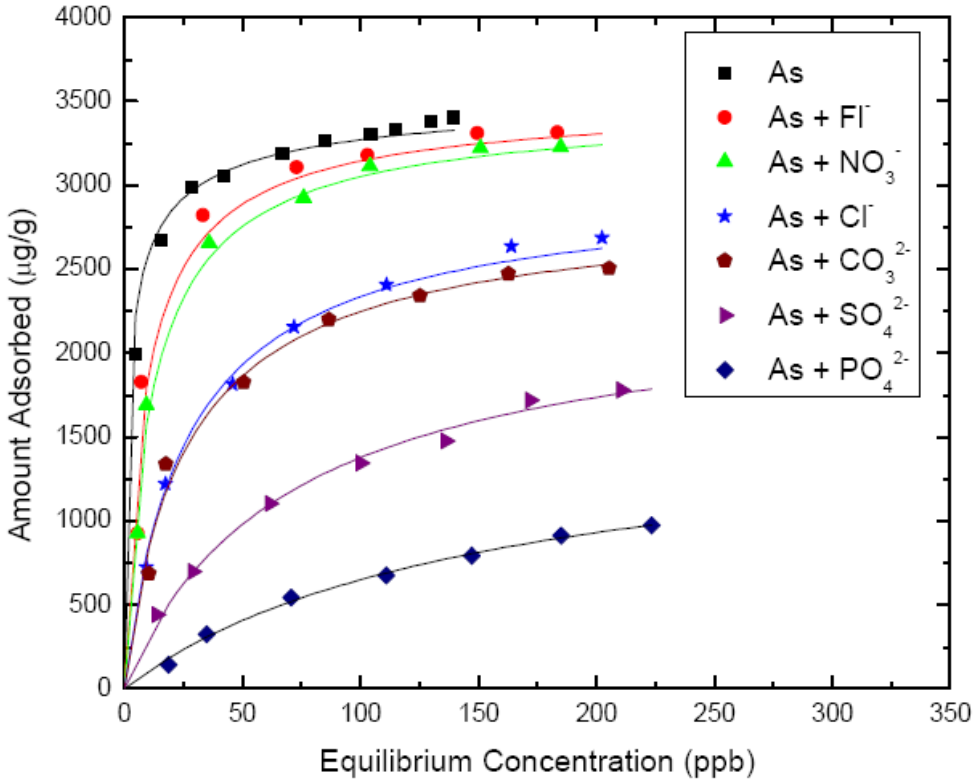

Figure 4.2. Adsorption isotherms for As(V) on conditioned LDH in the presence of various individual competing ions at a fixed initial concentration and the Sips fit.

For example, the K value in the presence of phosphates is ~93 times less than that for the pure As, while the q_s value is ~2.2 lower. Interestingly enough, for all competing anions the exponent n changes from the value of ~ 0.5 (that signifies a dual site adsorption mechanism) to a value that is much closer to 1.

Table 4.5. Sorption isotherm parameters for As(V) uptake on conditioned LDH in the presence of various competing ions

Sips Isotherm				
	q_s **(μg/g)**	K **(l/g)**	n	R^2
Arsenic	3619.9	0.649	0.58	0.91
Arsenic (Fluorides)	3516.2	0.143	0.88	0.94
Arsenic (Nitrates)	3479.3	0.107	0.91	0.98
Arsenic (Chlorides)	3015.5	0.043	0.95	0.99
Arsenic (Carbonates)	2910.9	0.047	0.93	0.98
Arsenic (Sulphates)	2386.6	0.017	0.97	0.99
Arsenic (Phosphates)	1678.1	0.007	0.98	0.99

Table 4.6. Reduction in the competing ion concentrations during the isotherm experiments as a function of As concentration

	Arsenic Concentration (ppb)	**Initial Ion Concentration (ppm)**	**Final Ion Concentration (ppm)**
Fluorides	20	1	0.51
	40	1	0.52
	80	1	0.54
	120	1	0.55
	160	1	0.56
	200	1	0.56
	240	1	0.56
Nitrates	20	5	4.54
	40	5	4.55
	80	5	4.56
	120	5	4.58
	160	5	4.60
	200	5	4.61
	240	5	4.63
	20	100	99.5

Chlorides	40	100	99.5
	80	100	99.5
	120	100	99.5
	160	100	99.5
	200	100	99.5
	240	100	99.6
Carbonates	20	5	4.28
	40	5	4.29
	80	5	4.30
	120	5	4.31
	160	5	4.32
	200	5	4.34
	240	5	4.35
Sulphates	20	100	99.3
	40	100	99.3
	80	100	99.3
	120	100	99.3
	160	100	99.3
	200	100	99.3
	240	100	99.3
Phosphates	20	1	0.42
	40	1	0.44
	80	1	0.44
	120	1	0.46
	160	1	0.46
	200	1	0.46
	240	1	0.46

4.4.3. Adsorption Kinetics

Figure 4.3 shows the adsorption kinetics of 20 ppb As solution for the initial solution pH of 8.0 measured in the presence of various individual competing ions at concentration levels typically present in the power plant effluents. It can be seen that phosphates have the most effect on As adsorption, with an almost 87% reduction in the final adsorption capacity, followed by sulfates causing a 53% reduction, and carbonates and chlorides which cause almost 29% reduction. Fluorides and nitrates, on the other hand, do not have much effect on the As adsorption, at least at the concentrations selected. All the batch

adsorption experiments were repeated thrice, and the average concentration values are plotted in the figure. The affect of these ions can be explained by the fact that the LDHs have greater affinities for anions with higher charge density i.e. the tendency of multi-charged anions to get adsorbed is more than that of monovalent anions. Similar results have been reported by You *et al.* where they study the release of As(III) adsorbed on calcined LDH as a function of different competing anions [*You et al.*, 2001] and the adsorption of Se on LDH as a function of total anion concentration [*You et al.*, 2001].

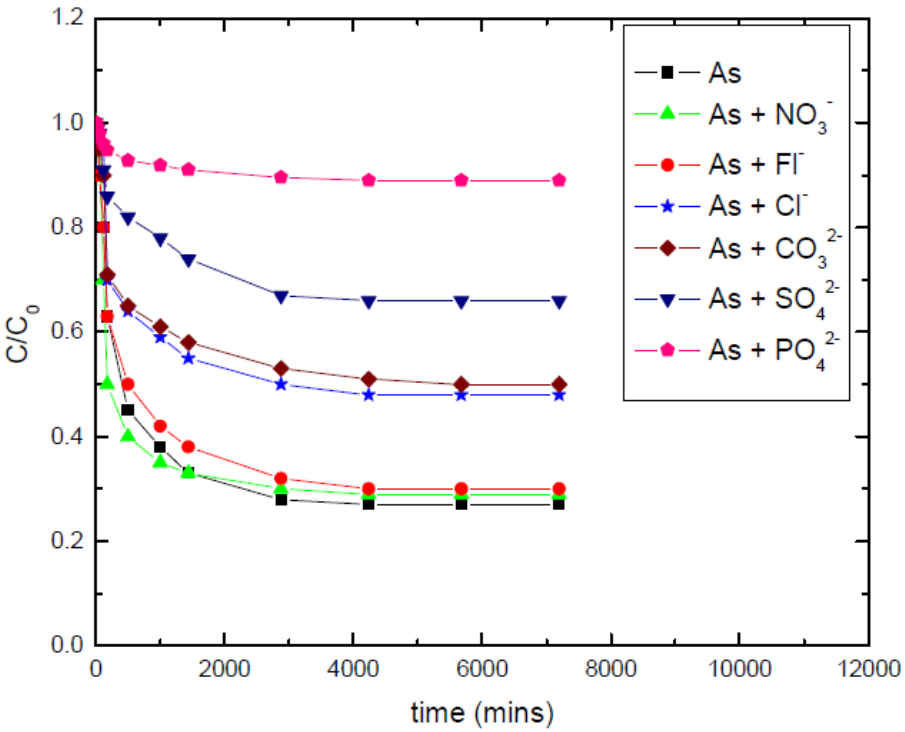

Figure 4.3. Adsorption of 20 ppb As solution as a function of time by (180-300 μm) LDH particles in the presence of various individual competing ions at concentration levels found in typical power plant effluents.

We analyzed the kinetic data using the HSDM and the BPM described in the previous section, in order to use the fitted parameters to predict packed column behavior. Figures 4.4a - 4.4g, in addition to the adsorption data also report the fitted lines obtained using the HSDM (the solid lines in the figure) and the BPM (the broken lines in the

figure). Table 4.7 reports the corresponding surface diffusivity values for the HSDM as well as the corresponding mesopore diffusivity and micropore diffusivity values for the BPM. It is seen from Table 4.7 that the surface diffusivity of the As anion decreases in the presence of the competing anions, being $8.31\times10^{-11} cm^2 s^{-1}$ for the As alone, and decreasing to $5.99\times10^{-11} cm^2 s^{-1}$ in the presence of phosphates.

In case of BPM, the basic assumption made is that the adsorbent particle is an agglomerate of a number of equal size, single crystal microparticles, and since we have no data about the size of the microparticle we report values of $\frac{D_\mu}{R_\mu^{\,2}}$ instead of D_μ. It also assumes that before the metal anion adsorbs inside the microparticle structure, it must be transported from the particle surface, through the intercrystalline region, to the surface of the microparticles. The diffusivity of this intercrystalline region is called the mesopore diffusivity, and it is observed that this diffusivity is not affected by the presence of the various ions and stays constant at a value of $0.48\times10^{-6} cm^2 s^{-1}$ irrespective of the various ions. However the micropore diffusivity ($\frac{D_\mu}{R_\mu^{\,2}}$) does depend on the presence of various ions and decreases in the presence of the competing ions form a value of $0.86\times10^{-6} s^{-1}$ for the As alone to $0.19\times10^{-6} s^{-1}$ in the presence of phosphates.

From both the isotherm as well as the kinetic adsorption experiments it can be concluded that the As adsorption capacity decreases in the presence of various individual competing ions in the order $PO_4^{2-} > SO_4^{2-} > CO_3^{2-} > Cl^- > NO_3^- \approx F^-$. The order observed is very similar to that observed by other research groups [*You et al.*, 20001; *Delorme et al.*, 2007; *Wang et al.*, 2009] as described above.

Table 4.7. Fitted diffusion coefficients for HSDM and BPM for the As experiments in the presence of various competing ions

	D_i (× 10^{11} cm^2 s^{-1})	R^2	D_M (× 10^6 cm^2 s^{-1})	$\frac{D_\mu}{R_\mu^2}$ (× 10^6 s^{-1})	R^2
As	8.31	0.75	0.48	0.86	0.75
As (Fl^-)	8.23	0.70	0.48	0.84	0.70
As (NO_3^-)	8.09	0.85	0.48	0.83	0.85
As (Cl^-)	7.57	0.83	0.48	0.59	0.83
As (CO_3^{2-})	7.32	0.88	0.48	0.47	0.88
As (SO_4^{2-})	6.97	0.89	0.48	0.39	0.89
As (PO_4^{2-})	5.99	0.84	0.48	0.19	0.84

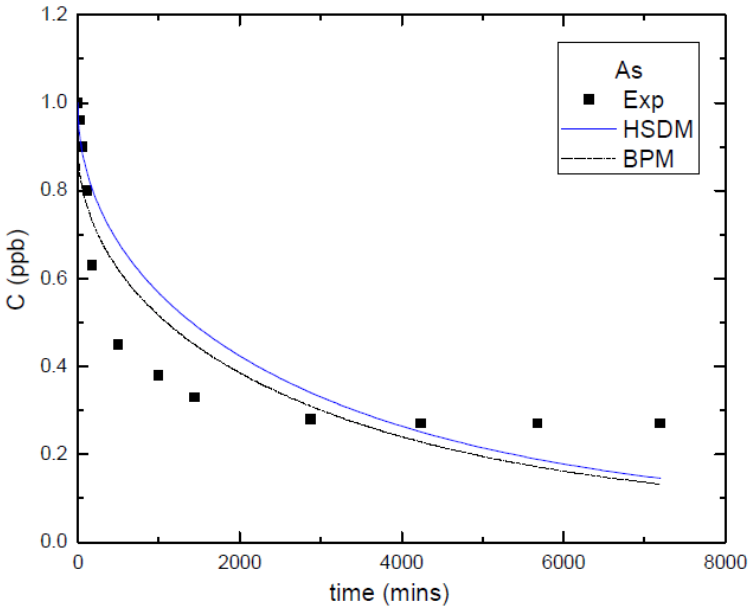

(a)

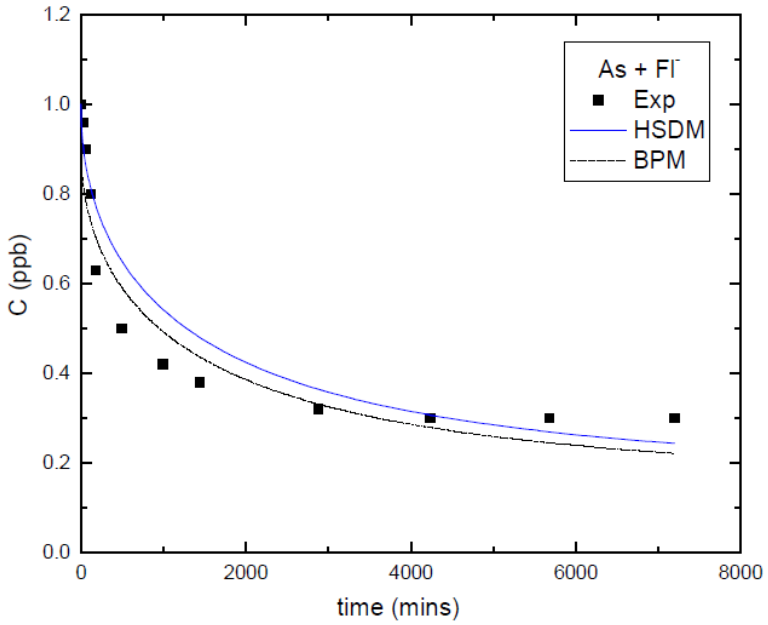
As + Fl-
Exp
HSDM
BPM
C (ppb)
time (mins)
0.0
0.2
0.4
0.6
0.8
1.0
1.2
0
2000
4000
6000
8000

(b)

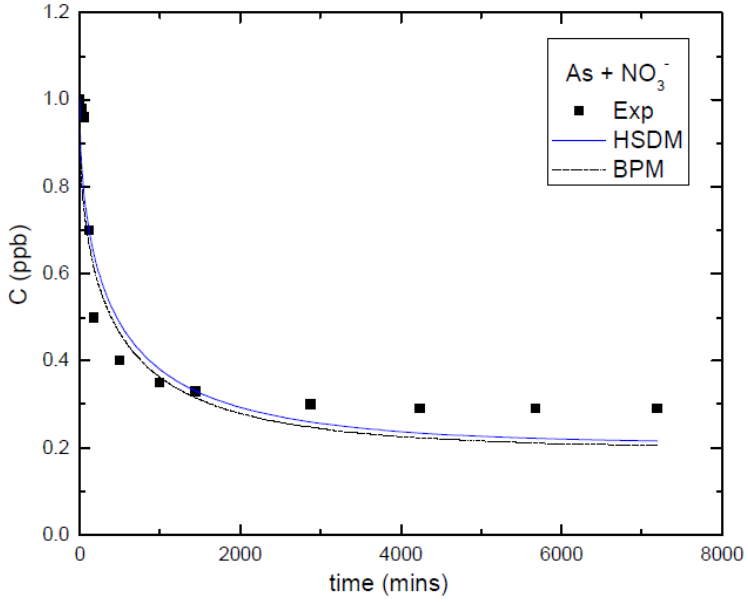
As + NO3-
Exp
HSDM
BPM
C (ppb)
time (mins)
0.0
0.2
0.4
0.6
0.8
1.0
1.2
0
2000
4000
6000
8000

(c)

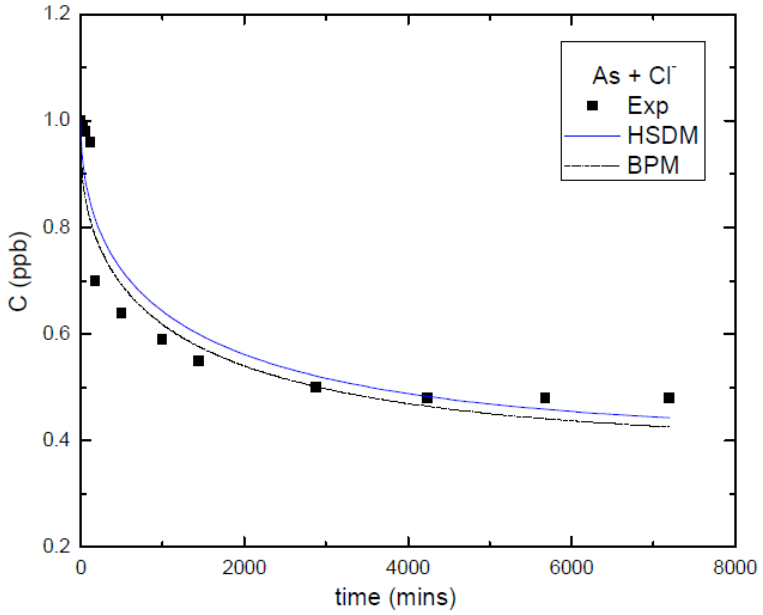
As + Cl-
Exp
HSDM
BPM
C (ppb)
time (mins)
1.2
1.0
0.8
0.6
0.4
0.2
0
2000
4000
6000
8000

(d)

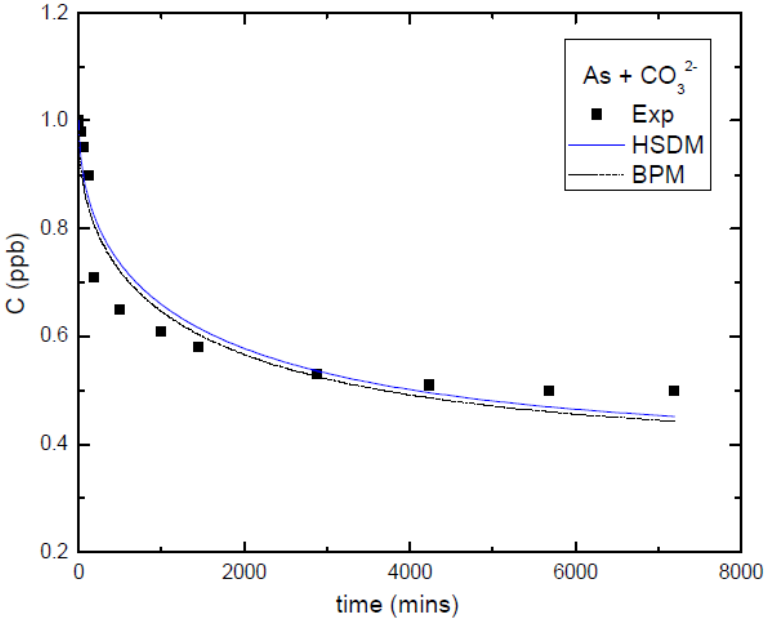
As + CO3 2-
Exp
HSDM
BPM
C (ppb)
time (mins)
1.2
1.0
0.8
0.6
0.4
0.2
0
2000
4000
6000
8000

(e)

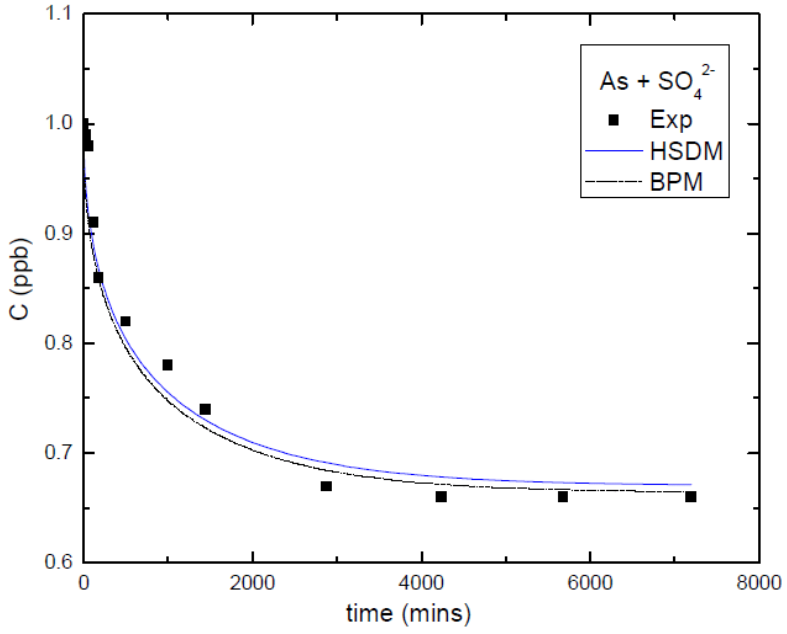

(f)

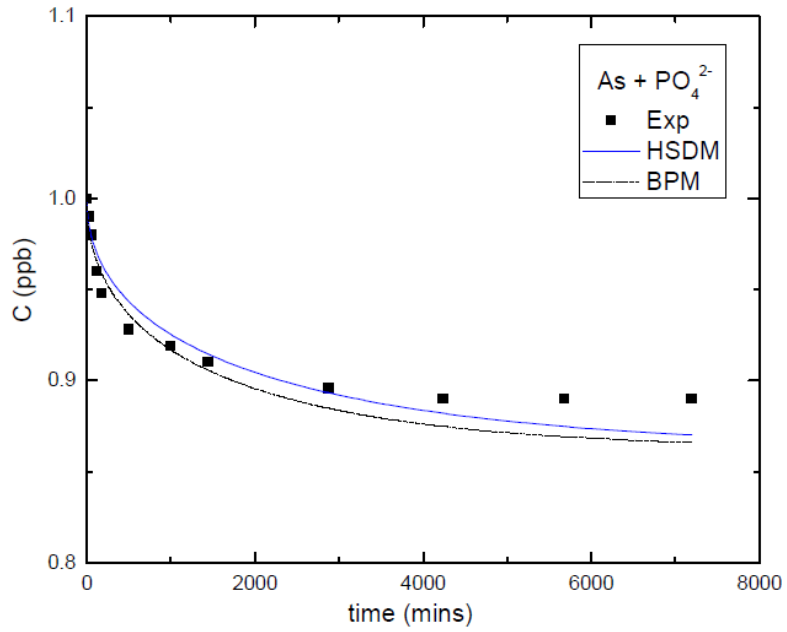

(g)

Figure 4.4. HSDM and BPM fits for the adsorption of 20 ppb As solution as function of time by (180-300 μm) LDH particles in the presence of various individual competing ions at concentration levels found in typical power plant effluents.

During the kinetic experiments of As adsorption by the LDH particles in the presence of various individual competing ions we also measured the reduction in the competing anion concentration for fluorides, nitrates, carbonates, and phosphates as a function of time and the results are shown in Figures 4.5 (for sulfates and chlorides the concentration changes are within the experimental error). It can be seen that the adsorption of these ions on LDH follows a similar pattern with that of As with fast adsorption first, followed then by a slow uptake.

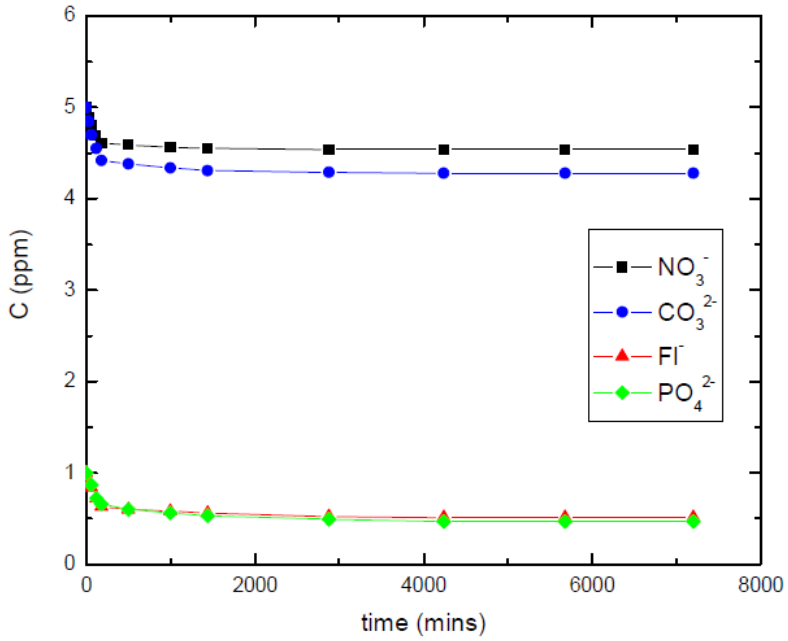

Figure 4.5. Reduction in the competing ion concentration as a function of time during As adsorption.

We also varied the initial concentration of the individual ions (from 10 ppb to 100 ppm) in the As adsorption experiments in order to understand the effect that the initial concentration levels of these ions has on adsorption kinetics. The results are shown in Figures 4.6a – 4.6f. It is observed that for fluorides and nitrates, if their initial concentration in the aqueous solution is 5 ppm and 100 ppb respectively, then they hardly

affect the As adsorption capacity on LDH, however chlorides, carbonates, sulphates and phosphates present at 100 ppb levels, cause 3%, 3%, 4% and 41% reduction respectively. On the other hand when these ions are present at 100 ppm levels, they reduce the As adsorption capacity by 22%, 22%, 29%, 42%, 53% and 96% for fluorides, nitrates, chlorides, carbonates, sulphates and phosphates respectively.

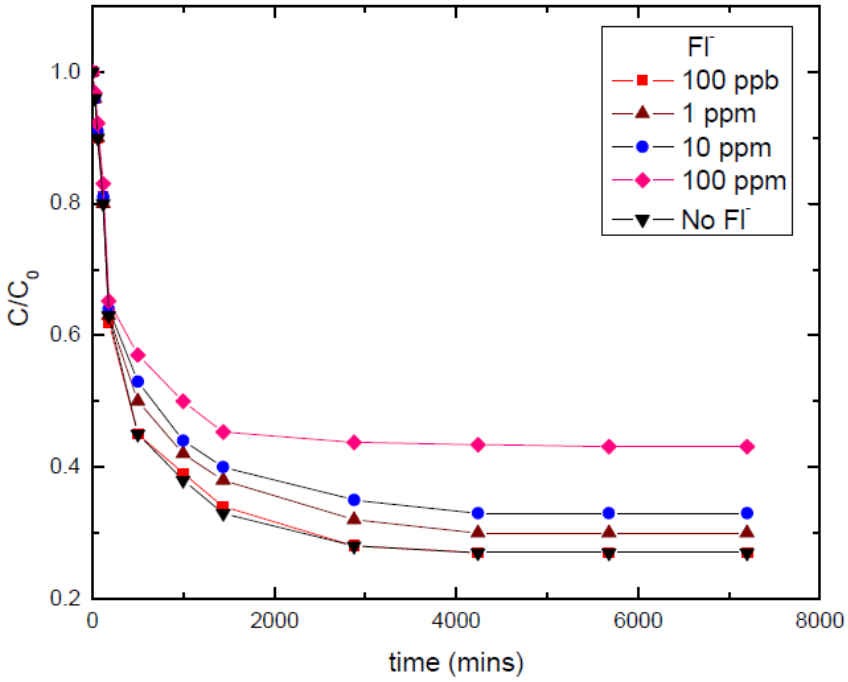

(a)

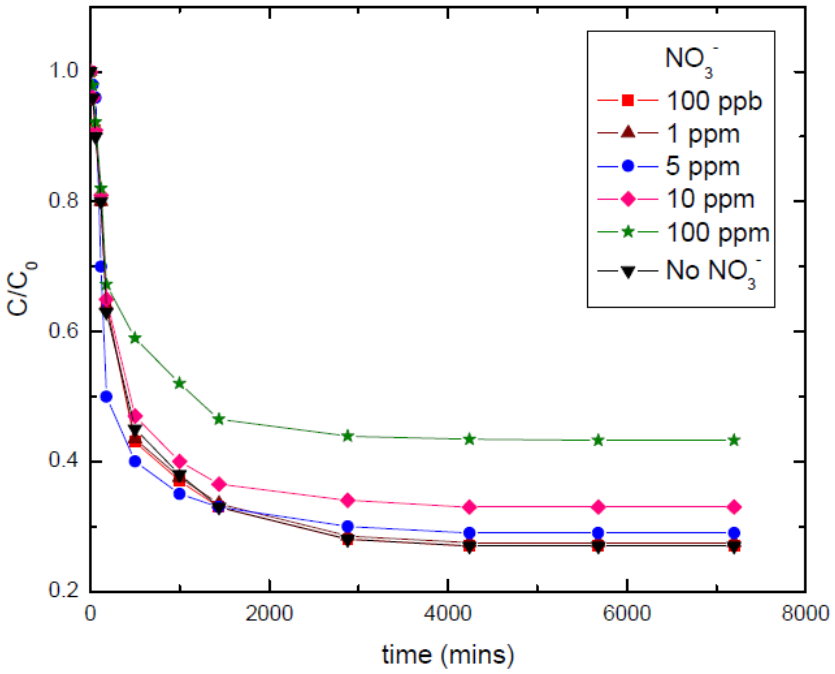
NO3-
100 ppb
1 ppm
5 ppm
10 ppm
100 ppm
No NO3-
C/C0
time (mins)
1.0
0.8
0.6
0.4
0.2
0
2000
4000
6000
8000

(b)

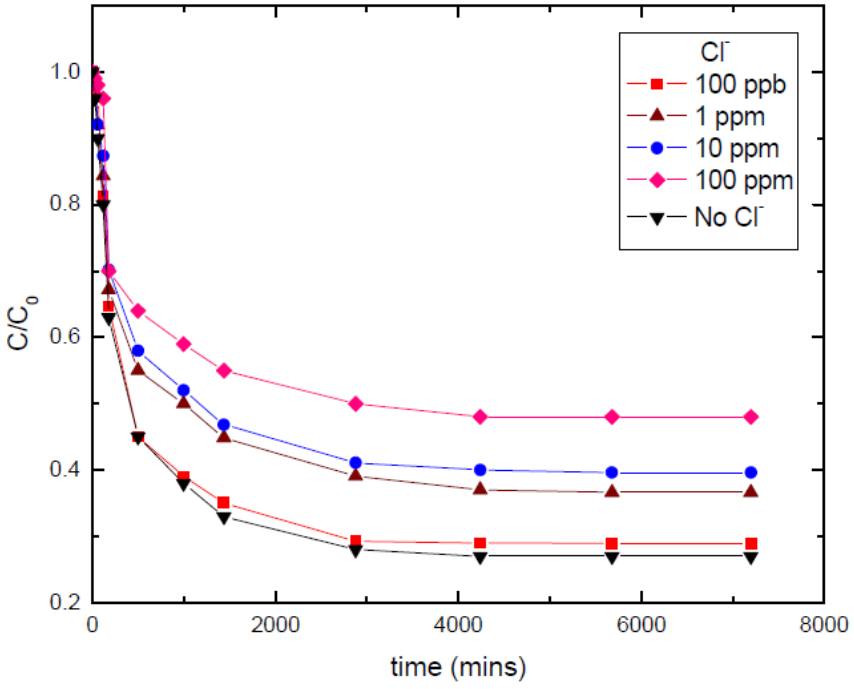
Cl-
100 ppb
1 ppm
10 ppm
100 ppm
No Cl-
C/C0
time (mins)
1.0
0.8
0.6
0.4
0.2
0
2000
4000
6000
8000

(c)

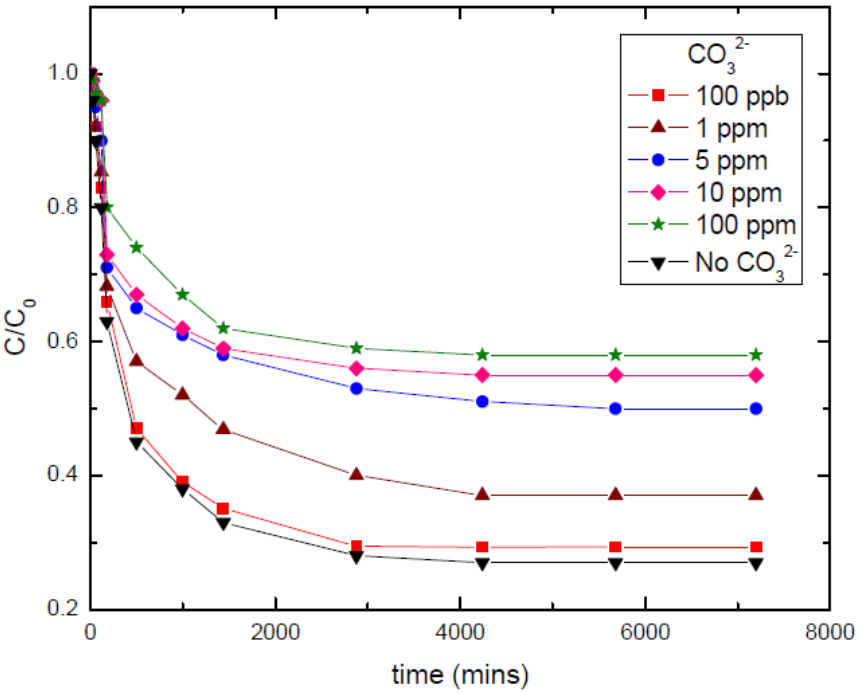
CO_3^{2-}
100 ppb
1 ppm
5 ppm
10 ppm
100 ppm
No CO_3^{2-}
C/C0
time (mins)
1.0
0.8
0.6
0.4
0.2
0
2000
4000
6000
8000

(d)

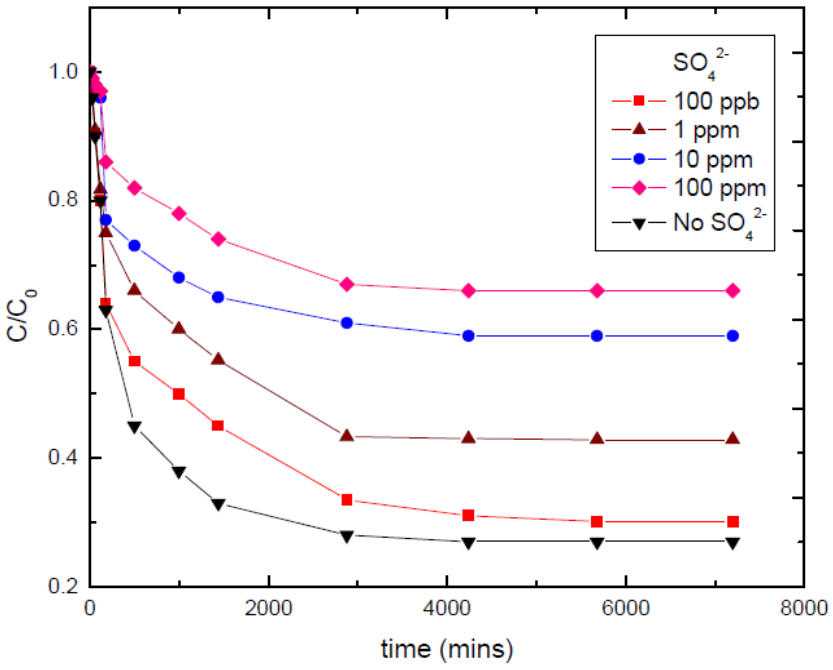
SO_4^{2-}
100 ppb
1 ppm
10 ppm
100 ppm
No SO_4^{2-}
C/C0
time (mins)
1.0
0.8
0.6
0.4
0.2
0
2000
4000
6000
8000

(e)

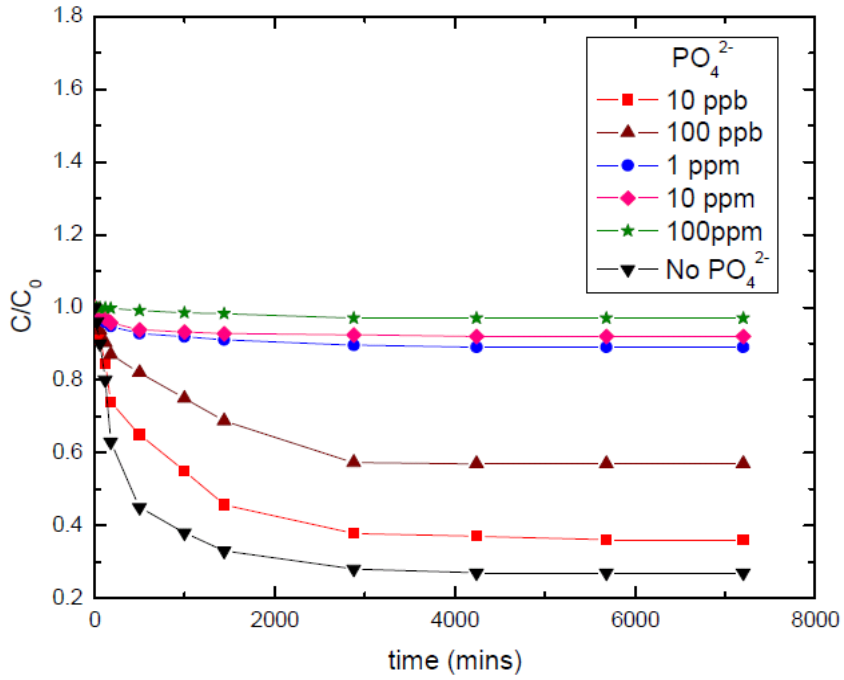

(f)

Figure 4.6. Reduction in As concentration as a function of time in the presence of various individual competing ions as a function of competing ion concentration.

Figure 4.7 shows the additive effect of the various ions on the As kinetics. It is observed that the As kinetics are not affected in presence of 1 ppm nitrates and 1 ppm fluorides. However when 1 ppm of chlorides are added to the system, the As adsorption capacity is reduced by 12% (chlorides if present just by themselves at a concentration of 1 ppm cause a 13% reduction in adsorption capacity of LDH). The adsorption capacity gets further reduced by 13% on addition of 1 ppm of carbonates (carbonates if present just by themselves at a concentration of 1 ppm cause a 14% reduction in adsorption capacity of LDH). One observes an additional 30% decrease upon the addition of 1 ppm of sulphates (sulphates if present just by themselves at concentration of 1 ppm cause a 22% reduction in adsorption capacity of the LDH) while an additional 37% reduction is observed upon the addition of 1 ppm of phosphates to the system (phosphates if present just by themselves at a concentration of 1 ppm causes a 85% reduction in adsorption

capacity of LDH). So it can be concluded that these ions have a cumulative effect being competitive with each other for the same sites on the LDH adsorbent.

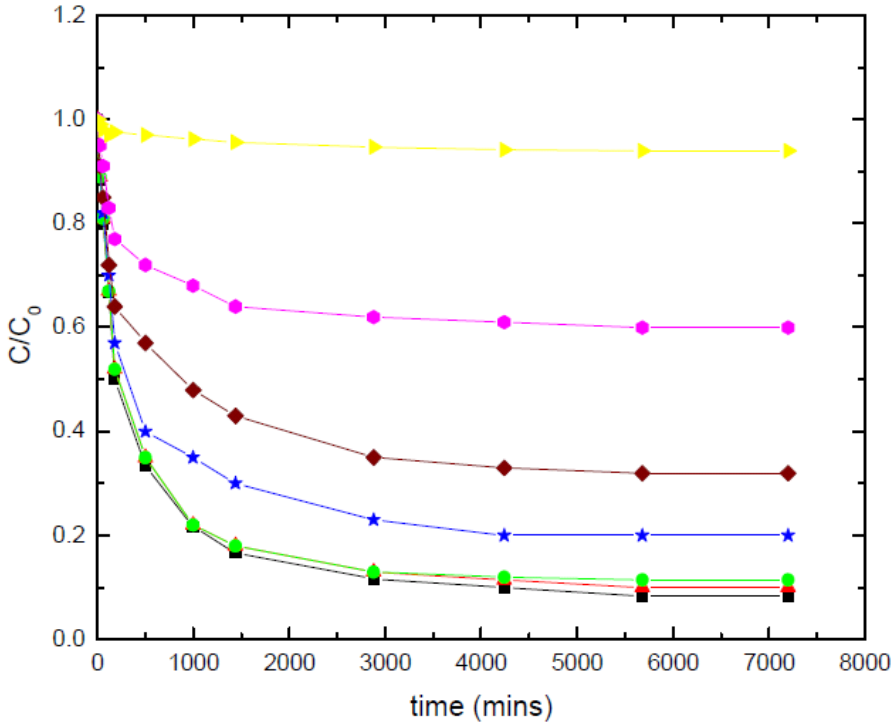

Figure 4.7. Adsorption of 60 ppb As solution as a function of time by (180-300 μm) LDH particles indicating the additive effect of various individual competing ions.

Black Line	As
Red Line	As + Fl^-
Green Line	As + Fl^- + NO_3^-
Blue Line	As + Fl^-+ NO_3^-+ Cl^-
Brown Line	As + Fl^- + NO_3^- + Cl^- + CO_3^{2-}
Pink Line	As + Fl^- + NO_3^- + Cl^- + CO_3^{2-} + SO_4^{2-}
Yellow Line	As + Fl^- + NO_3^- + Cl^- + CO_3^{2-} + SO_4^{2-} + PO_4^{2-}

4.4.4. Breakthrough Studies for As in the Presence of Individual Competing Ions

We have shown in the previous sections that the two models developed, i.e. the HSDM and BPM were able to successfully predict the column behavior as a function of various parameters such as flow rate, initial concentration, particle size and pH. We use here both these models in order to verify whether they are able to predict As adsorption in

a column even in the presence of competing ions. This is important in terms of process scale-up for the treatment of real power plant effluents. As described in the previous section, the performance of a packed-bed column is evaluated experimentally by monitoring the As concentration (and by comparing it with the feed concentration) as a function of the number of bed volumes (BV) that are treated.

The model equations can be found in the previous section describing the column experiments. The column parameters are given in Table 4.8 and the experimental breakthrough curves along with the HSDM and BPM predictions are shown in Figures 4.8a- 4.8g, where the dimensionless effluent concentration C/C_0 is plotted *vs.* dimensionless time τ (BV) at four different bed heights. The mass transfer coefficient used in the model is determined by the empirical correlation obtained by Williamson *et al.* [*Williamson et al.*, 1963] (refer to the appropriate Equation in the previous section on the column experiments). The time at which the concentration reaches its breakthrough value, $\frac{C}{C_0} = 0.05$, varies with the presence of individual competing ions, almost in the same order as observed in the batch experiments. In addition it can also be observed that the slope of the breakthrough curves decreases in the presence of various ions in the order $PO_4^{2-} > SO_4^{2-} > CO_3^{2-} > Cl^- > NO_3^- > F^-$. In Figures 4.8a – 4.8g, for example the breakthrough time τ_{br} predicted by HSDM at the exit of the column was 200591 for As and 160827, 144608, 79316, 80237, 26423 and 6127 for As in the presence of 1 ppm fluoride ions, 5 ppm nitrate ions, 100 ppm chloride ions, 5 ppm carbonate ions, 100 ppm sulphate ions, and 1 ppm phosphate ions respectively. The corresponding breakthrough times predicted by BPM are 209585 for As and 167640, 155867, 87582, 85238, 27701

and 7092, respectively. It can also be seen that both the HSDM and the BPM perform well in describing the experimental data even in the presence of the various competing ions.

Table 4.8. Properties of the fixed-bed column

Parameters		**Value**
Height, H (cm)		8.5
Diameter, D (cm)		0.7
Mass transfer coefficient, k_f (cm/min)		0.26
180-300 (μm)	**Solid density, ρ_s (g/cm^3)**	1.986
	Bed porosity, ε	0.27
	Particle Porosity, ε_M	0.31
	Arithmetic mean, d_{10} (μm)	274.5

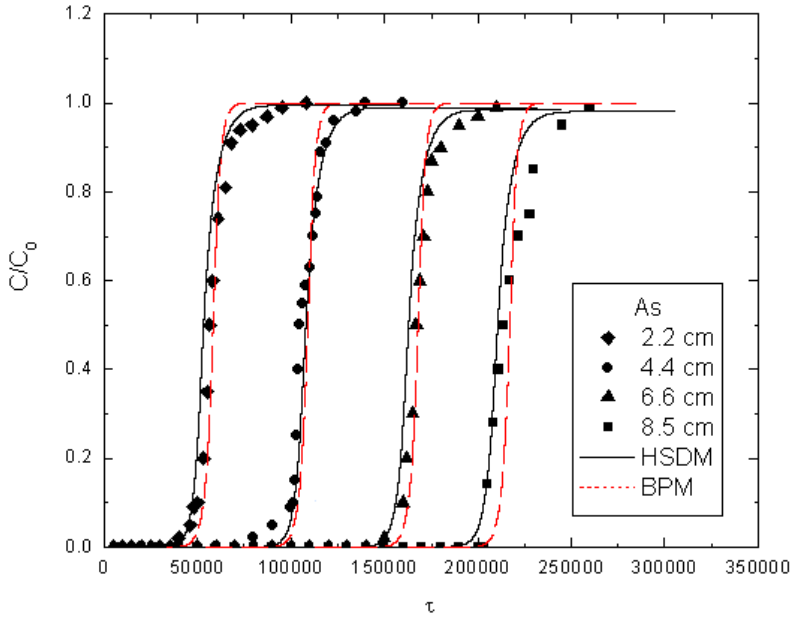

(a)

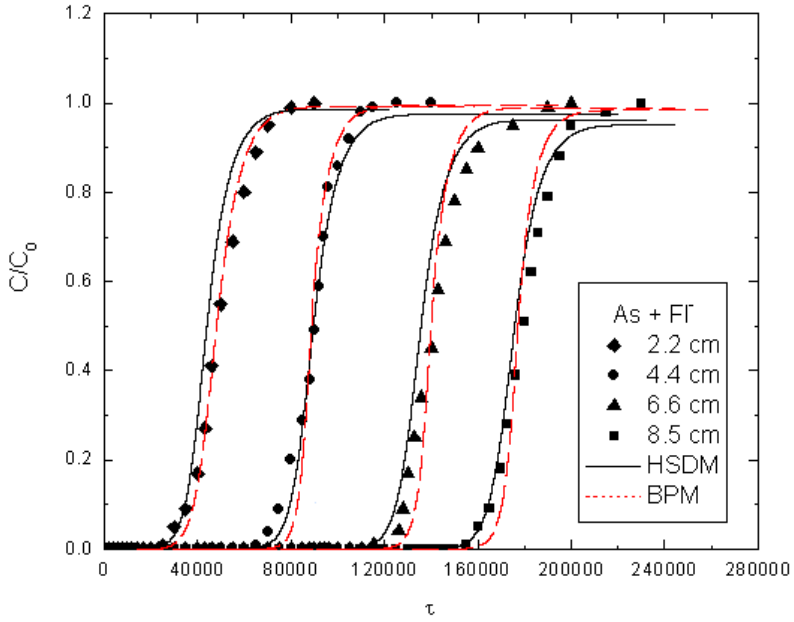
C/C0
τ
As + Fl-
2.2 cm
4.4 cm
6.6 cm
8.5 cm
HSDM
BPM

(b)

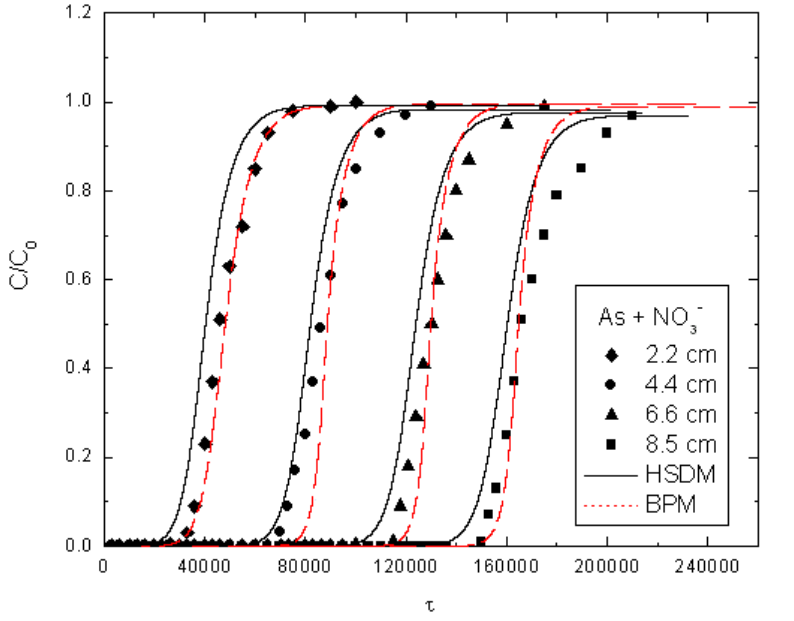
C/C0
τ
As + NO3-
2.2 cm
4.4 cm
6.6 cm
8.5 cm
HSDM
BPM

(c)

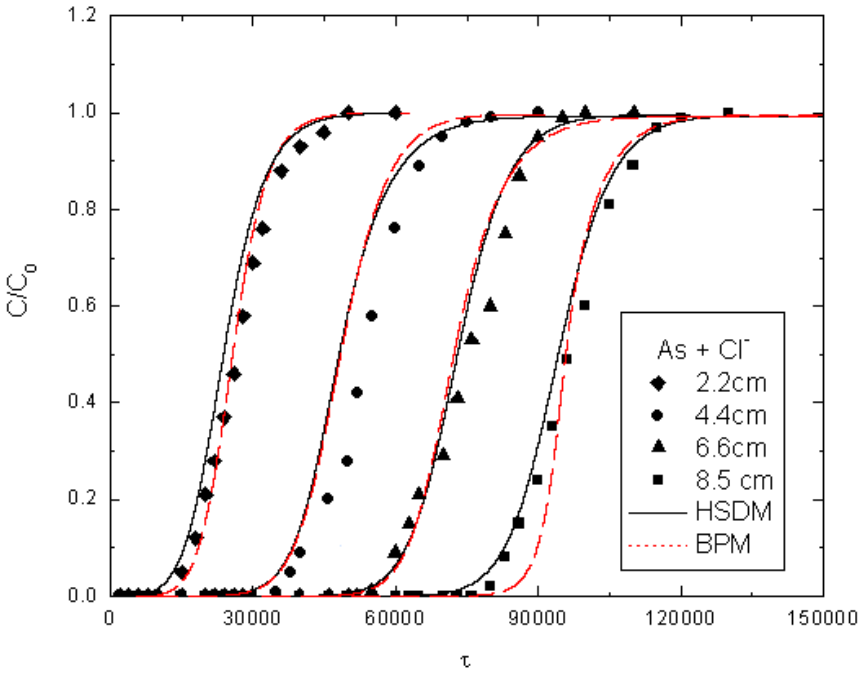
1.2
1.0
0.8
0.6
0.4
0.2
0.0
C/C0
0
30000
60000
90000
120000
150000
τ
As + Cl-
2.2cm
4.4cm
6.6cm
8.5 cm
HSDM
BPM

(d)

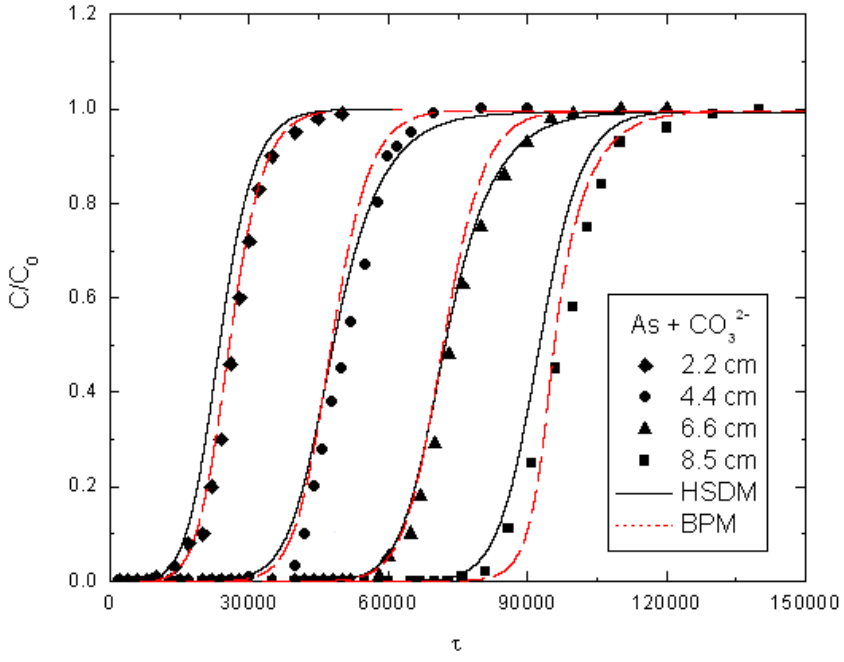
1.2
1.0
0.8
0.6
0.4
0.2
0.0
C/C0
0
30000
60000
90000
120000
150000
τ
As + CO3 2-
2.2 cm
4.4 cm
6.6 cm
8.5 cm
HSDM
BPM

(e)

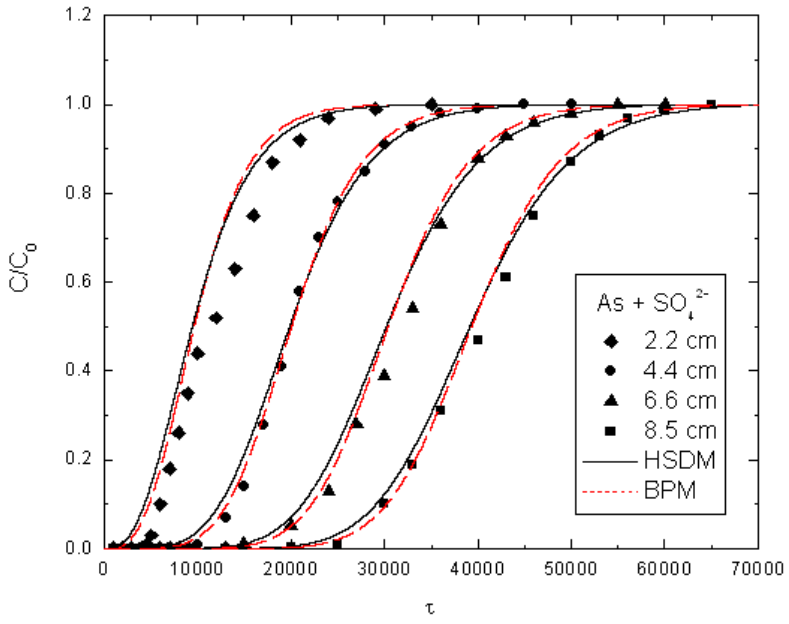

(f)

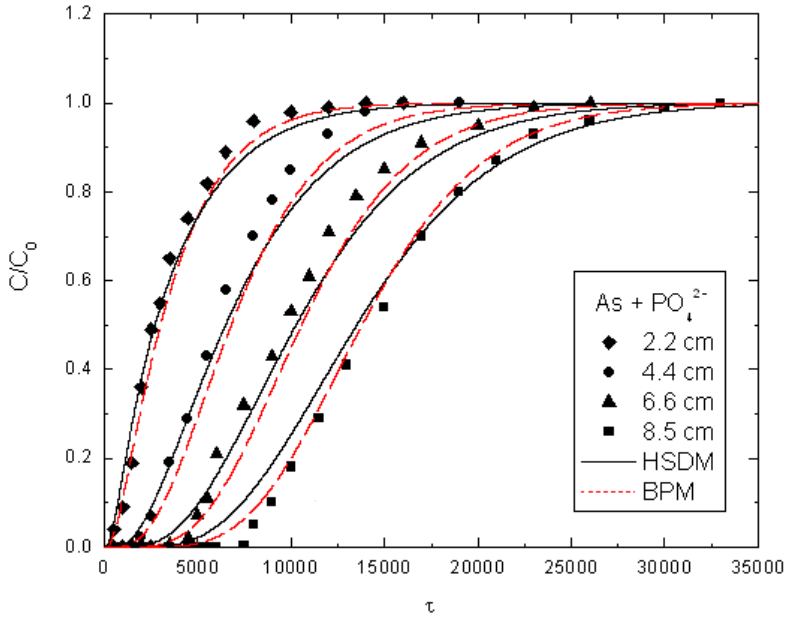

(g)

Figure 4.8. Adsorption of 20 ppb As solution by LDH in the presence of various individual competing ions at several column height locations in packed-bed experiments and the corresponding HSDM & BPM predictions.

4.4.5. Binary Adsorption Isotherms of As and Competing Ions

The binary adsorption isotherms of As(V) and the various anions on conditioned LDH are shown in 3-D plots in Figures 4.9a- 4.9f, where q_{As} (the amount of As adsorbed) and q_{Ion} (the amount of competing ion adsorbed) are plotted as a function of both C_{As} and C_{Ion} (the concentrations at equilibrium of As and the ion, correspondingly). It is observed in Figure 4.9 that the amounts of different competing ions absorbed are much (typically an order of magnitude) higher than the corresponding amount of As, which is consistent with the experimental adsorption data of the individual species, as reported above. The much high adsorption saturation capacities of the competing ions, when compared to As, show that not all the LDH adsorption sites are available to the As ionic species. This may be due to either the chemical nature of the sites or to the relatively large molecular size of the latter species [*Yoshikado et al.*, 2002; *Janz et al.*, 1962; *Kojima et al.*, 2003; *Rao*, 1980]. Therefore, in order to fit the binary isotherm experimental data we have used an extended multi-component Sips Isotherm, which however has been modified to take into account the presence of the two different adsorption sites on the adsorbent material. The concentration of sites where only anions other that As adsorb is given by the difference between the maximum saturation loading of the two species, that is, $q_{s,I} - q_{s,A}$, measured during the individual species adsorption experiments reported above. So the isotherm equations for the As and the competing ions, respectively, become [*Choy et al.*, 2000],

$$q_{e,A} = \frac{q_{s,A} K_A C_{e,A}{}^{n_A}}{1 + K_A C_{e,A}{}^{n_A} + K_I C_{e,I}{}^{n_I}} \tag{4.2}$$

$$q_{e,I} = \frac{(q_{s,I} - q_{s,A})K_I' C_{e,I}^{n_I'}}{1 + K_I' C_{e,I}^{n_I'}} + \frac{q_{s,A} K_I C_{e,I}^{n_I}}{1 + K_A C_{e,A}^{n_A} + K_I C_{e,I}^{n_I}} \quad (4.3)$$

where, $q_{s,A}$, K_A and n_A are the maximum sorption capacity, extended Sips constant and the extended Sips exponential factor for As, as measured during the As sorption experiments in the absence of competing anions ($q_{s,A}$ = 3619.9 μg/g, K_A = 0.65, n_A = 0.58). $q_{s,I}$ is the maximum sorption capacity for the individual ions, as noted above (values are reported in Table 4.4). K_I and K_I' are the extended Sips equilibrium constants, and n_I and n_I' are the two sets of extended Sips exponential factor for the two kind of sites available to the competing ions.

We have fitted K_I and n_I by using the As isotherm data first, and K_I' and n_I' by using the ion isotherm data. The fitted parameters are reported in Table 4.9 and the fitted plots are shown in Figure 4.9a-4.9f (solid lines) along with the experimental data (points).

Table 4.9. Fitted parameters for the binary isotherm data

	$q_{s,I}$ (μg/g)	K_I (l/g)	n_I	K_I' (l/g)	n_I'
Carbonates	46010.4	0.029	0.69	0.029	0.81
Sulphates	41868.4	0.026	0.72	0.019	0.83
Phosphates	38251.1	0.025	0.67	0.016	0.82
Fluorides	34927.2	0.018	0.71	0.013	0.85
Chlorides	32394.7	0.011	0.81	0.011	0.85
Nitrates	30017.3	0.006	0.86	0.006	0.92

It can be observed that the values of K_I' and n_I' are fairly close to K and n values reported in Table 4.4 for the individual ions, as expected because these parameters are for the sites that are only available to the ions without any competition from As and the

majority of ion adsorption occurs on these sites. K_1 and n_1 values for nitrates and chlorides are also close to the single anion values, but substantial difference exist for the more competitive anions, particularly the sulfates and phosphates.

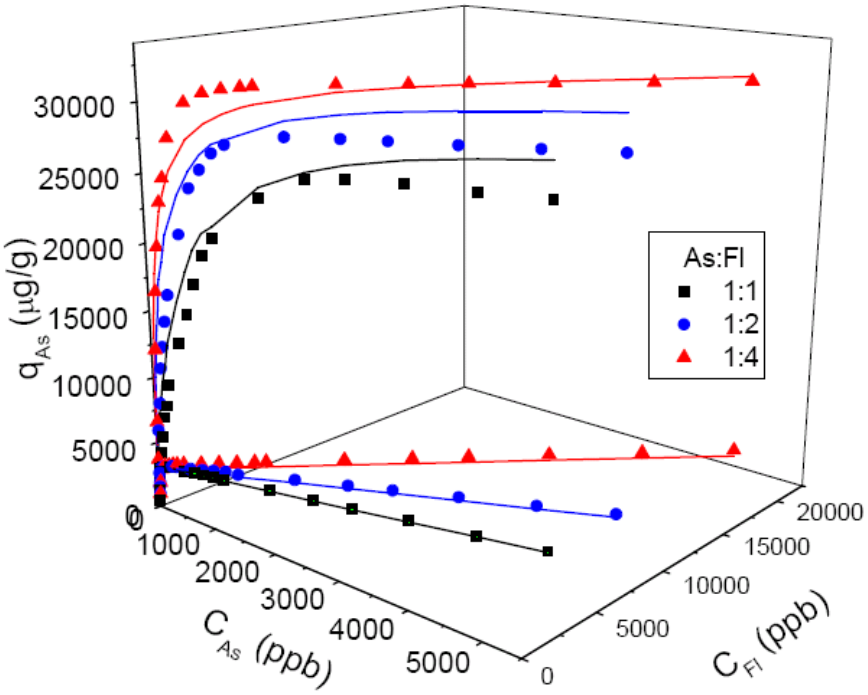

(a)

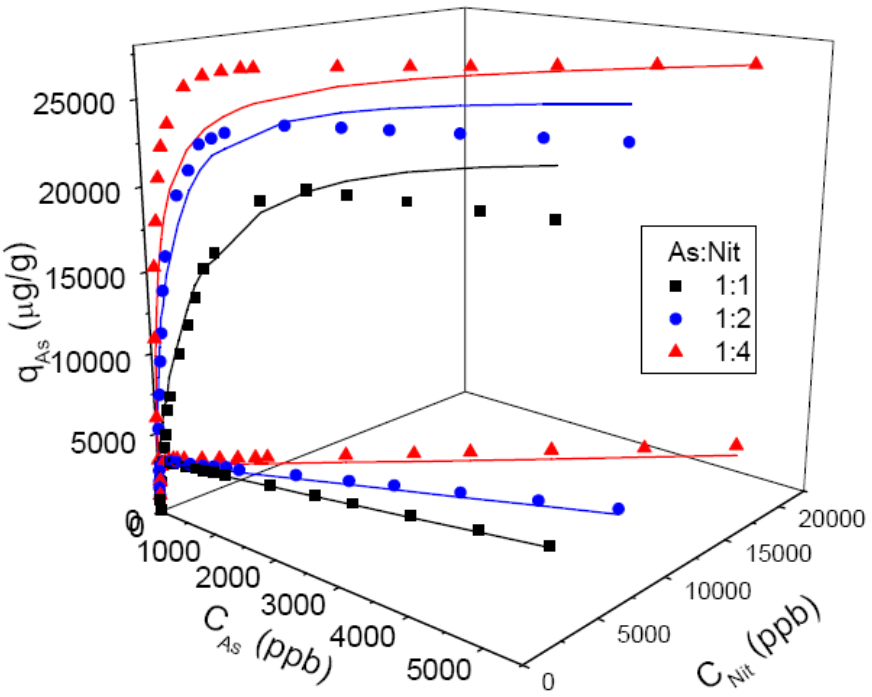
25000
20000
15000
10000
5000
0
q_{As} (µg/g)
1000
2000
3000
4000
5000
C_{As} (ppb)
0
5000
10000
15000
20000
C_{Nit} (ppb)
As:Nit
1:1
1:2
1:4

(b)

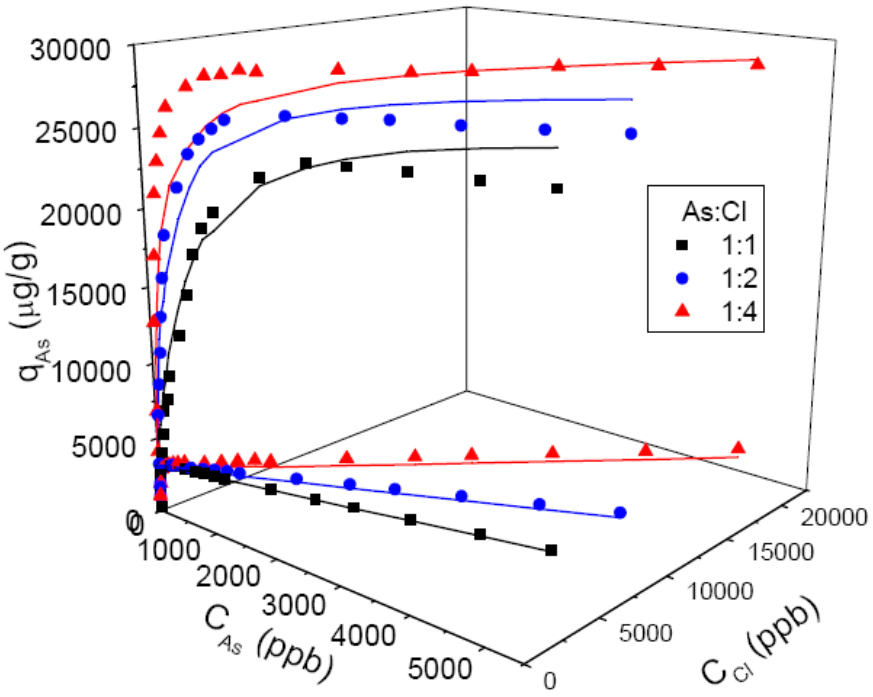
30000
25000
20000
15000
10000
5000
0
q_{As} (µg/g)
1000
2000
3000
4000
5000
C_{As} (ppb)
0
5000
10000
15000
20000
C_{Cl} (ppb)
As:Cl
1:1
1:2
1:4

(c)

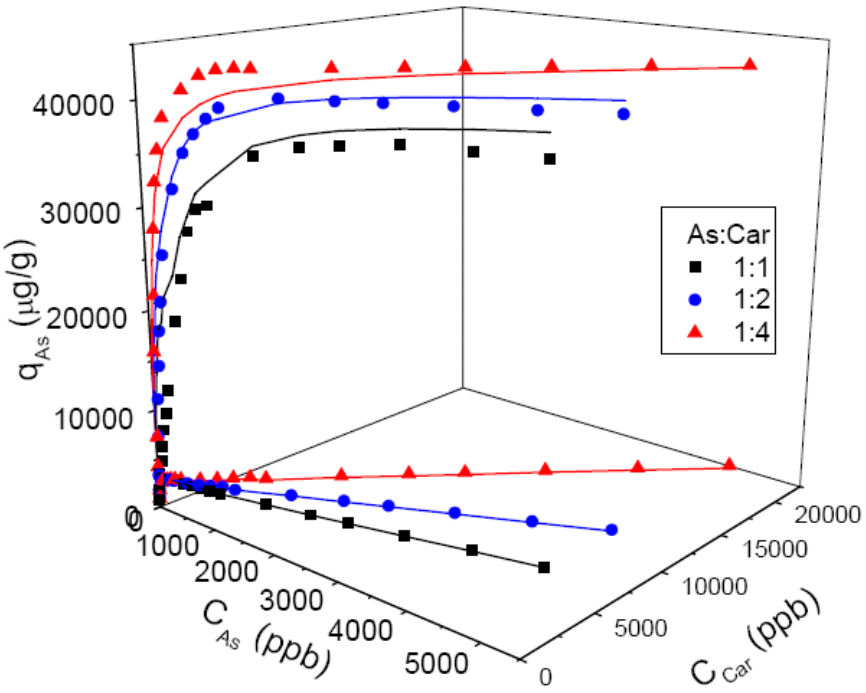
40000
30000
20000
10000
0
q_{As} (µg/g)
As:Car
1:1
1:2
1:4
0
1000
2000
3000
4000
5000
C_{As} (ppb)
0
5000
10000
15000
20000
C_{Car} (ppb)

(d)

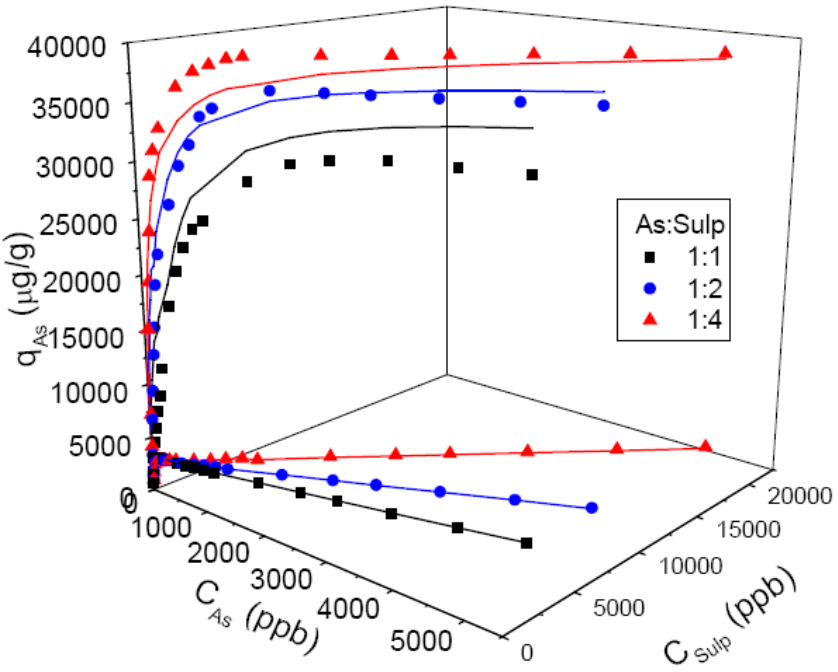
40000
35000
30000
25000
20000
15000
10000
5000
0
q_{As} (µg/g)
As:Sulp
1:1
1:2
1:4
0
1000
2000
3000
4000
5000
C_{As} (ppb)
0
5000
10000
15000
20000
C_{Sulp} (ppb)

(e)

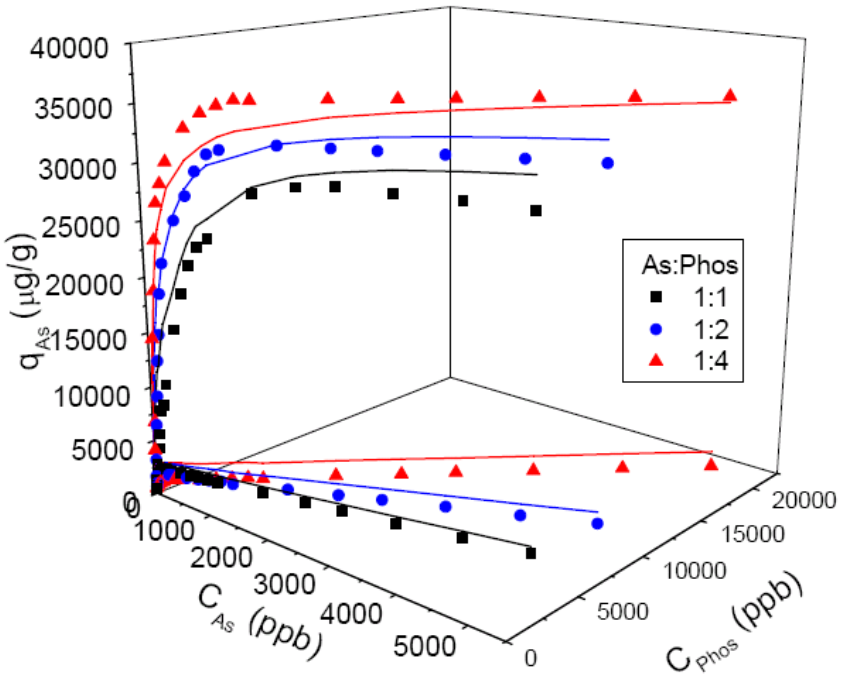

(f)

Figure 4.9. Binary adsorption isotherms for As(V) and the competing ions on conditioned LDH.

We also fitted the isotherm data reported in section 4.4.2. using the extended dual-site Sips isotherm and the fitted parameters are as shown in Table 4.10. The parameters for As, i.e., $q_{s,A}$, K_A and n_A were again taken to be that for As when it is present by itself, and $q_{s,I}$ is taken to be the maximum value for the ions when present by themselves. There is agreement between the values reported in Tables 4.9 and 4.10 for carbonates, nitrates and fluorides but also substantial discrepancies for the remaining anions which can be attributed to the fact that the initial molar ratios of the competing ions to the As ion are much higher in these experiments as compared to the binary experiments in Figure 4.9.

Table 4.10. Fitted parameters for the isotherm data with the power plant concentration ratios

	$q_{s,I}$ (μg/g)	K_I (l/g)	n_I	K_I' (l/g)	n_I'
Carbonates	46010.4	0.029	0.62	0.029	0.79
Sulphates	41868.4	0.018	0.59	0.018	0.59
Phosphates	38251.1	0.044	0.89	0.044	0.89
Fluorides	34927.2	0.018	0.71	0.018	0.96
Chlorides	32394.7	0.011	0.52	0.011	0.58
Nitrates	30017.3	0.006	0.61	0.006	0.93

4.4.6. Adsorption of Se in the Presence of Individual Competing Ions

The results of Se removal for both the conditioned and calcined LDH are reported in Figure 4.10 (the amount adsorbed in the absence of any competing ions is indicated by the horizontal line). It can be observed that the amount of Se adsorbed on conditioned LDH is half or less to that absorbed on calcined LDH. This is to be expected, as the calcined LDH regenerates itself in the presence of the Se aqueous solution, thereby absorbing larger amounts of Se, whereas in the case of the conditioned LDH, it just gets adsorbed or intercalated into the LDH by replacing the existing carbonate ions in the structure. It is also observed that the Se adsorption capacity on both conditioned and calcined LDH decreases in the presence of the various individual competing ions in the order of $PO_4^{2-} > SO_4^{2-} > CO_3^{2-} > Cl^- > NO_3^- > F^-$, i.e., the same order by which the As adsorption on LDH is affected by such anions. In addition, the results reported for the calcined LDH are similar to those reported in the prior publication by our group [*Yang et al.*, 2005].

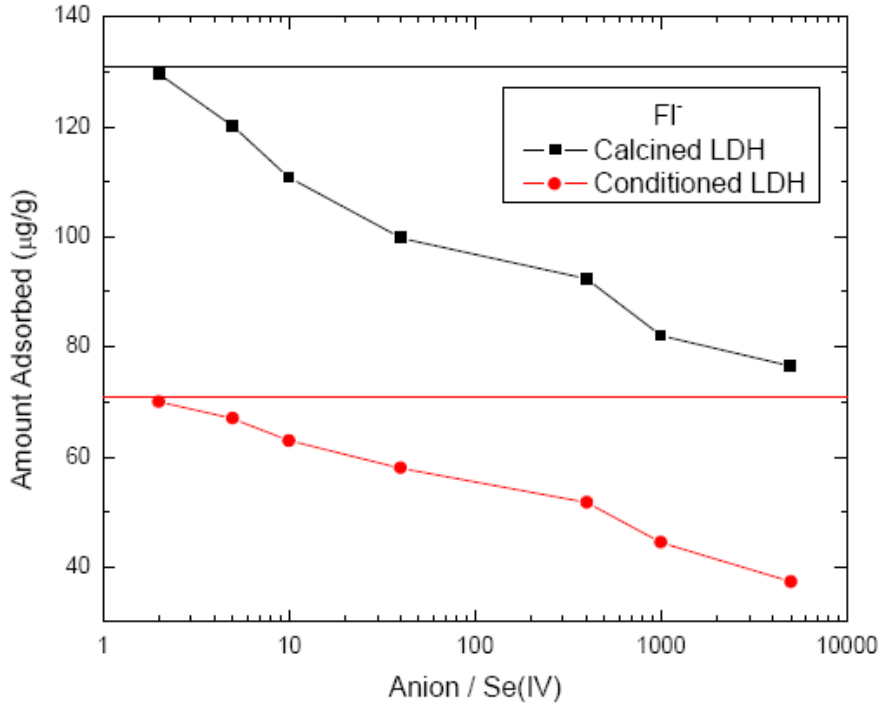
140
120
100
80
60
40
Amount Adsorbed (μg/g)
1
10
100
1000
10000
Anion / Se(IV)
F⁻
Calcined LDH
Conditioned LDH

(a)

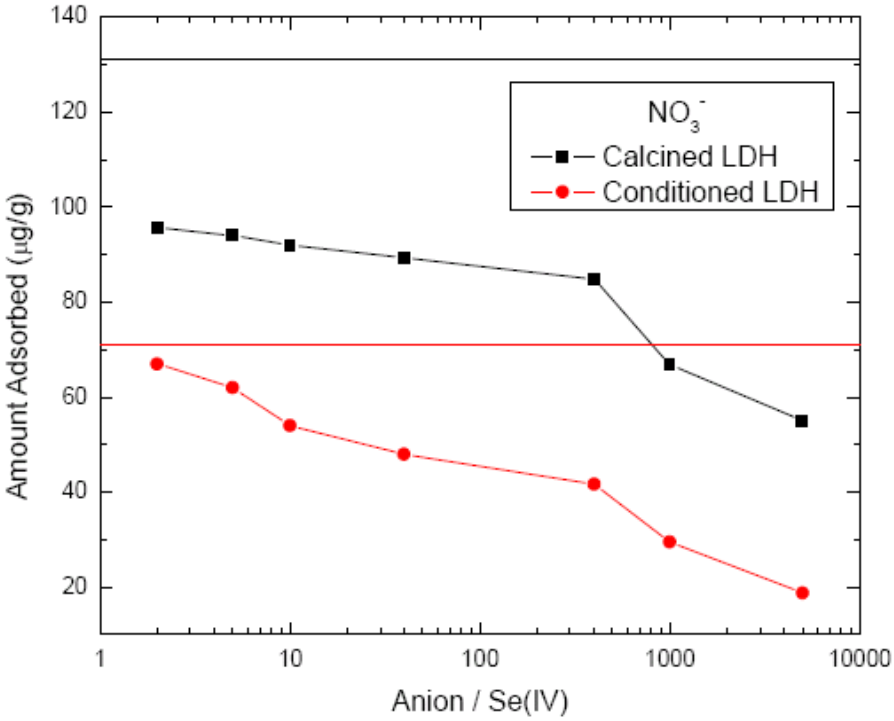
140
120
100
80
60
40
20
Amount Adsorbed (μg/g)
1
10
100
1000
10000
Anion / Se(IV)
NO3-
Calcined LDH
Conditioned LDH

(b)

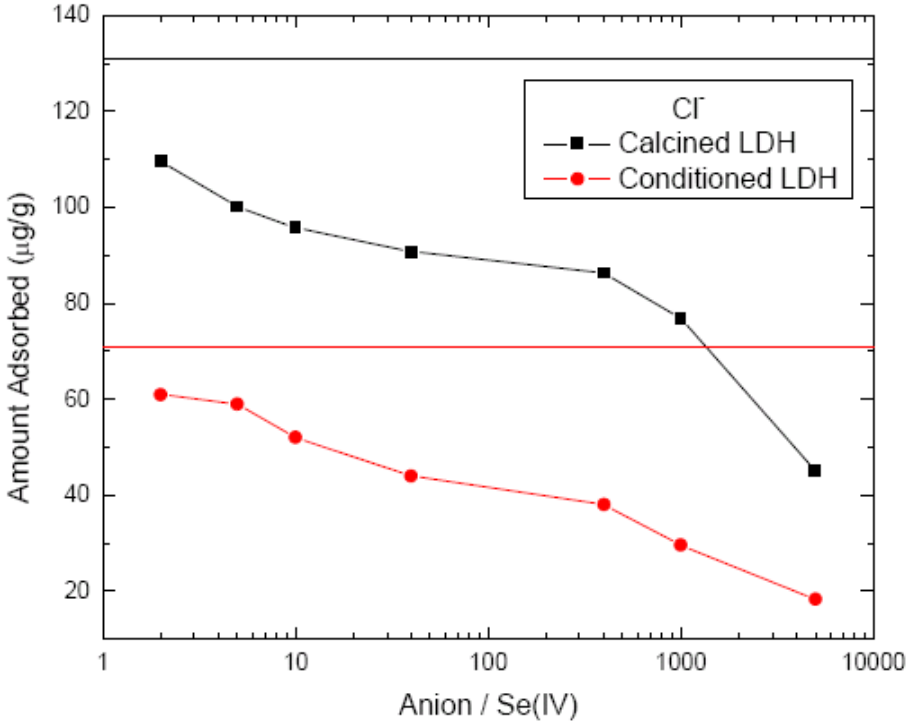
Cl-
Calcined LDH
Conditioned LDH
Amount Adsorbed (µg/g)
Anion / Se(IV)
140
120
100
80
60
40
20
1
10
100
1000
10000

(c)

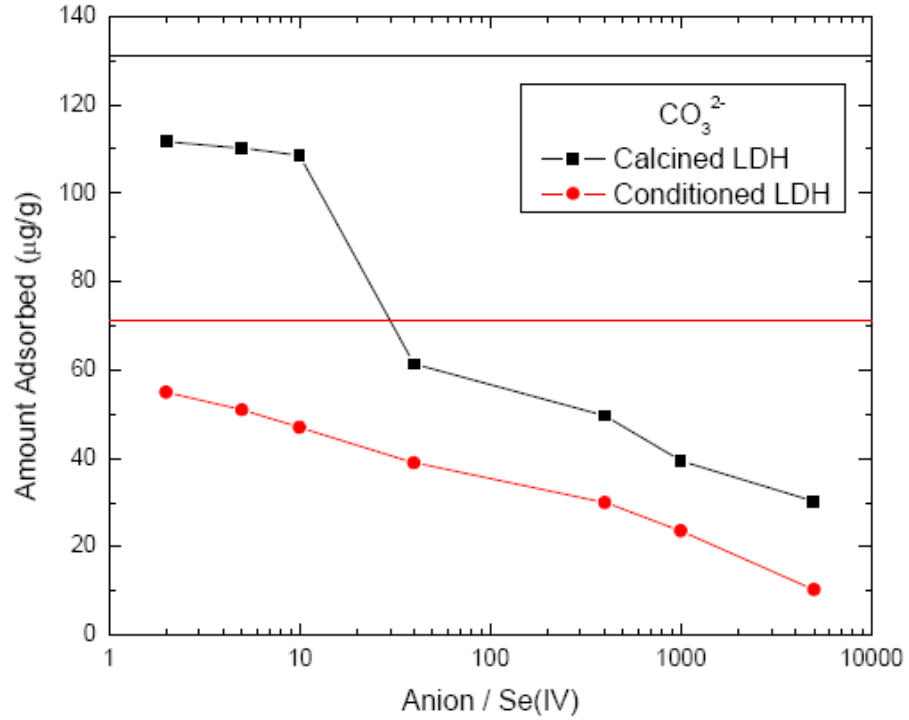
CO3 2-
Calcined LDH
Conditioned LDH
Amount Adsorbed (µg/g)
Anion / Se(IV)
140
120
100
80
60
40
20
0
1
10
100
1000
10000

(d)

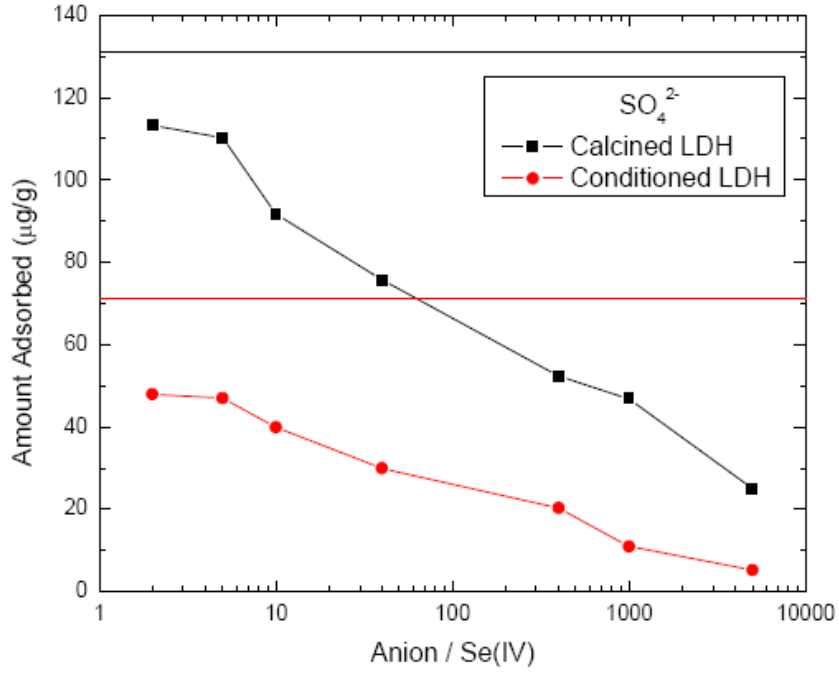

(e)

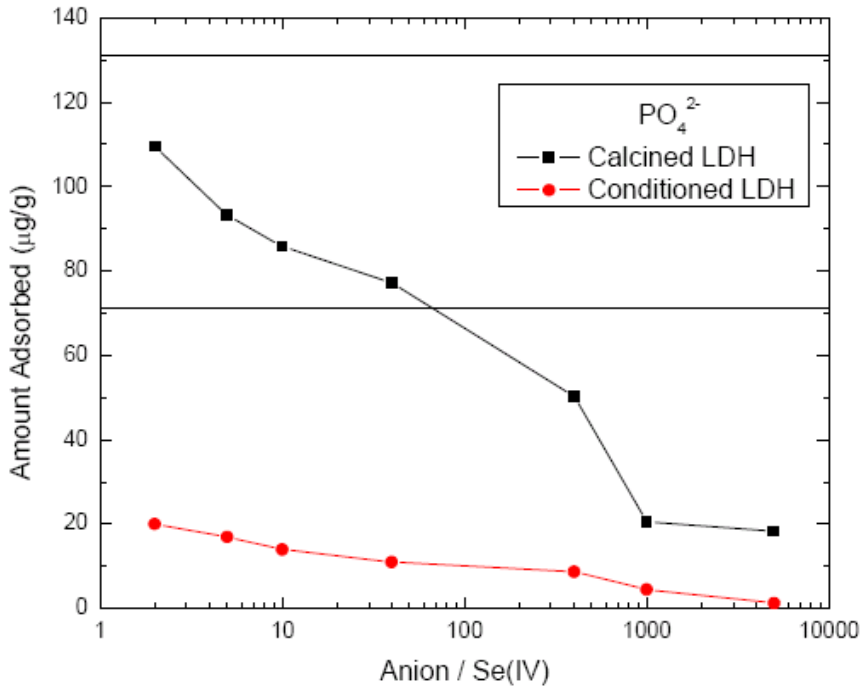

(f)

Figure 4.10. Adsorption isotherms for Se on calcined and conditioned LDH in the presence of individual competing ions.

4.5. Conclusions

Power plant effluent data were collected and it was found that these effluents contain fluorides, nitrates, chlorides, carbonates, sulphates and phosphates in addition to As and Se. The effect of these competing ions on As and Se adsorption by conditioned LDH has been investigated. Individual competing ions isotherms were measured. It was found that carbonates adsorb the most on LDH, while nitrates adsorb the least among the various ions present in the power plant effluents. Binary isotherms of As and the individual competing ions were also measured. The effect of each of these individual ions on the rates of As removal by the LDH, at concentration levels that are found in typical power plant effluents, was also studied. It was observed that nitrates and fluorides have almost no effect, whereas phosphates compete the most with the As for the adsorption sites on LDH. The experimental kinetic data were fitted with the homogeneous surface diffusion and bidisperse pore models. We also carried out column experiments in the presence of individual competing ions at concentration levels that are found in power plant effluents, and similar trends were observed as in the batch experiments. The HSDM and BPM were also able to predict the qualitative trends quite well. From the batch adsorption isotherm and kinetic experiments as well as the column experiments, it can be concluded that the As adsorption capacity decreases in the presence of various individual competing ions in the order of $PO_4^{2-} > SO_4^{2-} > CO_3^{2-} > Cl^- > NO_3^- > F^-$. For Se removal from aqueous solutions in the presence of individual competing ions, calcined LDH proved more effective than conditioned LDH. It can also be concluded that the Se adsorption capacity decreases in the presence of various individual competing ions in the order of $PO_4^{2-} > SO_4^{2-} > CO_3^{2-} > Cl^- > NO_3^- > F^-$.

5. Regeneration of the LDH

5.1. Introduction

For any adsorption process to be economical, the adsorbent material utilized should be reusable or easily regenerated. LDH can uptake anions from a solution by three different mechanisms: (1) by adsorption, (2) by intercalation through anion exchange, and (3) by intercalation through its reconstruction of its structure (for calcined LDH). The latter phenomenon is known as the "memory effect," which takes place when an LDH, usually containing carbonates in its interlayer, is calcined at temperatures that are high enough to eliminate most of the interlayer anions, and is then put in a solution of the same or different anion. While in solution, rehydration and reconstruction of the layered structure occurs with incorporation of the anions from the solution. The ability of LDH to "recover" their structure provides at least, in principle, the potential for reuse and recycle of the adsorbent, which is important for any large-volume applications.

5.2. Regeneration Experiments

Initially a 500 ml of 20 ppm As(V) solution was equilibrated with 100 mg of conditioned LDH (Mg-Al-CO_3-LDH) for 2 days, after which the saturated Mg-Al-hydrotalcite was separated from the reaction mixture by simple filtration, and the supernatant liquid was analyzed with ICP-MS for the remaining As concentration. The filtered hydrotalcite is then added to the regenerating solution, i.e., 1000 ml of 0.1M Na_2CO_3 solution in order to replace the potential exchangeable As(V) ions with the carbonate ions. The supernatant was withdrawn and concentrations of As were measured using ICP-MS, and the concentration of CO_3^{2-} was measured using titration, in order to have an idea of how much of the adsorbed As is removed from the LDH. This process

was repeated twice with shaking at 170 rpm for 8 h for each Na_2CO_3 addition. The solid phase was washed by distilled water two times, in order to make sure all As was removed from the solid phase. The regenerated hydrotalcite is then filtered again and dried at 60 °C for 24 h. The adsorption-regeneration process is repeated 15 times using the recycled LDH in 20 ppm As(V) solution. The reuse experiments were deemed complete after fifteen iterations. Table 5.1 shows the results for the various adsorption and regeneration cycles. It can be seen, that even after regenerating the adsorbent for ten times, the adsorption capacity still remained greater than 95%; when regenerated for an additional five times, for a total of fifteen times, the adsorption capacity dropped by only an additional 5%. Thus the regenerated LDH kept up to 90% of its initial adsorption capacity, which proves that conditioned LDH is a very effective adsorbent for As removal from water.

Table 5.1. Adsorption efficiency of recycled conditioned LDH

Recycle Times	**Adsorption of As (μg/g)**	**Adsorption Efficiency (%)**
	6124.28	100
1	6124.21	99.99
2	6119.05	99.91
3	6104.20	99.67
4	6074.23	99.18
5	6042.19	98.66
6	6017.21	98.25
7	5990.42	97.81
8	5951.94	97.19
9	5894.71	96.25
10	5856.43	95.63
11	5787.29	94.50
12	5724.73	93.48
13	5649.72	92.25
14	5592.19	91.31
15	5544.21	90.53

5.3. Conclusions

The regeneration experiments carried out proved that the conditioned LDH can be recycled for at least 15 times with a minimal loss of its adsorption capacity.

6. Cost Analysis for Treating Power Plant Effluents

This section focuses on the cost analysis for running a LDH column for treating power plant effluents. The basic assumptions made are:

Average As concentration in power plant effluents = 20 ppb

Typical power plant effluents = 5000 gal/min (GPM)

LDH Cost: $ 16/Kg LDH

The cost has been calculated as a function of the flow rate, inlet effluent As concentration and pH of the inlet stream, and the results are reported in Table 6.1. The sample calculations are shown in the Appendix.

Table 6.1. Cost analysis for treating power plant effluents

GPM	ppb	pH	Gallons treated/$
5000	20	8.0-8.5	27500
10000			18500
5000	20	8.0-8.5	27500
	100		13695
5000	20	4.0-5.0	110800
		6.5-7.5	55400
		8.0-8.5	27500

7. Second Generation Adsorbents

7.1. Introduction

Some of the avenues considered in this Section for modification in the LDH materials include:

- Varying the ratio of the M^{II}/M^{III} metal constituents.
- Substitution in the M^{II} and M^{III} position with selected other metal constituents.
- Substitution of the interlayer anion

The resulting second generation sorbents are tested for their sorption selectivity utilizing a model "wastewater" containing a predetermined amount of As oxyanion in solution.

7.2. Experimental

7.2.1. Preparation of Second Generation Adsorbents

7.2.1.1. Mg-Al-CO_3-LDH with a Mg/Al Molar Ratio of 2 and 4

The co-precipitation method described before was used to synthesize the LDH. To prepare the Mg-Al-CO_3-LDH with a Mg/Al molar ratio of 2, 140 ml of a solution containing 0.7 mol NaOH and 0.18 mol Na_2CO_3 was added all at once to a second solution containing 0.10 mol of $Mg(NO_3)_2 \cdot 6H_2O$ (90ml) and 0.05 mol of $Al(NO_3)_3 \cdot 9H_2O$ (90 ml) (corresponding to a Mg/Al ratio of 2) under vigorous stirring. The thick gel obtained was aged for 24 h at 333 K, followed by filtration and washing with distilled water, and was then dried at 333 K. ICP-MS analysis of the resulting LDH material indicated that its Mg/Al mole ratio is ~2.1, which is close to the Mg/Al ratio of the starting salts. To prepare a Mg-Al-CO_3-LDH with a Mg/Al molar ratio of 4, the co-precipitation method was again used, the only difference being that the second solution

this time contained 0.124 mol of $Mg(NO_3)_2 \cdot 6H_2O$ (90ml) and 0.031 mol of $Al(NO_3)_3 \cdot 9H_2O$ (90 ml) (corresponding to a Mg/Al ratio of 4). ICP-MS analysis of the resulting LDH material indicated that its Mg/Al mole ratio is ~3.9, again close to the Mg/Al ratio of the starting salts.

The conditioned Mg-Al-LDH was then obtained by first heating the original LDH in a muffle furnace at 773 K for 4 h, in an air atmosphere with heating and cooling rates of 2 $K \cdot min^{-1}$, and then shaking it in deionized water for 24 h (while changing the deionized water every 6 h), followed by drying in air atmosphere at 353 K for 12 h.

7.2.1.2. Mg-Al-NO_3-LDH with a Mg/Al Molar Ratio of 3

The Mg-Al-CO_3-LDH with a Mg/Al mole ratio of 3 was used to synthesize the Mg-AL-NO_3-LDH. The CO_3-LDH was calcined by heating it in a muffle furnace at 773 K for 4 h in an Ar atmosphere with heating and cooling rates of 2 $K \cdot min^{-1}$. The calcined material was then added to 280 ml of a solution containing 0.72 mol $NaNO_3$, through which N_2 was bubbled for 30 min, prior to adding the calcined material under vigorous stirring. The calcined LDH was left in the nitrate solution for 24 h with N_2 bubbling through it. The solution was then filtered, and the recovered NO_3-LDH was washed with decarbonated water and dried at 333 K.

7.2.1.3. Mg-Fe-SO_4-LDH with a Mg/Fe Molar Ratio of 3

The same co-precipitation preparation method, as with the Mg-Al-CO_3-LDH, was used to synthesize this LDH, the only difference being that instead of using $Al(NO_3)_3 \cdot 9H_2O$ we used $Fe(NO_3)_3 \cdot 9H_2O$. 140 ml of a solution containing 0.7 mol NaOH and 0.18 mol Na_2SO_4 was added all at once to a second solution containing 0.115 mol of $Mg(NO_3)_2 \cdot 6H_2O$ (90ml) and 0.04 mol of $Fe(NO_3)_3 \cdot 9H_2O$ (90 ml) (corresponding to a

Mg/Fe ratio of 3) under vigorous stirring. The thick gel obtained was aged for 24 h at 333 K, followed by filtration and washing with distilled water, and was then dried at 333 K. ICP-MS (inductively coupled plasma mass spectrometry) analysis of the resulting LDH material indicated that its Mg/Fe mole ratio is ~2.7, which is very close to the Mg/Fe ratio of the starting salts.

We have also used in the experiments in this section the Mg-Al-CO_3-LDH, with Mg/Al = 3.0, both in the uncalcined and the conditioned forms. To obtain different particle size fractions, the various LDH were crushed and sieved using standard testing sieves (VWR). The size fraction collected at 80-70 mesh (90-180 μm) was used for all the experiments reported in this section.

7.2.2. Sorption Isotherm Experiments

To compare the adsorption capacity of the various synthesized LDH, adsorption isotherm experiments were carried out. As(V) was the metal investigated in the study. The As(V) solutions used for the adsorption experiments were prepared by dilution from a 1000 ppm ICP standard solution (As(V) in 2% HNO_3 purchased from Exaxol) using deionized water. No effort was made to minimize contact with the atmospheric air during the preparation of the various solutions. The adsorption isotherm experiments were carried out in 1000 ml polyethylene bottles at a temperature of 298 K using various prepared LDH. 8 mg of the adsorbent was added to 500 ml of an aqueous solution of As(V) of varying concentrations, ranging from 40 ppb to 500 ppb. The bottles containing the LDH suspension and the As(V) solutions were placed in a reciprocal shaking water-bath (Precision Model 25) and were shaken at 170 rpm for at least 5 days in order for the adsorption on the conditioned LDH to reach equilibrium. 5ml samples from each bottle

were taken and centrifuged, and the As concentrations in the supernatant solutions were determined by ICP-MS.

7.3. Results and Discussion

7.3.1. Adsorption Isotherms

As before, the Sips isotherm is used to fit the adsorption isotherm data. The adsorption isotherms for As(V) on the various LDH are shown in Figure 7.1. The points represent the experimental data and the solid lines in the figure are the corresponding Sips fits. The various isotherm parameters (and the "goodness of fit", as manifested by the R^2) are reported in Table 7.1. Note that as the Mg/Al mole ratio decreases so does the As adsorption capacity of LDH. This could be explained by the fact that as the Mg/Al mole ratio decreases, the net positive charge on the layers increases, which in turn result in more electrostatic attraction between the positive layers and the negative interlayer ions. As a result the interlayer spacing decreases with the decreasing Mg/Al mole ratio [*Grover et al.*, 2009] and hence the incoming As ion has less space to enter, leading to a decrease in adsorption capacity. Similar results are also reported by Chitrakar and coworkers who have studied bromide uptake on Zn-Al-LDH and Mg-Al-LDH [*Chitakar et al.*, 2008]. However other researchers [*Harale,* 2008; *Barriga et al*, 2002] have reported that the adsorption capacity passes through a maximum as the Al content increases, but have failed to provide an explanation for the observed behavior. On the other hand, Wang and coworkers reported that the adsorption capacity of arsenate decreased from 1.56 to 1.08 to 0.36 mmol/g as the Mg/Al ratio increased from 2:1 to 3:1 to 4:1 in Mg-Al-NO_3-LDH [*Wang et al.*, 2009].

It is further observed that conditioning the adsorbent, increases its As adsorption capacity. Note furthermore, that while the LDH with a Mg/Al ratio of 3 and 4 have almost the same sorption capacity, the Mg/Al =2 LDH compound has a much smaller activity. We are not sure why the behavior of the conditioned materials is different from that of the uncalcined materials, and this is something that needs to be further investigated.

It is also observed that the NO_3-LDH was the most effective in adsorbing As ions from aqueous solutions followed by the conditioned LDH. The higher adsorption capacity of NO_3-LDH can be explained by the fact that the monovalent ions are easily replaced from the hydrotalcite structure as compared to the divalent ions like carbonates and sulphates. However among the divalent ions, carbonates have a greater affinity for the LDH structure as compared to sulphates and Fe has more affinity for As as compared to Al, leading to higher adsorption capacity of Mg-Fe-SO_4-LDH as compared to Mg-Al-CO_3-LDH with the same M^{2+}/M^{3+} ratio.

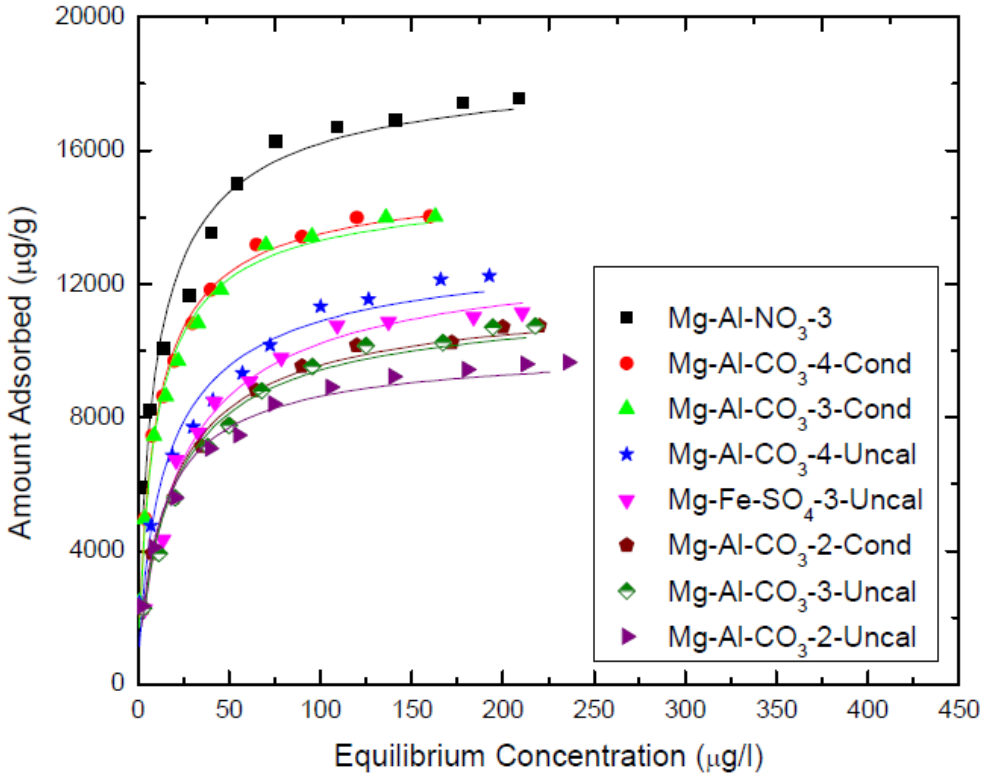

Figure 7.1. Adsorption isotherms for As on various second generation LDHs.

Table 7.1. Sorption isotherm parameters for As uptake on second generation LDHs

Sips Isotherm				
	q_s **(µg/g)**	K ***(l/g)***	n	R^2
Mg-Al-NO_3-LDH (Mg/Al=3)	18790.7	0.17	0.79	0.99
Mg-Al-CO_3-LDH (Mg/Al=4) Conditioned	15298.3	0.15	0.85	0.99
Mg-Al-CO_3-LDH (Mg/Al=3) Conditioned	15062.4	0.15	0.85	0.98
Mg-Al-CO_3-LDH (Mg/Al=4)	13397.7	0.11	0.81	0.99
Mg-Fe-SO_4-LDH (Mg/Al=3)	13186.5	0.07	0.86	0.98
Mg-Al-CO_3-LDH (Mg/Al=2) Conditioned	11834.4	0.08	0.86	0.99
Mg-Al-CO_3-LDH (Mg/Al=3)	11726.4	0.08	0.86	0.99
Mg-Al-CO_3-LDH (Mg/Al=2)	10226.9	0.11	0.84	0.98

7.4. Conclusions

The focus in this section was on the synthesis of second generation adsorbents and on comparing their adsorption capacity. We carried out batch isotherm experiments in which the adsorbent was exposed to the target metal in the presence of various synthesized LDH. The data indicate that the Mg-Al-NO_3-LDH was the most effective in removing the As from aqueous solutions followed by the conditioned LDH. However, the Mg-Al-NO_3-LDH is not practical for use with power plant effluents as the carbonates and other ions found in such water easily displace the nitrates from the LDH structure. It was also observed that the As removal capacity decreases with the decreasing Mg/Al molar ratio in the LDH structure.

8. Safe Disposal of the LDH Adsorbents

8.1. Introduction

The focus in this section is on the unique safe disposal features of the LDH. Limited tests early in our project indicated that the spent adsorbent met the TCLP test criteria, and thus, it can be disposed of as a non-hazardous solid waste. Further studies of this aspect of our work are described in this section. The successful completion of this task is important in terms of the safe disposal of the spent material, which is critical in terms of applying the proposed removal technology as an environmentally and user-friendly solution for the treatment of power plant effluents.

8.2. Experimental

Initially a 500 ml of 50 ppm As(V) solution was equilibrated with 5 g of conditioned LDH (Mg-Al-CO_3-LDH) for 2 days, after which the saturated Mg-Al-hydrotalcite was separated from the reaction mixture by simple filtration, and the supernatant liquid was analyzed with ICP-MS for its As concentration. This concentration was measured to be 450 ppb, indicating that 4955 μg As got adsorbed on 1 g of LDH.

The filtered hydrotalcite was then added to 500 mL of regular tap water contained in a 1 L plastic bottle, and was left there for one month. The supernatant solution was withdrawn at regular time intervals, and concentrations of As were measured using ICP-MS. It was found that even after one month, the As concentration in the solution was below 20 ppb, indicating that the As adsorbed on conditioned LDH does not desorbs even if the As-saturated LDH is left in water for 1 month.

The same test was repeated again, but this time the As-saturated LDH that was obtained was calcined at 600 °C for 4 h before being added to the 500 mL regular tap

water in a 1 L plastic bottle and left in storage for 1 month. The supernatant liquid was withdrawn at regular time intervals, and the concentration of As was again measured using ICP-MS. It was found, that even after 1 month, the As concentration in the solution was 0 ppb, indicating that the As adsorbed on calcined conditioned LDH does not elute even if the As saturated LDH is left in water for 1 month.

The As elution test was then repeated, but this time using the EPA test method 1311-TCLP, Toxicity Characteristic Leaching Procedure [www.ehso.com, Environmental Health & Safety Online]. For this test, the As-saturated LDH was put in contact with two different extraction fluids. The first extraction fluid contained 5.7 mL glacial CH_3COOH, 64.3 mL of 1N NaOH, and 930 mL of de-ionized water (pH = 5.0). The second extraction fluid contained 5.7 mL glacial CH_3COOH and 930 mL of de-ionized water (pH = 2.9). The solid was put in contact with the extraction fluid and rotated at 30 rpm for 20 h. After the extraction process is complete, the solid and liquid phases are separated by filtration. The As concentration in the liquid phase was analyzed and found to be 1.2 ppb and 0.5 ppb in extraction fluids 1 and 2, respectively. Note that the regulatory level for As in order for the waste to fail the TCLP test is 5 ppm [www.ehso.com, Hazardous waste fact sheet]), indicating that the As-saturated LDH passed the TCLP test.

The above three tests were also repeated for Se, and the Se saturated LDH also passed the TCLP test, with the Se concentration being 2.3 ppb in the extraction fluid 1, and 1.5 ppb in extraction fluid 2. Note that the regulatory level for Se in order for the waste to fail the TCLP test is 1 ppm [www.ehso.com, Hazardous waste fact sheet]).

8.3. Conclusions

The experiments carried out in this Section prove that the As- and Se-saturated LDH can be characterized as non hazardous waste.

9. Nomenclature

C	bulk liquid-phase concentration, (μg/l)
C_0	initial liquid-phase concentration, (μg/l)
$\overline{C}$	dimensionless bulk liquid-phase concentration
C_M	solute concentration in the intercrystalline pore space, (μg/l)
$\overline{C}_M$	dimensionless solute concentration in the intercrystalline pore space
C_{MS}	liquid-phase concentration at the solid-liquid interface, (μg/l)
$\overline{C}_{MS}$	dimensionless liquid-phase concentration at the solid-liquid interface
D	diameter of the column, (cm)
D_b	bulk diffusivity, (cm^2/s)
D_i	intraparticle diffusion coeffecient, (cm^2/s)
D_{i0}	diffusivity at zero loading, (cm^2/s)
$\overline{D}_i$	dimensionless intraparticle diffusion coeffecient
D_M	mesopore diffusivity, (cm^2/s)
$\overline{D}_M$	dimensionless mesopore diffusivity
D_μ	micropore diffusivity, (cm^2/s)
$\overline{D}_\mu$	dimensionless micropore diffusivity
G_0	superficial mass velocity of flow through the bed (g/cm^2 min)
H	height of the column, (cm)
K	Sips constant
K_A	Sips constant for As in extended Sips equation

k_f	external mass transfer coefficient, (cm/s)
K_I	Sips constant for individual competing ion in extended Sips equation
K_I'	Sips constant for individual competing ion in extended Sips equation for the sites only accessible to the ions
M	initial adsorbent mass, (mg)
n	exponential factor in the Sips-type isotherm
N	total number of experimental points in RMSD analysis
n_A	exponential factor for As in extended Sips equation
n_I	exponential factor for individual competing ion in extended Sips equation
n_I'	exponential factor for individual competing ion in extended Sips equation for the sites only accessible to the ions
q	solute concentration in the adsorbent particle, (μg/g)
Q	dimensionless solute concentration in the adsorbent particle
$\bar{q}$	volume-averaged adsorbate concentration in the whole particle, (μg/g)
$\bar{Q}$	dimensionless volume-averaged adsorbate concentration in the whole particle
Q_0	volumetric flow rate fed to the column, (ml/min)
q_e	solute adsorbed at equilibrium with the corresponding bulk concentration, (μg/g)
$q_{e,A}$	As adsorbed at equilibrium with the corresponding bulk concentration in the binary isotehrm, (μg/g)

$q_{e,I}$	Individual competing ion adsorbed at equilibrium with the corresponding bulk concentration in the binary isotherm, (μg/g)
q_s	maximum sorption capacity, (μg/g)
$q_{s,A}$	maximum sorption capacity of As in the binary isotherm, (μg/g)
$q_{s,I}$	maximum sorption capacity of the individual competing ion in the binary isotherm, (μg/g)
q_μ	solute concentration in the microsphere, (μg/g)
Q_μ	dimensionless solute concentration in the microsphere
$\overline{q}_\mu$	volume-averaged adsorbate concentration in the microsphere, (μg/g)
$\overline{Q}_\mu$	dimensionless volume-averaged adsorbate concentration in the microsphere
q_t	solute adsorbed at any time, (μg/g)
Re	Reynolds number
r_M	radial distance in particle, (cm)
R_M	particle radius, (cm)
r_μ	radial distance in microparticle, (cm)
R_μ	microparticle radius, (cm)
Sc	Schmidt number
Sh	Sherwood number
Sh$'$	Sherwood number
Sh$''$	Sherwood number

t time, (min)

t_R residence time in the column (min)

u average axial velocity of the flowing fluid in the interstitial spaces, (cm/min)

V initial volume of solution, (ml)

V' column volume coordinate, (cm^3)

V_0' total column volume, (cm^3)

$\overline{V'}$ dimensionless column volume coordinate

$x_{1,i}$ i_{th} experimental point value in RMSD analysis

$x_{2,i}$ i_{th} model prediction point value in RMSD analysis

z axial distance coordinate, (cm)

Greek Symbols

ε void fraction in the bed

ε_M void fraction of the porous region in the particle

ϕ_i mass fraction of particles with average radius equal to R_i

Γ tortuosity factor of the porous region in the particle

ρ particle density, (g/cm^3)

ρ_f density of water, (g/cm^3)

ρ_s solid density, (g/cm^3)

μ dynamic viscosity of water, (g/cm s)

ν kinematic viscosity of water, (cm^2/s)

η dimensionless particle radius

β	dimensionless microparticle radius
τ	dimensionless time
Λ	dimensionless Sips constant
χ	dimensionless mass transfer coefficient
ω	dimensionless solute concentration in the adsorbent particle
$\overline{\omega}$	dimensionless solute concentration in the microspheres
ψ	dimensionless group
$\overline{\psi}$	dimensionless group

10. Bibliography

Harale, A. A Hybrid Adsorbent-Membrane Reactor (HAMR) System For Hydrogen Production. *PhD Thesis*. University of Southern California, **2008**, 80.

Anthony, R.G.; Philip, C.V.; and Dosch, R.G. Selective adsorption and ion exchange of metal cations and anions with silico-titanates and layered titanates. *Waste Management*, **1993**, *13*(5-7), 503.

(ATSDR) Agency for Toxic Substances and Disease Registry, Toxicological Profile for Selenium, U.S. Public Health Service, U.S. Department of Health and Human Services, Atlanta, GA, **1989**.

Axe, L.; Trivedi, P. Intraparticle Surface Diffusion of Metal Contaminants and their Attenuation in Microporous Amorphous Al, Fe, and Mn Oxides. *J. Colloid Interf. Sci.*, **2002**, *247*(2), 259.

Badruzzaman, M; Westerhoff, P; Knappe, D. R. U. Intraparticle Diffusion and Adsorption of Arsenate onto Granular Ferric Hydroxide. *Wat. Res.*, **2004**, *38*, 4002.

Barriga, C.; Gaitan, M.; Pavlovic, I.; Ulibarri, M. A.; Hermosin, M. C.; Cornejo, J. Hydrotalcites as Sorbent for 2,4,6-trinitrophenol: Influence of the Layer Composition and Interlayer Anion. *J. Mater. Chem.*, **2002**, *12*, 1027.

Bowell, R. J. Sorption of Arsenic by Natural Iron Oxides and Oxyhydroxides in Soil. *Appl. Geochem.*, **1994**, *9*, 279.

Cavani, F.; Trifiro, F.; Vaccari, A. Hydrotalcite-type Anionic Clays: Preparation, Properties and Applications, *Catal. Today*, **1991**, *11*, 173.

Cen, P. L.; Yang, R. T. Analytical Solution for Adsorber Breakthrough Curves with Bidisperse Sorbents (Zeolites). *AICHE*, **1986**, *32*(10), 1635.

Chen, J. P.; Wang, X. Removing Copper, Zinc, and Lead Ion by Granular Activated Carbon in Pretreated Fixed Bed Columns. *Sep. and Purif. Technol*., **2000**, *19*, 157.

Chen, J. P.; Yoon, J. T.; Yiacoumi, S. Effects of Chemical and Physical Properties of Influent on Copper Sorption onto Activated Carbon Fixed Bed Columns. *Carbon*, **2003**, *41*, 1635.

Chitrakar, R; Tezuka, S; Sonoda, A; Sakane, K; Hirotsu, T. A New Method for Synthesis of Mg/Al, Mg/Fe, and Zn/Al Layered Double Hydroxides and Their Uptake Properties of Bromide Ion. *Ind. Eng. Chem. Res.*. 2008, *47*(14), 4905.

Choy, K. K. H.; Porter, J. F.; McKay, G. Langmuir Isotherm Models Applied to the Multicomponent Sorption of Acid Dyes from Effluent onto Activated Carbon. *J. Chem.*

Eng. Data. **2000**, *45*, 575.

Clifford, D.; Lin, C.C. Ion exchange, Activated Alumina and Membrane Process for Arsenic Removal from Groundwater. In Proceedings of the 45th Annual Engineering Conf., University of Kansas. **1995**.

Crepaldi, E.L; Tronto, J; Cardoso, L.P; Valim, J.B. Sorption of terephthalate anions by calcined and uncalcined hydrotalcite - like compounds. *Colloids and Surfaces A: Physicochem*. *Eng. Aspects*, **2002**, *211(2-3),* 103.

Dadwhal, M.; Kim, T. W.; Sahimi, M.; Tsotsis, T. T. Study of CO_2 Diffusion and Adsorption on Calcined Layered Double Hydroxides: The Effect of Particle Size. *Ind. Eng. Chem. Eng*., **2008**, *47*(16), 6150.

Dadwhal, M.; Ostwal, M. M.; Liu, P. K. T.; Sahimi, M.; Tsotsis, T. T. Adsorption of Arsenic on Conditioned Layered Double Hydroxides: Column Experiments and Modeling. *Ind. Eng. Chem. Eng*., **2009**, *48*(4), 2076.

Das, D. P.; Das, J.; Parida, K. Physicochemical Characterization and Adsorption Behavior of Calcined Zn/Al Hydrotalcite-like Compound (HTLs) Towards Removal of Fluoride from Aqueous Solution. *J. Colloid Inter. Sci.*, **2003**, *261*(2), 213.

Das, N. N.; Konar, J.; Mohanta, M .K.; Srivastava, S. C. Adsorption of Cr(VI) and Se(IV) from Their Aqueous Solutions onto Zr^{4+}-Substituted ZnAl/Mg-Al-Layered Double Hydroxides: Effect of Zr^{4+} Substitution in the Layer. *J. Colloid Interf. Sci.*, **2004**, *270*, 1.

Delorme, F.; Seron, A.; Gautier, A.; Crouzet, C. Comparison of the fluoride,arsenate and nitrate anions water depollution potential of a calcined quintinite, a layered double hydroxide compound. *J Mater Sci*., **2007**, *42*, 5799.

DeMarco, M.J., SenGupta, A.K., and Greenleaf, J. Arsenic removal using a polymeric/hybrid inorganic sorbent. *Wat. Res*., **2003**, *37*, 164.

Driehaus, W.; Jekel, M.; Hildebrandt, U. Granular Ferric Hydroxide - A New Adsorbent for the Removal of Arsenic from Natural Water. *J Water SRT – Aqua*. **1998**, *47*, 30.

El-Geundi, M.S. Homogeneous Surface Diffusion Model for the Adsorption of Basic Dyestuffs onto Natural Clay in Batch Adsorbers. *Adsor. Sci. Tech.,* **1991**, *8*(4), 217.

EPA Test Method 1311 - TCLP, Toxicity Characteristic Leaching Procedure. www.ehso.com, Environmental Health & Safety Online.
Ferguson, J.F.; Gavis, J. A Review of the Arsenic Cycle in Natural Waters. *Wat. Res.*, **1972**, *6*, 1259.

Grover, K.; Komarneni, S; Katsuki, H**.** Uptake of arsenite by synthetic layered double hydroxides. *Water Res*., 2009, *43*(15), 3884.

Guidelines for Drinking Water Quality, 2nd edition, Addendum to Volume 1, Recommendations World Health Organization, Geneva, 3. **1998**.

Han, R.; Zhang, J.; Zou, W.; Xiao, H.; Shi, J.; Liu, H. Biosorption of Copper(II) and Lead(II) from Aqueous Solution by Chaff in a Fixed-Bed Column. *J. Hazard. Mater.*, **2006**, *113*(1-3), 262.

Hayes, K.F.; Roe, A.L.; Brown, G.E.; Hodgson, K. O.; Leckie, J. O.; Parks, G.A. In Situ X-ray Absorption Study of Surface Complexes: Selenium Oxyanions on a-FeOOH. *Science*, **1987**, *238*, 783.

Hazardous Waste Fact Sheet: TCLP: Toxicity Characteristic Leaching Procedure and Characteristic Hazardous Wastes. www.ehso.com.

Hermosin, M.C.; Pavlovic, I.; Ulibarri, M. A.; Cornejo, J. Hydrotalcite as Sorbent for Trinitrophenol: Sorption Capacity and Mechanism. *Wat. Res.*, **1996**, *30*(1), 171.

Impellitteri, C. A.; Scheckel, K. G. The Distribution, Solid-Phase Speciation, and Desorption/Dissolution of As in Waste Iron-Based Drinking Water Treatment Residuals. *Chemosphere*. **2006**, *64*(6), 875.

Inglezakis, V. J.; Grigoropoulou, H. Effects of Operating Conditions on the Removal of Heavy Metals by Zeolite in Fixed Bed Reactors. *J. Hazard. Mater. B*, **2004,** *112*, 37.

Janz, G. J.; James, D. W. Molten nitrates as electrolytes: Structure and physical properties. *Electrochimica Acta*, **1962**, *7*(4), 427.

Kaczmarski, K; Bellot, J. Ch. Effect of Particle-Size Distribution and Particle Porosity Changes on Mass-Transfer Kinetics. *Acta Chromatographica*, **2003**, *13*, 22.

Kang, M.J.; Chun, K.S.; Rhee, S.W.; Do, Y. Comparison of Sorption Behavior of I^- and TcO_4^- on Mg/Al Layered Double Hydroxide. *Radiochim. Acta.*, **1999**, *85(1-2)*, 57.

Kim,Y. H.; Kim, C. M.; Choi, I.; Rengaraj, S.; Yi, J. H. Arsenic Removal Using Mesoporous Alumina Prepared via a Templating Method. *Environ. Sci. Tech.*, **2004**, *38*, 924.

Ko, D.C.K.; Porter, F.F.; McKay G. Effect of Concentration-Dependent Surface Diffusivity on Simulations of Fixed Bed Sorption Systems. *Trans IChemE.*, **2003**, *81A*, 1323.

Ko, D. C. K.; Porter J. F.; Mckay, G. Film-pore Diffusion Model for the Fixed-Bed Sorption of Copper and Cadmium Ions onto Bone Char. *Wat. Res.*, **2001**, *35*(16), 3876.

Ko, D.C.K.; Porter, F.F.; McKay G. Optimised Correlations for the Fixed-bed Adsorption of Metal Ions on Bone Char. *Chem. Eng. Sci.*, **2000**, *55*, 5819.

Kojima, T.; Miyazaki, Y.; Nomura, K.; Tanimoto, K. Density, Molar Volume, and Surface Tension of Molten Li_2CO_3-Na_2CO_3 and Li_2CO_3-K_2CO_3 Containing Alkaline Earth (Ca, Sr, and Ba) Carbonates. *J. Electrochem. Soc.*, 2003, *150*(11), E535-E542.

Kundu, S.; Gupta, A. K. Analysis and Modeling of Fixed Bed Column Operations on As(V) Removal by Adsorption onto Iron Oxide-Coated Cement (IOCC). *J. Colloid. Interf. Sci.*, **2005**, *290* (1), 52.

Kwon, T.; Tsigdinos, G. A.; Pinnavaia, T. J. Pillaring of Layered Double Hydroxides (LDHs) by Polyoxometalate Anions. *J. Am. Soc.*, **1988**, *110*(11), 3653.

Lazaridis, N. K.; Pandi, T. A.; Matis, K.A. Chromium (VI) Removal from Aqueous Solutions by Mg-Al-CO_3 Hydrotalcite: Sorption-Desorption Kinetic and Equilibrium Studies, *Ind. Eng. Chem. Res.*, **2004**, *43*, 2209.

Lee, L.K. The Kinetics of Sorption in a Biporous Adsorbent Particle. *AICHE*, **1978**, *24(3)*, 531.

Lee, T.Y; Ma, Y.H. Transient Diffusion in Solids with a Bipore Distribution. *AICHE*, **1976**, *22(1)*, 147.

Lepkowski, W. Arsenic Crisis in Bangladesh. *Chem. Eng. News*, **1998**, *76*(46), 27.

Lide, D.R. Hanbook of Chemistry and Physics. 77th Edition, **1996-1997**, 5-99.

Lin T.F.; Wu, J.K. Adsoprtion of Arsenite and Arsenate within Activated Alumina Grains. quilibrium and Kinetics. *Wat. Res.*, **2001**, *35*, 2049.

Malkoc, E.; Nuhoglu, Y. Removal of Ni(II) ions from aqueous solutions using waste of tea factory: Adsorption on a fixed-bed column. *J of Hazard. Mat.*, **2006**, *B135*, 328.

Manceau A.; and Charlet, L. The Mechanism of Selenate Adsorption on Goethite and Hydrous Ferric Oxide. J. Coll. Interface Sci., 1994, *168*(1), 87.

Manju, G. N.; Anirudhan, T. S. Treatment of Arsenic (III) Containing Wastewater by Adsorption on Hydrotalcite. *Indian J. Environ. Health*, **2000**, *42*(1), 1.

Manju, G. N.; Gigi, M. C.; Anirudhan, T. S. Hydrotalcite as Adsorbent for the Removal of Chromium (VI) from Aqueous Media: Equilibrium Studies. *Ind. J. Chem. Tech*., **1999**, *6*(3), 134.

Manning, B. A.; Goldberg, S. Adsorption and Stability of Arsenic (III) at the Clay Mineral-Water Interface. *Environ. Sci. Tech.*, **1997**, *31*, 2005.
Miyata S. Anion Exchange Properties of Hydrotalcite-Like Compounds. *Clays and Clay Minerals*, **1983**, *31*(4), 305-311.

Neal, R. H.; Sposito, G.; Holtzeland, K. M.; Traina, S. J. Selenite Adsorption on Alluvial Soils. 1. Soil Composition and PH effects. *Soil Sci. Soc. Am. J.*, **1987**, *51*(5), 1161.

O'Day P A.; Vlassopoulos D.; Meng X.; Benning L G. Advances in Arsenic Research: Integration of Experimental and Observational Studies and Implications for Mitigation. *American Chemical Society*, 2005, *915*.

Ohlendorf, H.M.; Hoffman, D.J.; Saiki, M.K.; Aldrich, T.W. Embryonic Mortality and Abnormality of Aquatic Birds – Apparent Impacts of Selenium from Irrigation Drainwater. *Sci. Total Environ.*, **1986**, *52*(1-2), 49.

Ouvrand, S.; Simonnot, M.O.; de Donato P.; Sardin, M. Diffusion-Controlled Adsorption of Arsenate on a Natural Manganese Oxide. *Ind. Eng. Chem. Res.*, **2002**, *41*, 6194.

Papelis, C.; Brown, G.E.; Packs, G.A. X-ray Absorption Spectroscopic Studies of Cadmium and Selenite Adsorption on Aluminum Oxides. *Langmuir*, 1995, *11*(6), 2041.

Parsons, S.A; Jefferson,B. Introduction to Potable Water Treatment Processes. *Blacwell Publishing*, **2006**, 4-5.

Pavan, P.C.; Crepaldi, E. L.; Valim, J. B. Sorption of Anionic Surfactants on Layered Double Hydroxides, *J. Colloid Interf. Sci.*, **2000**, *229*(2), 346.

Ramana, A.; and Sengupta, A.K. Removing Selenium(IV) and Arsenic(V) Oxyanions with Tailored Chelating Polymers. *J. Envir. Eng.*, **1992**, *118*(5), 755.

Rao, K.J. Ionic sulphate glasses. *Bull, Mater. Sci.*, **1980**, *2*(5), 357.

Raven, K. P.; Jain, A.; Loepert, R. H. Arsenite and Arsenate Adsorption on Ferrihydrite: Kinetic, Equilibrium and Adsorption Envelops. *Environ. Sci. Technol.I,* **1998**, *32*, 344.

Rhee, S. W.; Kang, M. J.; Kim, H.; Moon, C. H. Removal of Aqueous Chromate Ion Involving Rehydration Reaction of Calcined Layered Double Hydroxide (Mg-Al-CO_3). *Environ. Tech.*, **1997**, *18*, 231.

Roelofs, J. C. A. A.; Van Bokhoven, J. A.; Van Dillen, A. J.; Geus, J. W.; De Jong, K. P. The Thermal Decomposition of Mg-Al Hydrotalcites: Effects of Interlayer Anions and Characteristics of the Final Structure. *Chem.-Eur. J.*, **2002**, *8*(24), 5571.

Rives V. Layered Double Hydroxides. Nova Science Publishers. **2001**, 11-13.

Runkenstein, E; Vaidyanathan, A.S; Youngquist, G.R. Sorption by Solids with Bidisperse Pore Structures. *Chem. Eng. Science.*, **1971**, *26*, 1305.

Saha, B.; Bains, R.; Greenwood, F. Physicochemical Characterization of Granular ferric hydroxide for As (V) Sorption from Water. *Separation Science and Technology*. **2005**, *40*, 2909.

Scharfenaker, M.A. Whiteman's Halloween surprise: 10mg/l arsenic standard. *J. Am. Water Works Assosc.*, **2000**, *94*(1), 24.

Seida, Y.; Nakano, Y.; Nakamura, Y. Rapid Removal of Dilute Lead from Water by Pyroaurite-like Compound. *Wat. Res*., **2001**, *35(10)*, 2341.

Smith, E.H. Uptake of Heavy Metals in Batch Systems by a Recycled Iron-Bearing Material. *Wat. Res*., **1996**, *30(10)*, 2424.

Sperlich, A.; Werner, A.; Genz, A.; Amy, G.; Worch, E.; Jekel, M. Breakthrough Behavior of Granular Ferric Hydroxides (GFH) Fixed-Bed Adsorption Filters: Modeling and Experimental Approaches. *Water Research*. **2005**, *39*, 1190.

Steinberger, A.; Stein, E. D. Characteristics of Effluents from Power Plant Generating Stations in the Southern California Bight in 2000. in S. Weisberg and D. Elmore (eds.), Southern California Coastal Water Research Project Annual Report **2004**, Westminster, CA.

Thirunavukkarasu, O. S.; Viraraghavan, T.; Subramanian, K.S. Arsenic Removal from Drinking Water Using Granular Ferric Hydroxide. *Water S.A.* **2003**, *29*(2), 161.

Tien, C. Adsorption Calculations and Modeling. Butterworth-Heinemann. Boston, **1994**.

Trotz, M.A.; Porous Alumina Packed Bed Reactors: A Treatment Technology for Arsenic Removal, Ph. D. dissertation, Stanford University, Stanford, CA, **2002**.

Turk, T.; Alp, I.; Deveci, H. Adsorption of As(V) from water using Mg–Fe-based hydrotalcite (FeHT). *Journal of Hazardous Materials*. **2009**, *171*(1-3), 665.

Vaishya, R. C.; Gupta, S. K. Arsenic(V) Removal by Sulphate ModifiedIron Oxide-Coated Sand (SMIOCS) in a Fixed Bed Column. *Water Qual. Res. J. Canada*., **2006**, *41*(2), 157.

Villa, M. V.; Sanchez-Martin, M. J.; Sanchez-Camazano, M. Hydrotalcites and Organo-Hydrotalcites as Sorbents for Removing Pesticides from Water. *J. Environ. Sci. Health*, **1999**, *B34*(3), 509.

Vrijenhoek, E. M.; Waypa, J. J. Arsenic Removal from Drinking Water by a "loose" nanofiltration membrane. *Desalination*, **2000**, *130*(3), 265.

Wang, S. L.; Liu, C. H.; Wang, M. K.; Chuang, Y. H.; Chiang, P. N. Arsenate adsorption by Mg/Al–NO_3 layered double hydroxides with varying the Mg/Al ratio. *App. Clay Sc*.,

2009, *43*(1), 79.

Williamson, J. E.; Bazaire, K. E.; Geankoplis C. J. Liquid-Phase Mass Transfer at Low Reynolds Numbers. *Ind. Eng. Chem. Fund*, **1963**, *2*(2), 126.

Yang, L; Dadwhal, M; Shahrivari, Z; Ostwal, M; Liu, P.K.T; Sahimi, M; Tsotsis, T.T. Adsorption of Arsenic on Layered Double Hydroxides: Effect of the Particle Size. *Industrial & Engineering Chemistry Research*, **2006**, *45*(13), 4742.

Yang, L.; Shahrivari, Z.; Liu P.K.T.; Sahimi, M.; Tsotsis, T.T. Aqueous Solutions by Calcined and Uncalcined Layered Double Hydroxides (LDH). *Ind. Eng. Chem. Eng.*, **2005**, *44*, 6804.

Yoshikado, S; Ito, Y.; Reau J. M**.** Fluoride ion conduction in $Pb_{1-x}Sn_xF_2$ solid solution system. *Solid State Ionics*, **2002**, *154-155*, 503-509.

You, Y. W.; Vance, G. F.; Zhao, H.T. Selenium Adsorption on Mg-Al and Zn-Al Layered Double Hydroxides. *Appl. Clay Sci.*, **2001**, *20*, 13.

You, Y. W.; Zhao, H. T.; Vange, G. F. Removal of Arsenic from Aqueous Solutions by Anion Clays, *Environ. Tech.*, **2000**, *22*, 1447.

You, Y. W.; Zhao, H. T.; Vance, G. F. Removal of arsenite from aqueous solutions by anionic clays. *Environ. Tech*., **2001**, *22*(12), 1447.

11. Appendix

Sample Calculations for Power Plant Effluent Treatment

Assumptions:

Average As concentration in power plant effluents = 20 ppb

Typical power plant effluents = 5000 GPM

LDH Cost: $ 800 for 50 Kg ($ 16/Kg LDH)

Column Dimensions:

Height of Packing: $H = 6$ m

Diameter of Packing: $D = 0.9$ m

Volume of Packing: $V_{Packing} = \frac{\pi D^2 H}{4} = 3.82$ m^3

LDH needed for 1 column:

Density of LDH, $\rho_{bulk} =$ 1.37 g/cm^3

Bed Porosity, $\varepsilon =$ 0.27

LDH needed for 1 column, $Mass_{LDH} = (1-\varepsilon) V_{Packing} \rho_{bulk} = 3820.4$ Kg

Cost of LDH for 1 column: $3820.4 \times 16 =$ $ 61,126.4

Cost of LDH for 2 columns: $ 122,252.8 (when first column saturates, we will have the second column ready)

From our lab column experiments, 3.8 g of LDH treated 608 L of 20 ppb As solution fed at a flow rate of 10 ml/min before breakthrough (i.e. $C/C_0 = 0.05$ %)

Therefore, 3820.4 Kg will treat $= \frac{608}{0.0038}(3820.4) = 6.1 \times 10^8$ L $= 1.61 \times 10^8$ Gallons

Typical power plant effluent discharge = 5000 GPM

Total effluent volume discharged in 1 day $= 5000 \times 60 \times 24 = 7.2 \times 10^6$ Gallons

Therefore, 1 column will run for $= \frac{1.61 \times 10^8}{7.2 \times 10^6} = 22.4$ days before it saturates

Then we will switch to the other column. In the meantime we will regenerate this column using a Na_2CO_3 solution.

Amount of As adsorbed by the saturated LDH of first column

$= 6.1 \times 10^8 L \times 20 \frac{\mu g}{L} \times \frac{1}{10^9} \frac{Kg}{\mu g} = 12.2$ Kg As = 162.7 mol of As

Regeneration of LDH:

We will treat the used LDH with 500 Gallons water containing 1000 mol of Na_2CO_3. (mol of Na_2CO_3 used are much higher than As mol present, i.e. 162.7 mol, to ensure complete removal of As from LDH)

Amount of Na_2CO_3 needed $= 1000 * 106 = 106$ Kg of Na_2CO_3

106 Kg of Na_2CO_3 will cost $ 770

As concentration of this 500 Gallons of water will be $= \frac{12.2 \times 10^6 mg}{500 \times 3.78} = 6455.03$ ppm

If we regenerate each column 15 times, total cost of regeneration $= 770 \times 15 =$ $ 11,550

Operating cost = 20% of Initial Investment = 20% of $ 72676.4 = $ 14535.3

Conclusions

Total cost of 1 column (Initial cost + Regeneration + Operating Cost) = $ 61,126.4 + $ 11,550 + $ 14535.3 = $ 87211.7

Total effluent volume treated by this 1 column $= 1.61 \times 10^8 \times 15 = 2.4 \times 10^9$ Gallons

1 column will run for $= 22.4 \times 15 = 336$ Days

Effluent generated by regeneration $= 500 \times 15 = 7{,}500$ Gallons containing 6455.03 ppm As

Cost to treat: 27500 Gallons/$